UNIVERSITY OF LIVERPOOL

The Role of Decapping Factors During Nonsense-Mediated Decay (NMD) in *Aspergillus nidulans*

Thesis submitted in accordance with the requirements of
The University of Liverpool for the degree of
Doctor in Philosophy by

Izwan Bharudin

December 2016

ABSTRACT

RNA degradation is ubiquitous and it is clear that it must be carefully controlled to accurately recognise and target appropriate transcripts. There are several pathways for mRNA degradation and decapping is one of the critical steps in determining transcript stability. The focus of this study was the identification and characterisation of factors involved in decapping and their involvement in nonsense-mediated mRNA decay (NMD) in *Aspergillus nidulans*. Our studies have shown that disruption of two decapping factors, Dcp1 and the Nudix protein Dcp2, lead only to partial suppression of NMD. This distinguishes *A. nidulans* from *Saccharomyces cerevisiae*, where the two decapping factors are required for NMD. Deletion of *lsm1*, which encodes a component of a heptomeric complex, Lsm1-7, a known promoter of decapping, also partially supressed NMD. To our knowledge this is the first time that the role of Lsm's in NMD has been described. A similar result was observed when another Nudix family protein, NdxD, was disrupted. We propose that NdxD is a second decapping factor in *A. nidulans*. Disruption of other factors known to promote decapping and subsequent RNA degradation, Pat1, Dhh1 and Xrn1, did not affect NMD, demonstrating these factors are not required for NMD in *A. nidulans*. In order to quantify decapping, we set out to establish a simple and reliable assay to quantify the decapped transcripts. The method utilised splinted-ligation through which an RNA adaptor is ligated specifically to the 5' end of decapped transcripts with the help of splint primer. The primer has a complementary sequences to the RNA adaptor at its 3' end and the eight random nucleotides at the 5' end to facilitate hybridisation to any decapped transcript. qRT-PCR was utilised to amplify the ligation products for a specific transcript and used internal primers as a control to assess the relative level of decapped transcripts. This gave a good basis for quantifying the decapped transcripts, however further optimisation is required in order to develop a robust assay. Although it has been known that both Dcp1 and Dcp2 form a decapping complex in yeast, our studies showed that Dcp2 has a significant role in stabilising the *uaZ*$^{+}$ transcript, while deletion of *dcp1* did not. Fluorescence microscopy has shown that both of these proteins localise primarily to the expected P-body like structures, however, the major proportions of Dcp2 and Dcp1 did not co-localise and were therefore not interacting. These data suggest that the Dcp2 activity is not solely dependent on Dcp1, suggesting a divergence between *A. nidulans* and *S. cerevisiae*. Additionally, confocal microscopy was used to characterise the intracellular distribution of CutA and CutB, which are involved in 3' pyrimidine-tagging of transcripts, promoting decapping and degradation of mRNA. Using GFP and RFP tagged proteins, we determined that CutA is primarily localised in the cytoplasm whereas CutB is primarily, but not exclusively, located in the nuclei. Interestingly deletion of *cutB* lead to increased levels of CutA in the nuclei suggesting an interplay between the two proteins. Deletion of *dcp1* produces an aberrant polysome profile as determined by sucrose gradient centrifugation. The predominant peak correlated with the large (60S) subunit rather than the monosome (80S) peak observed for WT. The small (40S) subunit was also relatively high. These observations distinguished Δ*dcp1* from WT and the phenotype of the Δ*dcp2* strain was intermediate between the two. The accumulation of 60S peak in Δ*dcp1* included a relatively high proportion of 28S rRNA derived fragments. Northern analysis of these putative 60S degradation products and sequencing of two specific fragments suggest that in the Δ*dcp1* strain the ribosomes are being cleaved, possibly as part of an rRNA turnover mechanism. Although genetic analysis showed that both Δ*dcp2* and a point mutation, *dcp2* ^{E148Q}, which is likely to disrupt the nuclease activity, are both epistatic to *dcp1* with respect to this phenotype. Northern analysis indicates that the degradation products observed in Δ*dcp1*, Δ*dcp2* and WT strains appear very similar, even though the levels vary dramatically. This implies that Dcp2 is probably not directly responsible for these cleavage events or it is one of a number of activities cleaving the rRNA in what appears to be a similar way.

Acknowledgements

Firstly, I would like to thank my supervisor, Professor Mark X. Caddick who has given me the opportunity and undertaking this project and for all the help and guidance given, extreme patient and unpleasant task of reading and correcting this thesis. I would also like to thank Dr. Igor Morozov for all his useful advice.

I would also like to say a huge thank you to members of Lab G, Institute of Integrative Biology who made my time here enjoyable. Particular thanks goes to our group members, Amir, Ewan, Gwen, Danielle and Stefany who helping me a lot in the lab. I must also extend my gratitude to Jean Wood and Paul Loughnane for excellent technical assistance. Besides, I would like to thanks Dr. Marco Marcello, Dr. Pete Gould and Dr. Dave Mason for technical assistance in fluorescence microscopy work and Dr. Sean Connell for the help with the 3D mapping of ribosomal RNA.

Finally, I would like to thank my lovely wife, Anis Farhan Fatimi Ab Wahab, and my kids, Aisyah Nur Iman and Yusuf Abdul Rahman for putting up with me in the last three and a half years here in Liverpool. I am sure it's been difficult at times, but we manage to go through it. Besides, I would like to thank both my family in Malaysia for their endless support during my PhD. I am so lucky to have all of you as my family.

Last but not least, I would like to thank Malaysian government through Ministry of Higher Education and Universiti Kebangsaan Malaysia for given me a chance to pursue my PhD in the UK.

Abbreviations

ATP	Adenosine Triphosphate
bp	base pair
cDNA	complementary deoxyribonucleic acid
DNA	Deoxyribonucleic acid
dNTP	Deoxynucleotide phosphate
EDTA	Ethylenediaminetetraacetic acid
g	gram
Kb	kilobase
LB	Luria broth
mg	miligram
ml	mililitre
MOPS	3-(N-morpholino) propanesulfonic acid)
µl	microlitre
mRNA	messanger ribonucleic acid
mRNP	messanger ribonucleoprotein
NMD	Nonsense-Mediated Decay
PCR	polymerase chain reaction
PEG	Polyethylene glycol
PTC	Premature termination codon
qRT-PCR	quantitative real-time polymerase chain reaction
RNA	Ribonucleic acid
RPM	Revolutions per minutes
3’-UTR	three prime untranslated region
5’-UTR	five prime untranslated region

List of Tables

List of Figures.

Chapter 1

Chapter 2

Chapter 3

Chapter 4

Chapter 5

Chapter 6

CONTENTS

CHAPTER 1: INTRODUCTION

The central dogma provides an overview of how the genetic materials are expressed. Transcription, the production of messenger RNA (mRNA) from the DNA, is followed by the translation of mRNA into protein. In eukaryotes, transcription is carried out primarily in the nucleus, while translation occurs in the cytoplasm. Nuclear pre-mRNA needs to undergo several post-transcriptional modifications such as 3'-end processing and polyadenylation, 5'-capping and splicing before being transported into the cytoplasm (Millevoi and Vagner, 2010). The addition of the 5'-cap and poly(A) tail at the 3'-end of the mRNA are required to stabilise the transcript and also play important roles in the initiation and termination of translation. Consequently, there is a strong functional link between mRNA stability and translation.

1.1. General mechanism of mRNA decay

The stability of the eukaryotic mRNA primarily depends on the specific structures at its ends (Balagopal et al., 2012); theN^7-methyl guanosine cap (^{m7}G) at the 5'-end and poly(A) tail added at the 3′-end to the pre-mRNA in the nucleus (Shatkin and Manley, 2000). Both modifications are required to license mRNA export from the nucleus to the cytoplasm and protect the mRNA during this process. In addition to the ^{m7}G-cap structure protecting the mRNA from the 5′-to-3′ exonucleolytic degradation, it is bound and protected by the eIF4F protein complex (Sonenberg and Hinnebusch, 2009). The mRNA poly(A) tail, which is a poor substrate for the general 3'-5' exonuclease activity of the exosome, is also protected by poly(A)-binding proteins (Pab1) which shield it from degradation by exonucleases, primarily the deadenylases, and interacts with eIF4G (Sonenberg and Hinnebusch, 2009). Furthermore, the binding of eIF4F complex with Pab1 promotes the translation (Archer et al., 2015). There are two major pathways of mRNA degradation (Figure 1.1) and both are initiated by shortening of poly(A) tail (deadenylation) (Liu et al., 2008; Parker, 2012).

1.1.1. Deadenylation in eukaryotes

Deadenylation, which is the rate-limiting step in the degradation of most mRNAs, is mediated primarily by the Pan2-Pan3 and Caf1-Ccr4-Not deadenylase complexes (Balagopal et al., 2012; Funakoshi et al., 2007). The main cytoplasmic deadenylase is the Ccr4-Not complex which is evolutionarily conserved across eukaryotes (Parker and Song, 2004). It consists of nine different proteins subunits including the two nucleases, Ccr4 and Caf1 (Wiederhold and Passmore, 2010). The Pan2-Pan3 complex has a similar function to the Ccr4-Not complex (Tucker et al., 2001). Pan2, a member of the DEDD superfamily, is the deadenylase and Pan3 acts as a regulator. Although both complexes show similar activity their functional differentiation with respect to cytoplasmic deadenylation, remains unclear. It is postulated that Pan2-Pan3 acts to edit down the poly(A) tail to a certain length and Ccr4-Not complete the deadenylation (Yamashita et al., 2005). Co-immunoprecipitation studies show that Pan2 interacts with the Ccr4-Not complex component, Caf1, which led to the hypothesis of a two-step deadenylation process, where the two complexes act sequentially in a coordinated manner (Zheng et al., 2008). In many eukaryotes, which includes the vertebrates and some fungi, there is another deadenylase known as Poly(A)-specific RiboNuclease (PARN), which consist of a homodimer. Functionally, it differs from both the Ccr4-Not and Pan2-Pan3 complexes because it requires the mRNA 5’ cap to be activated (Yamashita et al., 2005).

1.1.2. Exosome-mediated decay

Deadenylated mRNAs can be degraded by the 3’-exonucleolytic decay pathway, involving the exosome complex (Franks and Lykke-Andersen, 2008). Studies have shown that distinct exosome complexes are present in the nucleus and cytoplasm (Houseley and Tollervey, 2009; Lykke-Andersen et al., 2009). The exosome ensures the balance of RNAs by facilitating normal RNA processing and turnover, as well as by participating in complex RNA quality-

control mechanisms and structural RNA maturation (Lykke-Andersen et al., 2009). The exosome contains a core of 10 components (Exo_{10}) which is evolutionarily conserved and is implicated in the to control the quality and quantity of most of the RNAs produced (Kowalinski et al., 2016). Although the core is present in both the nucleus and in the cytoplasm, it is bound by different cofactors in each location. In the nucleus, Rrp44/Dis3 is believed to possess the main 3′ exonuclease activity while the other nine non-catalytic core subunits (Exo_9) forms the central channel through which the RNA passes (Schneider et al., 2009; Wasmuth et al., 2014). However, recent studies have shown that Rrp6 also provides an additional RNase D−like hydrolytic 3′-exonuclease activity (Schneider and Tollervey, 2014). Associated with the nuclear exosome is the TRAMP complex which consists of an RNA helicase (Mtr4), a poly(A) polymerase (PAP) and a zinc knuckle protein (either *Air1* or *Air2*) within a 14-subunit assembly (Butler and Mitchell, 2010). However, in the cytoplasm, structural studies have shown that Exo_{10} functions together with the Ski complex (Kowalinski et al., 2016). Following mRNA degradation by the exosome, the remaining short mRNA, with the 5' cap structure, is degraded by a Dcps, a scavenger-decapping enzyme which contains the Histidine Triad (HIT) superfamily of pyrophosphatases (Milac et al., 2014).

1.1.3. The Xrn1 dependent 5'-to-3' decay pathway

Once the 3' poly(A) tail has been shortened to A_{15}, the decapping activator Pat1-Lsm1-7 complex is recruited to it, promoting 5' to 3' decay by a process called mRNA decapping (Tharun et al., 2000). The decapped transcript is then subject to 5' exonucleolytic decay, mediated by Xrn1 (Dunckley and Parker, 1999). Decapping occurs mainly by the activity of Dcp2, a Nudix family protein, together with its co-activator, Dcp1 (Parker, 2012; Valkov et al., 2016). The activation of this complex will generate 5'-monophosphorylated mRNAs (Chang et al., 2014), thus providing the substrates for rapid degradation by Xrn1 (Coller and Parker,

2004). There are several key factors which control decapping such as deadenylation and accessibility of the 5' cap structure, which is enhanced by the dissociation of the cytoplasmic cap-binding proteins. Association of Dcp1-Dcp2 to the 5'-cap involves assembly of an mRNP complex including many activators of decapping: Dhh1, Pat1, Edc3 and the Lsm1-7 complex (Coller and Parker, 2004; Parker, 2012).

The exonuclease, Xrn1, plays a crucial role in transcription, RNA metabolism and RNA interference (Chang et al., 2011). It is highly conserved in all eukaryotes, including well-characterised orthologues in *D. melanogaster* (Pacman) (Nagarajan et al., 2013), *C. elegans* (XRN1) (Newbury and Woollard, 2004) and *S. cerevisiae* (Xrn1p) (Solinger et al., 1999). Xrn1 is primarily located in the cytoplasm, localising to P-bodies and involved in various RNA degradation processes including the general turnover of decapped mRNAs (Parker and Song, 2004), nonsense-mediated decay and microRNA decay (Bail et al., 2010; Gatfield and Izaurralde, 2004). Its importance is underlined by being essential for proper development in mammals (Newbury and Woollard, 2004). Studies have shown that Xrn1 physically interacts the C-terminus of Pat1 of the Pat1-Lsm1-7 complex (Nissan et al., 2010). Moreover, the C-terminus of Xrn1 also interacts with Dcp1-EVH1 domain and a DCP1-binding motif (DBM) (Braun et al., 2012), consistent with the coordination of Xrn1 activity with mRNA decapping. A simplified overview of mRNA decay is illustrated in Figure 1.1.

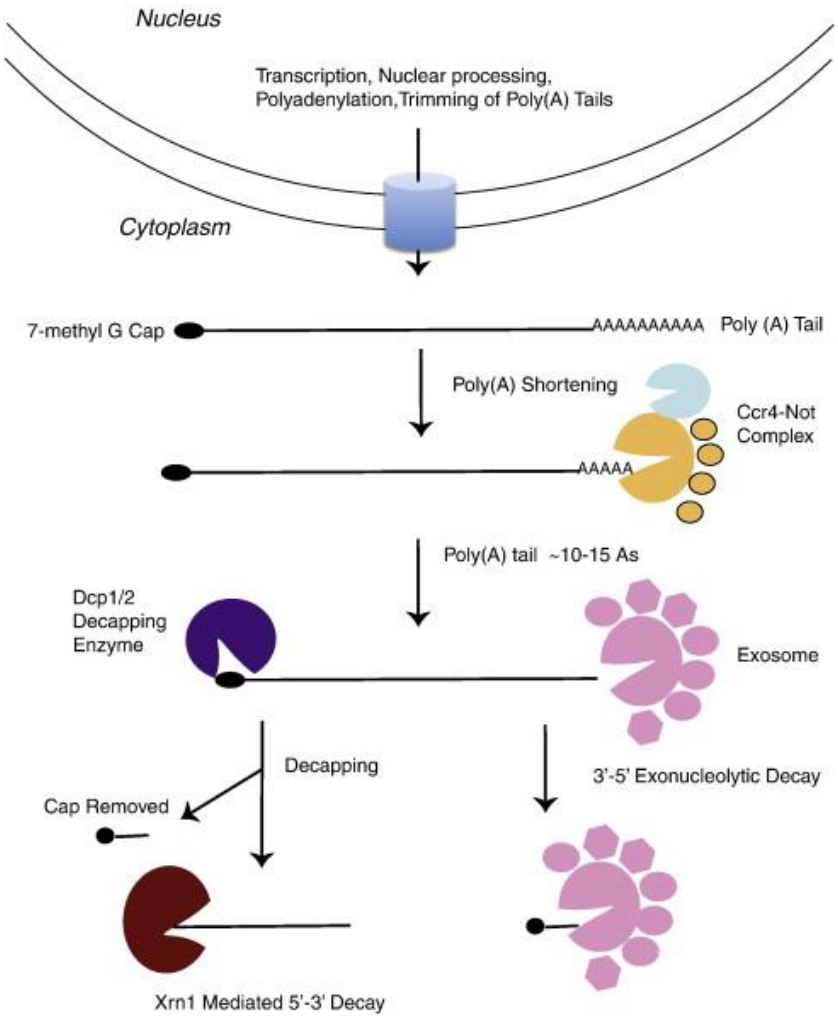

Figure 1.1. General mechanism of mRNA decay. mRNAs are generated in the nucleus and then translocate to the cytoplasm. Degradation of mRNAs started with the poly(A) shortening (catalysed by the CCR4–NOT and PAN2–PAN3 complexes-complexes not shown) until the poly(A) tail length is about 10-15 nucleotides. Next, decapping enzyme (Dcp2/Dcp1) will remove the cap structure which known as decapping process. Then, the decapped transcripts were subjected to 5' exonucleolytic decay pathway, mediated by Xrn1. Alternatively, they are degraded by the exonucleolytic 3´ to 5´ exosome decay pathway.
(Adapted from (Balagopal et al., 2012)).

1.2. Decapping protein

1.2.1. Dcp2-Dcp1 the conserved core of decapping complex

In the past few years, decapping has emerged as the critical step which initiates the process of mRNA degradation (Coller and Parker, 2004). Dcp2 has been identified as the main decapping enzyme in *S. cerevisiae* (Coller and Parker, 2004). It catalyses the hydrolysis of 5'-7-methylguanosine (m^7GpppN) cap from the mRNAs and releases m^7GDP and 5'-mono-phosphorylated mRNA which is a substrate of rapid degradation by Xrn1 (Song et al., 2013). Dcp2, a member of Nucleoside Diphosphate linked to X (Nudix) hydrolase family proteins, contains a catalytic Nudix domain and an RNA-binding motif (known as Box-B helix) at the C-terminus and a regulatory domain at the N-terminus (Chang et al., 2014; Coller, 2016; She et al., 2008; Valkov et al., 2016). Studies have shown that the N-terminus and Nudix domains of Dcp2 are enough to promote decapping *in vitro* (Harigaya et al., 2010). However, *in vivo* Dcp1 is essential in activating Dcp2 (Coller, 2016).

In addition to Dcp2, recent studies have shown that other Nudix family proteins posses mRNA decapping activity (Song et al., 2013). The Nudix protein are phosphohydrolases which cleave a phosphate bond in their substrate to create two products. Studies have revealed that Nudt2, Nudt3, Nudt12, Nudt15, Nudt16, Nudt17 and Nudt19 from mice, are all able to effect decapping, although their relative activities vary significantly (Song et al., 2010; Song et al., 2013).

Dcp1, is the main activator of Dcp2 and is important in accelerating decapping in yeast (Parker, 2012). It contains EVH1 domain at the N-terminus which serves as a binding site for the Dcp2 regulatory domain (She et al., 2008; Valkov et al., 2016). Moreover, the EVH1 domain also serves as the binding site for other decapping activators such as Edc1 and Edc2, which interact through its proline recognition site (Borja et al., 2011). Kinetic studies also show that this interaction stimulates Dcp2's decapping activity 1000-fold, in yeast (Borja et al., 2011).

Structural studies of *S. pombe* Dcp2 has shown that Dcp2 exists in two confirmations, open and closed, with the closed complex being more active than the open confirmation (She et al., 2008). It has been shown that in the closed form the N-terminal regulatory domain interacts with the Nudix domain, activating catalysis (Figure 1.2) (She et al., 2008; Valkov et al., 2016). However, there are no direct contacts between the Dcp2 Nudix domains and Dcp1 EVH1, so it remains unclear how Dcp1 activates Dcp2 (Coller, 2016; Valkov et al., 2016).

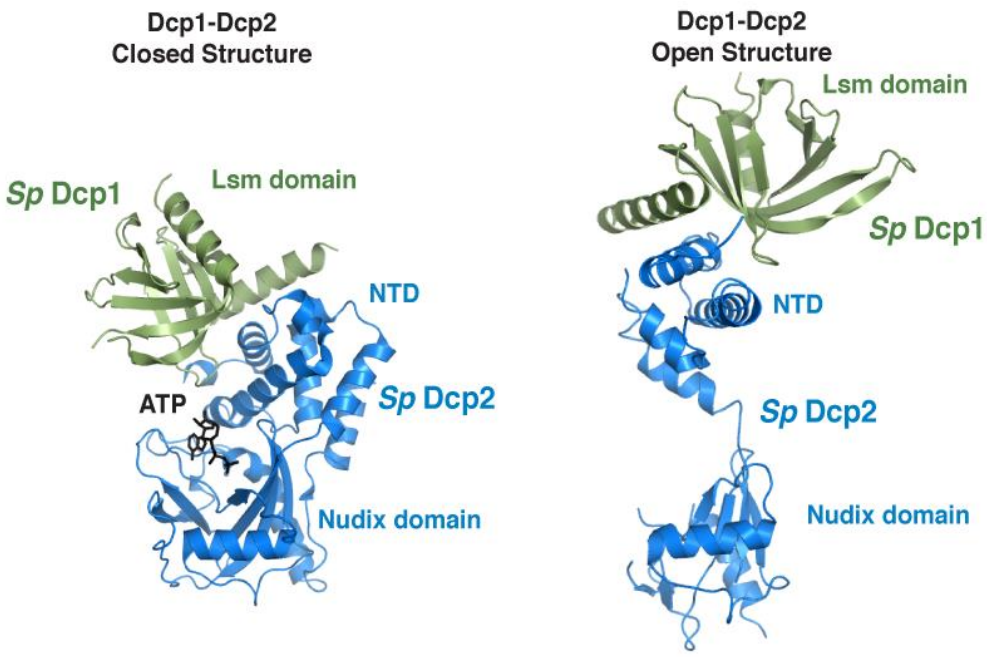

Figure 1.2. Crystal structures of the closed and open structure of *S. pombe* Dcp1-Dcp2. Dcp1 is depicted in green while Dcp2 N-terminal domain (NTD) and Nudix domain in blue, ATP analog in black. Adapted from (Sharif, 2014).

1.2.2. Nudt16, the second enzyme for decapping

Nudt16 is a Nudix family protein initially identified in Xenopus as a nucleolar U8 snoRNA binding protein and shown to possess decapping activity (Ghosh et al., 2004). This protein is capable of binding and decapping the U8 snoRNA, in the presence of either Mg^{2+} or Mn^{2+} as the cation source, *in vitro* (Ghosh et al., 2004). Although Nudt16 is conserved in metazoans, there is no known orthologue of Nudt16 found in *S. cerevisiae*, *C. elegans* or Drosophila (Taylor and Peculis, 2008). Interestingly, studies in mammalian cells demonstrated that Nudt16 is a cytoplasmic protein capable of regulating the stability of a subset of mRNAs, acting as a second cytoplasmic mRNA decapping enzyme (Song et al., 2010).

Characterisation of Nudt16 has been less extensive than Dcp2. However, studies in mammalian cells have revealed that both proteins were used differentially in specified mRNA decay processes; Dcp2 was preferred in NMD rather than Nudt16 while Dcp2 and Nudt16 are used differentially for specific groups of transcripts with 3' ARE elements, which regulate transcript stability (Li et al., 2011).

1.2.3. Decapping activators

Decapping is enhanced by a group of proteins known as mRNA decapping activators (Coller and Parker, 2004). In *S. cerevisiae*, proteins such as Pab1p, Lsm1–7p, Pat1p, Dhh1p and others (Coller and Parker, 2004; Nissan et al., 2010). Additionally, several factors which enhance decapping (e.g. Edc1, Edc2, and Edc3) have been identified (Fenger-Gron et al., 2005; Franks and Lykke-Andersen, 2008). Most of these components are well conserved across eukaryotes.

The decapping activators have different functions in addition to promoting decapping. Dhh1, a DEAD-box RNA helicase was identified as a general inhibitor of translation (Coller and Parker, 2004; Sweet et al., 2012). Like Pat1, it blocks the formation of the 48S pre-initiation

complex (Coller and Parker, 2004; Franks and Lykke-Andersen, 2008; Nissan et al., 2010). Dhh1 has well-characterised orthologues in different organism such as Rck/p54 (humans), Me31D (*D. melanogaster*), CGH-1 (*C. elegans*) and Xp54 (*X. laevis*) (Franks and Lykke-Andersen, 2008). Dhh1 has also been shown to represses translation *in vivo* and associates with the mRNA on the polysome fractions (Sweet et al., 2012). Another important protein complex in decapping is the Lsm1-7 complex, which associates with the 3′ end of oligoadenylated mRNAs *in vivo* (Tharun et al., 2000). This complex consist of seven Sm-like proteins and protects the last 20–30 nucleotides of the message (He and Parker, 2001). Additionally, the Lsm1-7 complex forms a larger complex with Pat1 which protects the deadenylated 3'-end of mRNA from the exosome degradation; thus promoting the decapping pathway (Nissan et al., 2010; Parker, 2012). Pat1 is a multifunctional protein which binds to various proteins such as the Dcp1-Dcp2 complex (Nissan et al., 2010), Dhh1 (Nissan et al., 2010; Sharif, 2014), Xrn1, in yeast (Nissan et al., 2010) and the Ccr-Not4 complex in *Drosophila* (Haas et al., 2010). Interactions between Pat1 and Dcp1-Dcp2 complex activates the catalytic activity of Dcp2 (Nissan et al., 2010). Structural studies of Pat1-Lsm1-7 complex from yeast revealed that the heptameric ring, formed by the Lsm proteins, interacts with the C-terminal domain of Pat1 via Lsm2 and Lsm3, and not the cytoplasm specific component, Lsm1 (Sharif and Conti, 2013).

Three enhancers of decapping (Edc) proteins have been described. Two of them (Edc1 and Edc2) are specific to yeast (Schwartz et al., 2003) whereas Edc3 is highly conserved in eukaryotes (Fenger-Gron et al., 2005; Franks and Lykke-Andersen, 2008). Edc1 and Edc2 act by binding to the mRNA substrate and enhancing the activity of the decapping enzyme (Schwartz et al., 2003) while Edc3 interacts directly with multiple decapping factors, including Dcp2 and Dcp1 and thus activates the decapping complex on the target mRNAs (Decker et al., 2007; Franks and Lykke-Andersen, 2008). Like Dhh1, another decapping activator, Scd6, also

represses translation *in vitro* by limiting the formation of a stable 48S pre-initiation complex (Nissan et al., 2010). Scd6 is an RNA-binding protein and shares a number of structural features with Edc3 (Fromm et al., 2012). In yeast, Scd6 interact directly with Dcp2 (Nissan et al., 2010), however, it did not modify the catalytic activity of the Dcp1:Dcp2 decapping complex *in vitro* (Fromm et al., 2012).

Table 1.1. Decapping and 5' – 3' exonuclease factors

Factor	Functions
Dcp2	Catalytic subunit: Nudix family member mRNA decapping enzyme Releases m^7GDP and 5'p-RNA
Dcp1	Stimulatory subunit: EVH1 family member Blocked by eIF4E bound to cap
Xrn1	Major cytoplasmic 5' – 3' exonuclease Requires 5' monophosphate
Pat1	Activates general mRNA decapping Serves as scaffolding protein for decapping complexes Interacts with Lsm1-7 complex Promotes P-bodies assembly
Lsm1-7 complex	Required for efficient decapping Forms heptometric ring complex and binds oligo- or adenylated mRNAs
Dhh1	Required for efficient decapping of translating mRNAs Member of DEAD-box RNA helicase family
Edc1/Edc2	Two small RNA-binding proteins Directly bind and stimulate Dcp1/Dcp2
Edc3	RNA binding protein Binds directly and stimulates Dcp2 Served as scaffold for decapping factors
Scd6	RNA-binding protein related to Edc3 Represses translation by binding to eIF4G

Adapted from (Parker, 2012).

1.3. Nonsense-Mediated Decay (NMD)

The process of translation involves four steps; initiation, elongation, termination and ribosome recycling (Nurenberg and Tampe, 2013). Nonsense-mediated decay (NMD) serves as an mRNA-surveillance mechanism. It is translation-dependent and promotes the rapid degradation of mRNAs undergoing premature translational termination (Kervestin and Jacobson, 2012; Peccarelli and Kebaara, 2014). There are several mechanisms by which transcripts with a premature termination codon (PTC) can be produced; genes harbouring nonsense or frameshift mutations, alternative splicing events or splicing defects, bicistronic mRNAs, transcripts of pseudogenes, gene insertions, including transposable elements, and genes that are subject to programmed rearrangements (He et al., 2003; Kervestin and Jacobson, 2012; Thompson and Parker, 2007). The truncated proteins produced by the presence of a PTC could potentially have toxic effects on the cell and this mechanism protects the organism by limiting their expression (Brogna and Wen, 2009). Unlike premature termination, generally, translational termination does not lead rapid transcript degradation, allowing for repeated rounds of translation (Durand and Lykke-Andersen, 2013).

There are three main NMD factors which are evolutionary conserved across eukaryotes, known as UP-Frameshift protein 1; Upf1, Upf2 and Upf3 (Brogna and Wen, 2009; Conti and Izaurralde, 2005; Kervestin and Jacobson, 2012; Peccarelli and Kebaara, 2014). Upf1 is a group 1 RNA helicase with ATPase activity (He et al., 2013). Studies have shown that Upf1 is recruited to the PTC in an inactive form, being activated by Upf2, which acts as a bridge for Upf1 and Upf3 (Chamieh et al., 2008). Deletion of genes encoding Upf1 and Upf2 stabilises PTC-containing RNAs in *S. cerevisiae* (Leeds et al., 1991), *C. elegans* (Page et al., 1999), *Drosophila* (Gatfield and Izaurralde, 2004) and humans (Lykke-Andersen et al., 2000). In *C. elegans*, the Upf proteins are known as SMG proteins (Conti and Izaurralde, 2005; Kervestin and Jacobson, 2012). Besides acting as a key player in NMD, Upf1 has various functions such

as modulating telomerase function and controlling the telomere length (Isken and Maquat, 2008), it is involved in non-NMD RNA degradation such as staufen1 (STAU1)-mediated mRNA decay (SMD) (Park and Maquat, 2013) and replication–dependent histone mRNA decay (Mullen and Marzluff, 2008b).

1.3.1. NMD in yeast and *C. elegans*

Translational termination involves several proteins including the eukaryotic release factors (eRF1 and eRF3), eukaryotic initiation factor 4G (eIF4G) and the cytoplasmic poly-A binding protein (PABPC) (Kervestin and Jacobson, 2012; Sonenberg and Dever, 2003). Normal translational termination occurs when the ribosome reaches the stop codon which is located in close proximity to both the 3' poly(A) tail and the 5′ 7-methylguanosine (m^7G) cap of the mRNA which associate via protein-protein interactions. The ribosome recruits eRF1-eRF3 and this interaction is promoted by PABPC and eIF4G, which is bound to the 5'cap binding complex. Thus the circularised mRNA promotes efficient translation termination and ribosome recycling (Lykke-Andersen and Jensen, 2015). However, NMD occurs when eRF3 fails to interact with PABPC, leading to recruitment and activation of the Upf complex. This process is known as the faux-UTR (false-UTR) (Amrani et al., 2004; Brogna and Wen, 2009; Kervestin and Jacobson, 2012) (Figure 1.3(a)).

1.3.2. NMD in mammalian cells

The activation of NMD in mammalian systems involved a group of proteins known as the exon junction complex (EJC). It consists of at least the core proteins Y14, MAGOH, barentsz (BTZ) and eIF4AIII, and one effector of nonsense-mediated decay (NMD), Upf3 (Lykke-Andersen et al., 2001; Lykke-Andersen and Jensen, 2015). During splicing, Upf3 binds to the core complex of Y14, MAGOH, BTZ and eIF4AIII, Upf2 joining the complex in the cytoplasm (Kervestin

and Jacobson, 2012). This complex remains associated with the mRNA until it is displaced by the first round of translation. Another complex, consisting of Upf1, eRF1-eRF3, SMG1, SMG8 and SMG9, known as SURF (SMG1–UPF1–release factor) is formed and recruited to ribosomes stalled at a PTC (Brogna and Wen, 2009; Kervestin and Jacobson, 2012; Yamashita et al., 2009). If the PTC is upstream from an intron splice site Upf1 binds to Upf2; this leads to the formation of the DECID (decay inducing) complex, UPF1 phosphorylation and activation of its ATPase activity (Kervestin and Jacobson, 2012). Upf1 phosphorylation promotes its interaction with SMG6, an endonuclease that can cleave the mRNA, and with the SMG5–SMG7 complex, which promotes mRNA deadenylation and decapping (Eberle et al., 2009; Isken and Maquat, 2008; Kashima et al., 2006; Kervestin and Jacobson, 2012) (Figure 1.3 (b)).

a)

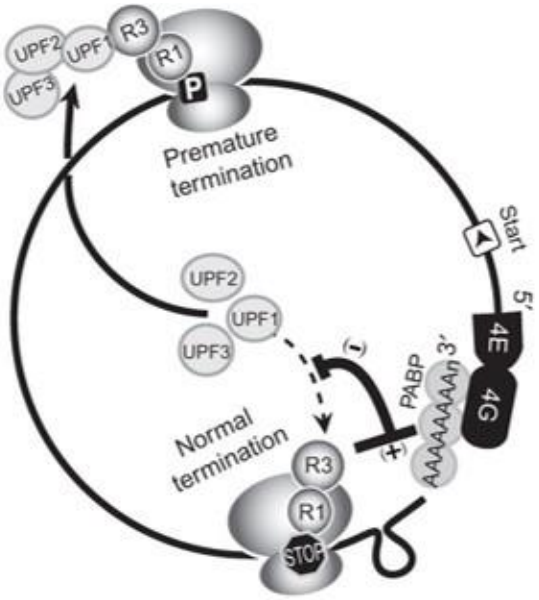

b)

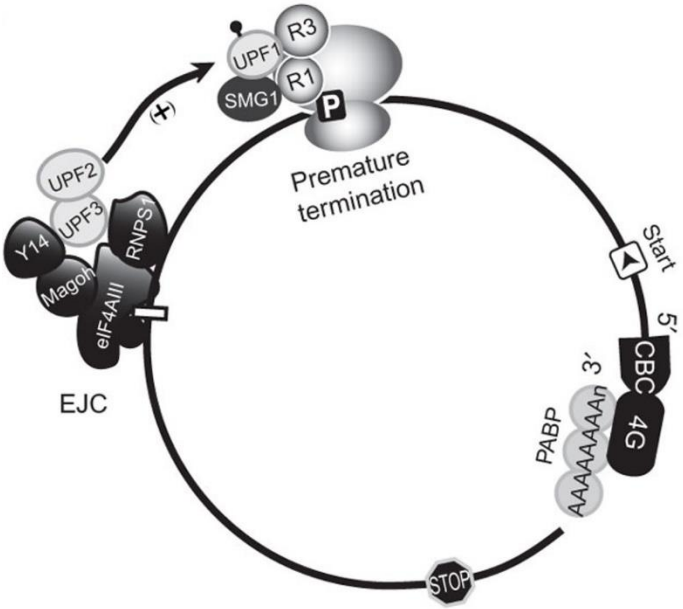

Figure 1.3. Model of NMD in different organisms. a) The faux-UTR model in yeast and *C. elegans*. Premature termination activates the interaction between Upf proteins with the eRF1-eRF3 complex, which will interacts with PABP, thus leads to the NMD.
b) The exon-junction complex model (EJC) in mammalian cells. The interaction of EJC complex and SURF complex with the help of Upf proteins; which leads the binding of SMG6, an endonuclease that cleaves the mRNA. This interaction leads the mRNA deadenylation and decapping. Taken from (Brogna and Wen, 2009; Kervestin and Jacobson, 2012).

1.4. RNA degradation in *A. nidulans*

Analysis of RNA degradation in *A. nidulans* was initially focused on *areA*, which encodes a transcription factor responsible for the global regulator of nitrogen metabolism (Morozov et al., 2001). Modulation of the transcription factors activity in response to the quality and quantity of available nitrogen was localised three important regions of *areA* (Platt et al., 1996). Two of these regions located within the coding region and one within the 3′-UTR of the *areA* transcript. This highly conserved RNA sequence and has been shown to be essential and sufficient for regulated degradation of the mRNA (Morozov et al., 2000; Platt et al., 1996). The regulated degradation of the *areA* is determined by the level of glutamine in the cell and it was also shown that a wide range of other genes involved in nitrogen metabolism was regulated at the level of RNA stability (Morozov et al., 2001).

Investigating the underlying mechanism of regulated transcript stability determined that mRNA decay is generally initiated by the shortening of the poly(A) tail and rapidly degraded primarily via the decapping-dependent pathway as had been found in other systems (Coller and Parker, 2004; Morozov et al., 2010a; Mullen and Marzluff, 2008a). The Ccr4-Caf1-Not complex, and not Pan2-Pan3, was shown to be the deadenylase activity responsible and studies have shown that both *A. nidulans* Caf1 and Ccr4 are functionally distinct deadenylases *in vivo*. Caf1 is required for the regulated degradation of specific transcripts, whereas Ccr4 is responsible for basal degradation (Morozov et al., 2010a). Regulated degradation of specific transcripts in response to glutamine correlates with their deadenylation rate (Caddick et al., 2006; Morozov et al., 2000) and this correlation is lost in strains deleted for *caf1* (Morozov et al., 2010a). Importantly, the rate of deadenylation in *A. nidulans* is highly variable between transcripts and can be regulated (Morozov et al., 2012). One key RNA binding protein involved in glutamine signaled RNA degradation was identified as RrmA (Krol et al., 2013). This has a RNA recognition motif and was identified as a protein that can bind specifically the 3’ UTR

of *areA*. In addition to its role in glutamine signaling RrmA it has a wide domain of activity including roles in amino acid biosynthesis and the oxidative stress response.

Work to characterise poly(A) tail length determined that deadenylation to a threshold length of ~A_{15} triggers decapping and rapid degradation of the mRNA in *A. nidulans*, which is consistent with other organisms (Parker, 2012). This work also showed that at this threshold length of A_{15} non-templated pyrimidine (C and U) nucleotides were added to the transcript 3' end (3'-tagging) by the ribonucleotidyltransferase, CutA, and CutB (Morozov et al., 2012). CutA was originally identified as the putative cytoplasmic activity whereas CutB was predicted to be nuclear with a proposed role as the polyA polymerase associated with the TRAMP complex. Disruption of *cutA* and/or *cutB* retard transcripts degradation (Morozov et al., 2012). Disruption Edc3, an enhancer of decapping, or CutA reduced the numbers of P-bodies formed in *A. nidulans.* The coincidence of 3' tagging with decapping, its requirement for normal rates of RNA degradation and CutA's involvement in P-body formation are all consistent with 3' tagging having a role in promoting RNA degradation (Morozov et al., 2010b). Work in a wide range of organisms, including *Schizosaccharomyces pombe, Arabidopsis thaliana* and humans all supports the notion that 3' tagging plays an important role in mRNA function and one key aspect is the promotion of its decapping and degradation (Morozov et al., 2012; Mullen and Marzluff, 2008a; Rissland and Norbury, 2009).

1.5. NMD in *A. nidulans*

The first studies of NMD in *A. nidulans* lead to the characterisation of *nmdA* (an orthologue of *upf2*) (Morozov et al., 2006). Strains bearing the mutant allele, *nmdA1,* increased the stability of several PTC-containing transcripts: *hxA* (encoding xanthine dehydrogenase), *uaZ* (encoding urate oxidase), *pacC* (encoding the transcription factor mediating regulation of gene expression by ambient pH), and *palB* (encoding a protease involved in pH signal transduction). Additionally, *nmdA1* stabilised pre-mRNA (unspliced) transcripts. Subsequent work identified

another key NMD factor, Upf1 and demonstrated that this was also required for NMD (Morozov et al., 2012). Intriguingly unpublished data has shown that NMD in *A. nidulans* is not dependent on the decapping protein Dcp2 (Morozov and Caddick, personal communication) unlike the situation in *S. cerevisiae*. Analysis of both *uaZ*$^{+}$ and the NMD substrate *uaZ14* revealed that both transcripts were subject to decapping in the respective Δ*dcp2* strains (Figure 1.4). These data suggest that an alternative decapping activity is present in *A. nidulans.*

The role of 3' tagging was investigated within the context of NMD and it was shown that NMD induces a high frequency of 3' tagging (Morozov et al., 2012). Interestingly this RNA tagging was not associated specifically with short poly(A) tails, as had been previously observed for wild-type transcripts. However, disruption of *cutA* and/or *cutB* did not suppress NMD although decapping of NMD substrates correlated with deadenylation. This supports the hypothesis that deadenylation-independent decapping is promoted by 3' tagging and perhaps there is additional RNA degradation mechanism involved in effecting this surveillance mechanism in *A. nidulans* (Morozov et al., 2012). An intriguing observation was that in strains disrupted for 3' tagging NMD substrates were greatly enriched within the polysome fraction, though the basis of this was not determined. It was also observed that disruption of Upf1 and NmdA/Upf2 led to reduced levels of 3' tagging of transcripts not subject to NMD. This implicated the NMD components in activating deadenylation-dependent 3' tagging. In mammalian system, Upf1 plays a direct role in the 3' tagging and degradation of human histone mRNAs in response to repression of DNA synthesis (Mullen and Marzluff, 2008a). Recent unpublished data has shown that in *A. nidulans* histone mRNAs are also subject to 3' tagging in response to blocking DNA synthesis. This correlates with mRNA degradation and is Upf1 dependent (Morozov and Caddick, personal communication).

A key role of mRNA 3' tagging is to recruit the Lsm1-7 complex which is known to promote decapping (Hoefig et al., 2013; Mullen and Marzluff, 2008a). This role is consistent with involvement in deadenylation-dependent degradation, NMD, and regulated transcript degradation. The involvement of the Upf1 in promoting 3' tagging outside the context of NMD is intriguing. A model linking deadenylation-dependent decapping with NMD, which integrates the role of Upf1 has been proposed (Morozov et al., 2012). This suggests that the deadenylated transcripts mirror NMD in that the absence of poly(A) binding protein in close proximity to the terminating ribosome leads to Upf1 recruitment which in turn promotes 3' tagging. In the case of histone mRNA 3' tagging, Upf1 is known to activate the tagging. In all cases, it is, therefore, likely that the Lsm1-7 complex will be recruited and we would, therefore, predict that Lsm proteins would play a direct role in all three degradation pathways, including NMD.

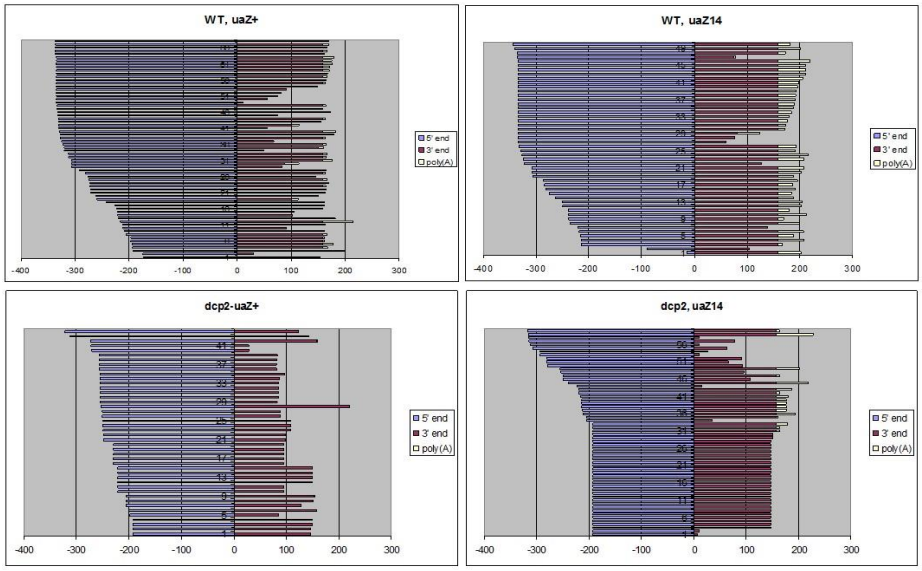

Figure 1.4. cRT-PCR analysis of natively decapped *uaZ*$^{+}$ and *uaZ14* in WT and Δ*dcp2* strains. Total RNA was extracted from WT, *uaZ14*, Δ*dcp2* and Δ*dcp2 uaZ14* strains and subject to cRT-PCR as described by Morozov et al., (2010). The products were cloned and sequenced to determine the position of the 5' and 3' ends of a random sample of transcripts. The results are displayed indicating the length of the 5' (blue line) and 3' (red line) and poly(A) tail (yellow line). As can be seen decapped and 5' degraded transcripts were identified in all strains, indicating that decapping is not dependent on Dcp2 in *A. nidulans*. (Morozov and Caddick, unpublished data).

1.6. Project aims

Decapping is the critical step in the 5'-3' mRNA decay pathway and its regulation is, therefore, critical in determining mRNA stability and gene expression. Previous studies have shown that 3' tagging by CutA and CutB promotes decapping of transcripts, although it has a less well-defined role in NMD. In this study, we undertook to characterise the role of known factors involved decapping (i.e Dcp1, Dcp2, Lsm1, Xrn1, Dhh1, Pat1) and investigate their contribution to NMD. Additionally, we aimed to identify other proteins that may account for the residual decapping activity observed in Δ*dcp2* strains. The links between 3' tagging, decapping, NMD, and translation are a primary focus.

This work was undertaken in *A. nidulans* as a model eukaryote which is amenable to molecular and genetic analysis, with a well-annotated genome. Importantly it has proved to be a good model system for the study of RNA degradation mechanism and appear more typical than the major model, *S. cerevisiae*, particularly with respect to 3' tagging of mRNA.

CHAPTER 2: MATERIALS AND METHODS

2.1 Buffers and solutions for general molecular biology

APPENDIX 1a

2.2 *Aspergillus nidulans* strains, oligonucleotides and maintenance

2.2.1 Oligonucleotides.

All synthetic oligonucleotides used in this project were syntheses by Sigma. These are listed in Table 2.1**.**

Table 2.1. Primer sequences used in mutant validation

Oligonucleotide	primer sequence (5' – 3')
Int_pyrG forward	ACATCCTCACCGATTTCAGC
Int_pyrG reverse	TCCCAGCCTTCTTTCTGGTA
Int_dcp1 forward	CGATCAACAGAATCGAAGCA
Int_dcp1 reverse	AAGACCCAAAGCCCGTAAAT
DCP1_Fwd.3'	GCCTGGTGGTAGTGCATCTT
Dcp1_rev.5'	GCTTCGGCAATCTCAAAAAG
Int_dcp2 forward	AGTGGAACTGTCGGCTCATC
Int_dcp2 reverse	AGGATCGTGATTGGTGAAGC
Dcp2.Int.F1	CTACACAGGCCCGTTCAACT
Dcp2.new.R4	ATCACCGGGAACAACAAGAC
Dcp2.Gib.3pF	GTGCCTCCTCTCAGACAGGCTGAGCTGCATAT GTCTGTG
Dcp2.Gib.CT.R	GCCTGCACCAGCTCCTTTGCTCCCTTTAGC GACTCC
Dcp2.Int.F2	CCGTTCAACTCATCTCACCA
Dcp2.New.R3	TTTGCTCCCTTTAGCGACTCC
Int_xrn1 forward	GTACGAATTCGAGCGTGTGA
Int_xrn1 reverse	GCACACCAAGTCGCTGTAAA
Int_scd6 forward	ATTTCCGTTGCCTTCCTTCT
Int_scd6 reverse	CTTGAGGTGGTTGTTGCAGA
Int_pat1 forward	CATCCCTTTATTGCGTTGCT
Int_pat1 reverse	GCGTATGGGTAAGCACCAAGT
Int_dhh11 forward	TGATGCAAATCCAGATCCAA
Int_dhh1 reverse	GTTTTGCCTGTGCCATTCTT
Int_lsm1 forward	ACGAGATGGGAGAAAGCTGA
Int_lsm1 reverse	GCCGAGCTCTTGTAGCTTGT
Int_lsm5 forward	AGTCTCGCATTGGAATCGTC
Int_lsm5 reverse	AGGAGGATTTTTGGCAGCTT
UP1TAG F	GGAGCTGGTGCAGGCGCTGGAG

UP2 pyrG R	CTGTCTGAGAGGAGGCACTGAT
Int_nkuA forward	CGCCCAACGACCCTGACG
Int_nkuA reverse	TCCCCGCCGAATTTGTATGC
cutBF3.pyrg	GTGCCTCCTCTCAGACAGATTTTGCACGGGTAT GGAAATTTCTGC
cutB.CT Rev.Tag	GCCTGCACCAGCTCCGCTGACCGCGATGAGCCC
CutA.intF2.miniT	CAACCAAAGCGAGAACAAAACTTGCCCAACAGA ACCTTG
cutA.CT.R2	TGGAAAAGGACTTCGAGGCCCCCTTTC CTCAAAGAC
Tag.F.cutA	GAAAGGGGGCCTCGAAGTCCTTTTCCAGGGTC CTGGAGCTGGTGCAGGCGCT
PyrG.Rev.cutA	CAAATAAGGCCTGTCTGAGAGGAGGCACTGATGC
cutA.F3.pyrG	TCTCAGACAGGCCTTATTTGGCCCTCTTTTTATG
Int_ndxA forward	ACGGGGGTACATGTCGATAA
Int_ndxA reverse	CTGAAAACCGCATCTCTGCT
ndxA F1	TGACAGGGTACCAATGCAAA
ndxA R1	TCTTGATGACGGCGATGTAG
ndxA For	TCCTATAGGCCCTAGCCACA
ndxA Rev	CGTCGCTGACCTGATAAAGG
ndxA CT Gib R	GCCTGCACCAGCTCCGTTCAAAACAGGC TGAAAACC
ndxA Gib F3	GTGCCTCCTCTCAGACAGCACCCGCTACGA TGTTACCT
ndxA.R4	GCTACTGTTCTTTCTTGAAGTCAAAT
Int_ndxB forward	AACGAAGCAAAGTGGACGAG
Int_ndxB reverse	GCTTGGGATTTTGGTTTTCA
ndxB F1	TCGGAGAAGCGTTTATGTCC
ndxB R1	GCTTCGGCAATCTCAAAAAG
ndxB F	CGTTGTCTTGAACCCTCCAA
ndxB R	GATTTCCAGCATTCCGTGTT
ndxB Gib F3	GTGCCTCCTCTCAGACAGAGATTGTCCATTTCGCCACT
ndxB CT Gib Rev	GCCTGCACCAGCTCCGAGCTTCAGTTTCTTCGCCA
ndxB.R4	TGGACTGGGATCCTTCTCTG
Int_ndxD forward	AGTTGGCTTTATCCGCCTTT
Int_ndxD reverse	GGTTGTCGTCACATCAGCAG
ndxD F1	GCGTCGTCCCATTATCAAAA
ndxD R1	GAACTTCGGTTTAACGCCTCT
ndxD For	CCGCCTTACTATCCCTCTCC
ndxD Rev	CCATGCTGGTAACGAGGCT
ndxD CT Gib Rev	GCCTGCACCAGCTCCTCTCTTCATGGAACTTCGGTTT
ndxD Gib F3	GTGCCTCCTCTCAGACAGTCTTCAAGCTAGG GCTGGAC
ndxD R4	TTCGGTTTAAAATCCATGCTG
GFP_diag forward	CTACCTGTTCCATGGCCAAC
GFP_diag reverse	GATGTTTCCGTCCTCCTTGA
18S forward	GGAAACTCACCAGGTCCAGA
18S reverse	GCTATTTAAGGGCCGAGGTC
uaZ forward	TCAAGACATTTGCCGAGGAG
uaZ reverse	CTTGTGCCAGCTCAGATCAA

actA.qPCR.fwd	CCTTCTCCACTACCGCTGAG
actA.qPCR.rev	ACCTGACCATCAGGCAGTTC
des.qpcr.fwd	ACCATCGTCTATGGGCTCAC
des.qpcr.rev	ACGCTTAGGGTTCTGCTTCA
28S_Nort_3end_Fwd	TCGATGTCGGCTCTTCCTAT
28S_Nort_3end_Rev	CAGCCGCAAAAACCAATTAT
28S_Int2_3end_Rev	GCGCTTGGTTGAATTTCTTC
28S_Nort_5end_Fwd	GGTAGGGATACCCGCTGAAC
28S_Nort_5end_Rev	ACGGGATTCTCACCCTCTCT
Int.28S.4seq.Fwd	GCCAATCCTTATCCCGAAGT
Int.28S.4seq.Rev	CACGCCAGGTCGTACTCATA
5' RNA adapter	UUUGGAUUUGCUGGUGCAGUACAACUAG GCUUAAUACUCGAGUCCGACG
5' Primer PCR	GATTTGCTGGTGCAGTACAACTAGGC
5'-PCR_2	TGGTGCAGTACAACTAGGCTTAATA
Splint_8N	TGAGCTCAGGCTGCNNNNNNNN
Splint_6N	TGAGCTCAGGCTGCNNNNNN
Splint_4N	TGAGCTCAGGCTGCNNNN
uaZ.decapped.rev	ACAAAGGAGTGTGAGTGTGGTTT
uaZ.int.fwd	AGCTGCCCGCTATGGTAAG
uaZ.int.rev	GTGCGTGATGATGTTGGTATG
gdhA.decapped.rev	GTACAGAAGCGACGAATTTCAGAGT
gdhA.int.fwd	GAGCCCGAGTTCGAGCAG
gdhA.int.rev	CCACCACCCATGTTTAGTCC
hxA.decapped.rev	GTAATAACGTGTTTCCCATCGAC
hxA.int.fwd	TATTACAACCGTCGCAATCG
hxA.int.rev	GGCATGGTAAAGCTTCTTGG

Table 2.2. *Aspergillus nidulans* strains used in this study.

Genotype	Stock Number	Source
Wild Type (WT): *veA*$^{+}$	1048	This laboratory
yA$_{2}$ *hxA5 pantoB*$_{100}$	294	This laboratory
uaZ14 pantoB$_{100}$	230	This laboratory
Δ*dcp1 hxA5 yA*$_{2}$ *pyroA*$_{4}$ *pantoB*$_{100}$ Δ*nkuA:argB*	999	This work
Δ*dcp1 uaZ14 pyroA*$_{4}$ *pantoB*$_{100}$ Δ*nkuA:argB*	972	This work
Δ*dcp1 hxA5 yA*$_{2}$ Δ*nkuA:argB*	1190	This work
Δ*dcp1 uaZ14 pantoB*$_{100}$ Δ*nkuA:argB*	1191	This work
Δ*dcp1 yA*$_{2}$ *pantoB*$_{100}$ Δ*nkuA:argB*	1194	This work
Δ*dcp1 pantoB*$_{100}$ Δ*nkuA:argB*	1193	This work
Δ*dcp2 hxA5 yA*$_{2}$ *pyroA*$_{4}$ *pantoB*$_{100}$ Δ*nkuA:argB*	740	This laboratory
Δ*dcp2 uaZ14 pantoB*$_{100}$	947	This laboratory
Δ*dcp1* Δ*dcp2 uaZ*$^{+}$ Δ*nkuA:argB*	1125	This work
Δ*dcp1* Δ*dcp2 uaZ14* Δ*nkuA:argB*	1126	This work
Δ*xrn1 hxA5 yA*$_{2}$ *pyroA*$_{4}$ *pantoB*$_{100}$	1000	This work
Δ*xrn1 uaZ14 pyroA*$_{4}$ *pantoB*$_{100}$ Δ*nkuA:argB*	973	This work

Δdhh1 hxA5 yA$_2$ pantoB$_{100}$	970	This work
Δdhh1 uaZ14 pyroA$_4$ ΔnkuA:argB	916	This laboratory
Δlsm1 hxA5 yA$_2$ pantoB$_{100}$	971	This work
Δlsm1 uaZ14 pyroA$_4$ pantoB$_{100}$ ΔnkuA:argB	910	This laboratory
Δpat1 hxA5 yA$_2$ ΔnkuA:argB	1078	This work
Δpat1 uaZ14 pyroA$_4$	948	This laboratory
ΔndxA pantoB$_{100}$	1136	This work
ΔndxA uaZ14	1137	This work
ΔndxB pantoB$_{100}$	1127	This work
ΔndxB uaZ14 pyroA$_4$ pantoB$_{100}$	1128	This work
ΔndxD pantoB$_{100}$	1125	This work
ΔndxD uaZ14	1131	This work
ΔndxA Δdcp2	1140	This work
ΔndxA Δdcp2 uaZ14 pyroA$_4$	1139	This work
ΔndxB Δdcp2 pyroA$_4$ pantoB$_{100}$ ΔnkuA:argB	1134	This work
ΔndxB Δdcp2 uaZ14 pyroA$_4$ ΔnkuA:argB	1129	This work
ΔndxD Δdcp2 pantoB$_{100}$ ΔnkuA:argB	1132	This work
ΔndxD Δdcp2 uaZ14	1130	This work
Δdcp2 Δxrn1 uaZ14	982	This laboratory
ΔndxA Δxrn1 uaZ14	1253	This work
ΔndxB Δxrn1 uaZ14	1282	This work
ΔndxD Δxrn1 uaZ14	1256	This work
Δdcp1 dcp2^{E148Q} (pyrG$_{89}$) pyroA$_4$ pantoB$_{100}$	1293	This work
dcp2^{E148Q} (pyrG$_{89}$) pyroA$_4$	1294	This work
ndxA:GFP:AfpyrG pabaB$_{22}$ riboB$_2$ ΔnkuA (pyrG$_{89}$) :argB	1203	This work
ndxD:GFP:AfpyrG pabaB$_{22}$ riboB$_2$ΔnkuA (pyrG$_{89}$) :argB	1204	This work
ndxB:RFP:AfriboB pyrG$_{89}$ pabaB$_{22}$ ΔnkuA (riboB$_2$) :argB	1205	This work
ndxD:RFP:AfriboB pyrG$_{89}$ pabaB$_{22}$ ΔnkuA (riboB$_2$) :argB	1206	This work
dcp2:GFP:AfpyrG pyroA$_4$ (pyrG$_{89}$)	1239	This work
dcp1:GFP:AfpyrG pyroA$_4$ (pyrG$_{89}$)	541	This laboratory
cutA:GFP:AfpyrG pyroA$_4$	1241	This work
ndxA:RFP:AfriboB dcp1:GFP pyroA$_4$ pyrG$_{89}$ pabaB$_{22}$ ΔnkuA (riboB$_2$) :argB	1291	This work
ndxB:RFP;AfriboB dcp1:GFP pyroA$_4$ pyrG$_{89}$ pabaB$_{22}$ ΔnkuA (riboB$_2$) :argB	1277	This work
ndxD:RFP:AfriboB dcp1:GFP pyroA$_4$ pyrG$_{89}$ pabaB$_{22}$ ΔnkuA (riboB$_2$) :argB	1278	This work
cutA:GFP cutB:RFP pyrG$_{89}$ pabaB$_{22}$ ΔnkuA	1259	This work
ΔcutB cutA:GFP:AfpyrG pyroA$_4$ ΔnkuA:argB	1261	This work
ΔcutA cutB:GFP:AfpyrG ΔnkuA:argB	1262	This work
dcp2:RFP:AfriboB dcp1:GFP pyroA$_4$ pyrG$_{89}$ pabaB$_{22}$ ΔnkuA (riboB$_2$) :argB	1287	This work

---

2.3. *Aspergillus nidulans* solution and media

APPENDIX 1b

2.4. Maintenance and growth of *A. nidulans* strains

A. nidulans stock cultures were kept as conidiated mycelia using premade glycerol stocks from the Protect Microorganism Preservation System (Technical Service Consultant Ltd) at -80˚C. For the preparation of conidial suspensions to inoculate liquid cultures, strains were grown on minimal media (MM) (Appendix 1b) containing 3% agar (w/v) with appropriate supplements for 3-4 days at 37˚C. Conidial were scrapped from the plates and resuspended in 10 ml 0.01% Tween, and grown into 200 ml MM in 1 litre flask. Liquid cultures were incubated at 30˚C in an orbital incubator at 200 rpm for 16 hours. Mycelia were harvested by filtration through Miracloth (Calbiochem Corp.), washed with cold water and dried by blotting with paper towel.

2.5. *Aspergillus nidulans* genetic techniques.

2.5.1. Crosses

For sexual crosses the procedure is as described by (Todd et al., 2007). The parental strains, with complimentary auxotrophic and preferably colour markers, were inoculated alternately on a fully supplemented agar plate. After 3 days of incubation at 37˚C, the junction of growth between the two parental strains was transferred to unsupplemented MM agar plate with NO_3^- as nitrogen source. The plate were very thick (~50 ml/ dish), and the mycelia were inoculated under the surface of the agar. The plates were incubated for 14 days or more at 37^o C. Mature cleistothecia were picked and rolled on a 1% MM plate to clean it from other debris. The cleistothecia were then individually squashed in a vial containing 2 ml of sterile water and vortex vigorously. A loop full of ascospore suspension was then inoculated onto complete medium (CM) (Appendix 1b) and incubated at 37˚C for 2 days. Ascospore suspensions that appeared to have the re-assortment of markers were plated out in dilution series onto fully supplemented MM. After 3 days, 23 progenies were randomly picked and inoculated onto a

master plate, which also containing both parental strains and a WT control. The master plates were incubated at 37˚C for 3 days before replica plating onto test media.

2.6. Plate tests

The progeny were grown on different supplements to check the growth requirements. Plates were scored after 2 days of incubation at 37˚C.

Table 2.3 Plate test to check the growth requirements of progenies

Allele	Function disrupted	Phenotypic characterisation
hxA5	(purine hydroxylase 1)	inability to use hypoxhantine as sole nitrogen source (Glatigny and Scazzocchio, 1995) (Morozov et al., 2006)
uaZ14	(urate oxidase)	inability to grow on uric acid as sole nitrogen source (Morozov et al., 2006)

2.7. Generating *A. nidulans* mutants

The protocol for transformation in this study was based on the method developed by Dr Joan Tilburn (Tilburn et al., 1983), and modification made by Dr Berl R.Oakley ((Szewczyk et al., 2007). All the glassware used in this method was acid washed to remove any detergent traces which could rupture the protoplasts (Magdalena Mos 2010).

2.7.1. Generating protoplasts of *A. nidulans*

10^8 of fresh conidia were inoculated into 25 ml fully supplemented CM and grown overnight at 30° C with agitation at 200 rpm. After 14 h growth, the culture was harvested using a sterile funnel lined with miracloth (Calbiochem). The cells were transferred to a new falcon tube containing 8 ml of CM, 8 ml of 2 x protoplasting solution (1.1 M KCl, 0.1 M citric acid pH 5.8, and 2 g of VinoTaste Pro lysing enzyme (Novozymes). The cells were incubated with gentle shaking at 30 °C for 2 hours. Then the protoplasts were filtered through a sterile sintered glass funnel containing glass wool and washed with an equal volume of protoplast

wash solution (1 M sorbitol, 10 mM Tris-Cl, pH 7.5). The mixture was centrifuge at 3,100 *g* (Megafuge 1.0R, Heraeus) for 12 minutes at 4 °C. The supernatant was discarded and the pellet re-suspended with 1 ml protoplast wash solution and transferred to a 1.5ml tube. The mixture was centrifuge at 6,500 *g* for 2 minutes and the washing step was repeated for another 2 times. The pellet was re-suspended in 500 µl transformation solution (1M sorbitol, 10mM CaCl, 10mM Tris-Cl, pH 7.5). Protoplasts were counted and diluted to 1 x 10^8 for transformation.

2.7.2. Transformation of *A. nidulans* strain

Up to 50 µl DNA was added to 150 µl protoplasts and the mixture was transferred to a plastic universal containing 50 µl PEG solution (60 % Polyethylene glycol 6000 10 mM CaCl, 20 mM Tris-Cl, pH 7.5 and incubated on ice for 20 minutes. 1 ml PEG solution was added and the mixture was incubated at room temperature for 5 minutes. Then, 5 ml transformation solution was added and the mixture was incubated on ice. Then, 15 ml of regeneration media (minimal media (1% glucose, 2% salt solution v/v pH 6.6 (Appendix 1b)) with 1 M sucrose, 1% glucose) were added into the mixture and layered on top of regeneration media plates. Plates were incubated at 30 °C overnight and transferred to 37 °C for another 2 to days until transformants had appeared.

2.8. *Escherichia coli* strains, growth, maintenance and manipulation

The *E. coli* strain used in this project was DH5-alpha™ (DH5α) (Thermo).

2.8.1. *Escherichia coli* growth and maintenance

E. coli was grown on Luria-Bertani (LB) agar, or in LB liquid media in orbital incubator (200rpm), at 37˚C for all standard protocols. Long term storage of *E.coli* strains was achieved

using a Protect Microorganism Preservation System (Technical Service Consultant Ltd) and stored at -80˚C.

2.8.2. Antibiotics and plasmids

PCR products were cloned into pGEMT-Easy™ (Promega) which has an ampicillin resistance gene. For selection and maintainence of plasmids within *the E. coli*, 50 µg/ml ampicillin (amp) was added to the solid or broth media.

2.8.3. Plasmid DNA isolation

Small scale plasmid preps were performed using the GeneJET Plasmid Miniprep Kit (Thermo Scientific) according to manufacturer's instructions.

2.8.4. Restriction digests

Restriction digests of plasmids were performed with standard restriction enzymes (NEB) according to manufacturer's instructions. Plasmid DNA was normally digested for at least 120 minutes at 37˚C.

2.8.5. Ligation of DNA fragments

All DNA fragments were ligated using the T4 DNA Ligase (Promega) according to manufacturer's instructions.

2.8.6. DNA purification

DNA fragments from agarose gels were extracted using QIAquick Gel Extraction Kit (Qiagen) according to manufacturer's instructions.

2.9. Molecular techniques for the manipulation of DNA

2.9.1. Small-scale *A. nidulans* genomic DNA preparation

Genomic DNA extraction was carried out from strains grown SC with 1% (w/v) agar. Hyphae and conidia were transferred to a sterile 2.0 ml microcentrifuge tube containing glass beads (180 µm) and 1 ml of extraction buffer (100 mM Tris pH 8.0, 1.4 M NaCl, 10 mM EDTA, 2% CTAB).The mixture was homogenized using a PowerLyzer® 24 Bench Top Bead-Based Homogenizer (MO-Bio) at 3,000 rpm for 90 sec. The suspension was incubated at 65˚C for 10 minutes before centrifugation for 2 min. 700 µl of supernatant was transferred to a new 2 ml tube containing 2 µl RNase (100mg/ml) and the tube was incubated at 37˚C for 30 min. Equal volume of phenol: chloroform : isoamyl alcohol (v/v, 25:1) were added. The mixture was vortex and centrifugated at maximum speed for 2 min. 600 µl of the aqueous phase were transferred to a new 2 ml tube and repeat the chloroform extraction one more time. An equal volume of isopropanol was added to the aqueous phase and the mixture was incubated on ice for 5 minutes. Then, the mixture was spun at maximum speed for 5 min and the pallet was washed twice with 70% ethanol. Pellets were air dried on bench for 5 min before dissolving it with 150 µl nuclease-free water. The genomic DNA was used directly for PCR or store at -20 ˚C.

2.9.2. Nucleic acid quantification

The quantity and quality of DNA and RNA was measured with NanoDrop-1000 (Thermo Scientific) using a 1 µl sample per measurement.

2.9.3. Agarose gel electrophoresis of DNA and RNA

Agarose gel electrophoresis of DNA was performed in Fisher brand horizontal electrophoresis gel tanks (Fisher Scientific) using agarose (Bioline) at a concentration

between 1% to 2% (w/v) in 1X TAE (0.4 M Tris-acetate, 1 mM EDTA) buffer. Gels were run at 100 V until the bromophenol dye reached ¾ of the gel length. DNA was stained by the addition of 2 µl Midori Green (NIPPON Genetics EUROPE) per 100 ml agarose gel for visualization under the UV light using the U-Genius (Syngene Imager). Hyperladder 1/Hyperladder 1kb and Hyperladder IV (Bioline) were used as a molecular weight marker.

2.9.4. Polymerase Chain Reaction (PCR) from genomic and plasmid DNA

2.9.4.1.Standard PCR

PCR analysis was carried out using 5 µl of 2X BioMix^{TM} Red (Bioline), 1 µl genomic DNA (0.1 µg), 0.1 µl of forward primer (10µM), 0.1 µl of reverse primer (10µM) and 3.8 µl of nuclease-free water. All the forward and reverse primers used in this experiment are listed in Table 2.1. The standard PCR program was as follows; 3 min at 95 °C, followed by 30 amplification cycles (30 seconds at 95 °C, 30 seconds annealing at 57 °C, and 30 seconds at 72 °C) and final extension at 72 °C for 10 min.

2.9.5. Fusion PCR

Amplification of more than one fragment which will be fused together were performed using the Phusion High-Fidelity DNA Polymerases (Thermo Scientific). Oligonucleotides were designed as in illustrated in Figure 2.1. Annealing temperature and extension times varied with primers and product sizes.

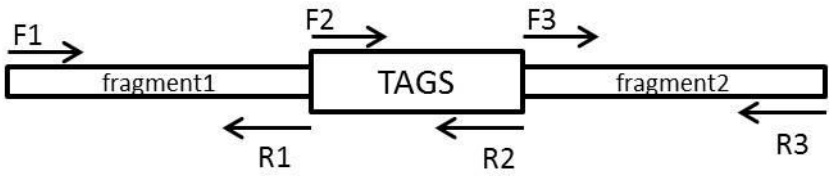

Fig 2.1. Oligonucleotide design for Fusion PCR. The principles for this experiment were adapted from (Morozov et al., 2010).

Three different fragments were amplified individually using three different PCR reactions with three different primer combinations F1/R1, F2/R2 and F3/R3. The 5' of primers directing fusion (R1/F2 and R2/F3) were complementary. All the PCR products with the correct size were gel extracted and then used in the Fusion PCR utilising F1/R3 primer combination. The reaction mixture for fusion PCR as below:

2 flanking DNA fragments (~100ng)	- 1 µl
DNA-TAG fragment (200ng)	- 1 µl
Primer F1 (20 mM)	- 1.25 µl
Primer R3 (20 mM)	- 1.25 µl
dNTPs (10 mM)	- 1 µl
Phusion High-Fidelity DNA Polymerases	- 1 µl
nuclease-free water	- 43.5 µl

The fusion PCR were performed using the program as follow:

Predenaturation	- 98 °C, 30 seconds
<u>12 cycles</u>	
Denaturation	- 98 °C, 10 seconds
Ramp down	- to 67 °C, 0.1 °C/second
Primers annealing	- 67 °C, 30 seconds
Ramp up	- to 72 °C, 0.2 °C/second
Extension	- 72 °C, 3 minutes
<u>12 cycles</u>	
Denaturation	- 98 °C, 10 seconds
Ramp down	- to 67 °C, 0.1 °C/second
Primers annealing	- 67 °C, 30 seconds
Extension	- 72 °C, 3 minutes
Ramp up	- to 72 °C, 2 °C/second
Increase by 5 seconds every cycle	
<u>12 cycles</u>	
Denaturation	- 98 °C, 10 seconds
Ramp down	- to 67 °C, 0.1 °C/second
Primers annealing	- 67 °C, 30 seconds
Extension	- 72 °C, 4 minutes
Ramp up	- to 72 °C, 0.2 °C/second
Increase by 20 seconds every cycle	
Final Extension	- 72 °C, 5 minutes

2.10. Molecular techniques for the manipulation of RNA

To minimise degradation of RNA by ribonucleases, all the consumables were autoclaved twice. Disposable gloves were worn at all times during the preparation of materials and solutions used as well as during the extraction and handling the RNA. Diethyl pyrocarbonate (DEPC) water were prepared and used to prepare the solutions.

2.10.1. RNA preparation from *A. nidulans*

Strains were grown in 200 ml minimal medium with nitrate as N source and incubated overnight at 30˚C with agitation at 200 rpm. After 16 h growth 0.1mg/ml uric acid was added to the cells for 2 h prior to harvesting. This step was carried out to induce the expression of the *uaZ* gene. Mycelia were harvested and washed with cold water twice and pressing it between the paper towels before transfer immediately to liquid nitrogen. Then, frozen mycelia were ground using a DEPC-treated mortar and pastel. The powdered cells were added to 800 µl of lysis buffer (100 mM Tris-Cl pH 8.0, 600 mM sodium chloride, 10 mM EDTA, 5% sodium dodecyl sulphate, SDS) and 800 µl of phenol was added then vortexed vigorously. Supernatants were phenol:chloroform (1:1) extracted followed by 5 M lithium acetate precipitation. Pellets were then washed with 70% ethanol before dissolving in DEPC-water. The RNA was then treated with DNase1 (Thermo) for 30 min to remove contaminating DNA. The RNA was then subject to chloroform extraction and re-precipitation before being dissolved in DEPC-treated water for subsequent analysis.

2.10.2. Northern blotting

2.5 grams of agarose (Bioline) was melted in 206 ml DEPC water. When cooled to 50º C , 25 ml of 10X MOPS (20mM MOPS, 5 mM sodium acetate, 1mM EDTA) and 14 ml formaldehyde were added to the agarose solution. This was mixed and poured into the gel

mould. RNA samples were prepared by adding 10 µl 2X sample buffer (50 µl formamide, 18 µl 37% formaldehyde (~ 2.2 M), 10 µl 10X MOPS buffer and 3 µl 10X Dye Solution (50% glycerol, 0.3% Bromophenol Blue). Samples were then denatured at 65 ˚C for 10 minutes and transferred to ice prior to loading. The gel was submerged in 1X MOPS and the samples were run for 3 hours at 100 V. After electrophoresis, the RNA was transferred from the gel to Zeta-Probe GT (BioRad) blotting membrane in 10X SSC (1.5 M NaCl, 0.15 M Na-Citrate, pH 7.0) overnight. Then, the membrane was rinsed in 2X SSC twice for 10 minutes and air dried. RNA was fixed to the blot by vacuum drying for 45 minutes at 80 ˚C. Membrane was then hybridized to radiolabelled (α^{32}P – dCTP) DNA probes at 65 ˚C followed the recommended protocols for Zeta-Probe membrane. Imaging was conducted using a Molecular Dynamics STORM™ scanner and quantification was done using ImageQuant TL Software (GE Healthcare Life Sciences).

2.10.3. Quantitative real-time polymerase chain reaction (qRT-PCR)

For each sample, 2 µg of total RNA was reverse transcribed with random hexamers using the Tetro reverse transcriptase enzyme (Bioline). cDNA samples were diluted 50 fold in H_2O for qPCR analysis. Three transcripts were investigated in this study; the internal control gene (18S rRNA) and the genes of interest;*uaZ* and *hxA*). The sequences of the PCR primers used in this study are given in Table 2.1. PCR eactions of 20 µl were set up with 10 µl 2X SensiFAST SYBR Hi-ROX Kit (Bioline), 1 µl of forward primer (10 µM), 1 µl of reverse primer (10 µM), 6 µl RNase-free water and 2 µl template. PCRs were conducted using the StepOnePlus™ Real-Time PCR System (Applied Biosystems) with the following settings: 2 min at 95 °C, 40 amplification cycles (each 5 seconds at 95 °C, 10 seconds annealing at 57 °C, and 5 seconds at 72 °C with endpoint fluorescence detection). Gene expression analysis was carried out using comparative Ct method (Livak and Schmittgen, 2001)

2.11. Confocal Microscopy

Conidia were resuspended in 0.01% Tween water and vortex.1 µl of the suspension was applied to the bottom of the glass cell culture dish (Greiner Bio-One) and let it dry at 37 °C for about 10 minutes before the addition of 300 µl of fully supplemented liquid MM. The cultures were then incubated at 30 °C for 14 hours. To simultaneously stain nuclei 1 µl of a 20 µg/ml DAPI (4′,6-Diamidino-2-phenylindol Dihydrochloride) were added to the media and sample were incubated at 37 °C for 20 minutes. Immediately prior to microscopy the media with DAPI was removed by aspiration and 300 µl of fresh media added and this procedure was repeated twice. Imaging of the hyphae was undertaken using the Zeiss microscopes LSM710 with Plan-Apochromat Fluar 63x1.4 NA objective, utilising Zeiss ZEN and Zeiss LSM software respectively. Green Fluorescence Proteins (GFP) was excited with a 488 nm laser and imaged using fluorescence emission bandwidth of 492-530 nm. Red Fluorescence Proteins (RFP) was imaged with 561 nm DSP excitatory laser using a fluorescence emission bandwidth 571-630 nm. DAPI was excited by a short arc mercury lamp and emission was detected between 426 and 479 nm. The contrast of all images was enhanced linearly using Fiji (ImageJ) software (Schindelin et al., 2012).

2.12. Computational analysis

2.12.1. Sequence analysis and phylogenetic reconstruction

PCR Primers and hybridisation probes were designed using Primer3 online tools (http://biotools.umassmed.edu/bioapps/primer3_www.cgi). All alignments of protein sequences was done using MEGA5 package (Tamura et al., 2011) while the Muscle program (Edgar, 2004) was used for multiple alignments of protein sequences using the default

parameters. To assess the internal support of tree branches, heuristic bootstrap analyses with 1000 replicates were performed.

2.12.2. Databases

- The *Aspergillus* genome database (http://www.aspgd.org/)
- National Center for Biotechnology Information (NCBI) database (http://www.ncbi.nlm.nih.gov/)
- Conserved domain database (http://www.ncbi.nlm.nih.gov/Structure/cdd/wrpsb.cgi)

2.12.3. Online tools

- Basic Local Alignment Search Tool (BLAST) (http://www.ncbi.nlm.nih.gov/)
- Protein sequence analysis tools (http://www.expasy.ch/)

2.13. Polysome fractionation

800µl of lysis buffer (20 mM Tris-Cl pH 8.0, 140 mM potassium chloride, 1.5mM magnesium chloride, 0.5 mM DTT, 1% Triton X-100, 0.1 mg/ml cyclohexamide, 1mg/ml heparin and 6µl RNasin) were added to the ground mycelia and incubated on ice with agitation for 10 min. The samples were centrifuged at 4000g at 4˚C for 5 min. Supernatant was transferred to a new tube and centrifuged again to remove any contamination. About 800 µg of RNA was loaded onto sucrose gradient. Gradient were centrifuged at 37,000 rpm in 4˚ C for 2 hours and 50 min. 1.1 ml gradient were collected and phenol extraction was carried out. Then, the samples were precipitated for overnight in -20˚ C.

2.14. Capped and decapped assay

2.14.1. Annealing of RNA adaptor with decapped transcripts using splinted primers

a) Prepare the 10X annealing buffer 250 µl KCl (3M), 200 µl Tris-HCl (1M, pH 7.5), sterile water (up to 1 mL).
b) Assemble the following reaction in 0.25 mL tube:

10X annealing buffer	-	5 µl
RNA adaptor (100 pmol)	-	5 µl
Splint-primer 8N (100 pmol)	-	5 µl
DEPC-H_2O	-	5 µl

c) Add 2 µl of annealing mix (From 2.14.1 (b)) with 20 µg of total RNA and the tube were sequentially incubated at 95°C for 1 min, 65°C for 1 min, 60°C for 1 min, 50°C for 1 min, 40°C for 1 min, 30°C for 1 min and finally to 25°C for 2 min.

2.14.2. Ligation of RNA adaptor with decapped transcripts using splinted primers

a) In the meantime, prepare the 2X ligation buffer (132 µl Tris-HCl (1M, pH 7.5), 20 µl $MgCl_2$ (1M), 2 µl DTT (1M), 10 µl ATP (100mM), 750 µl 20% Polyethylene Glycol (PEG; MW 6000), sterile water 86 µl.
b) Prepare the ligation mix as below:

2X ligation buffer	-	31 µl
T4 RNA Ligase 1 (20U/µl) (NEB)	-	1 µl
SUPERase.In™ RNase Inhibitor (10U/µl) (Thermo)	-	1 µl
DEPC-H_2O	-	5 µl

c) Add 7.5 µl of ligation mix to the tube at 2.14.1 (c) and mix it by pipetting up and down gently.
d) The tube was incubated at 16˚C for at least 16 hours in Thermoblock.

2.14.3. DNase1 treatment and cDNA synthesis

a) 85 µl of DEPC-H_2O were added to the splinted ligation mixture (From 2.14.2 (d)). 2 µl of DNase1 (1000U) (Thermo) and 5 µl of 10X DNase1 buffer (Thermo) were added to the mixture.
b) The tube was incubated at 37˚C for 60 minutes.
c) 100 µl of phenol:chloroform:isoamyl alcohol (25:24:1) was added to the mixture and vortex.
d) The tube was centrifuged at 15,000 rpm for 10 minutes at 4˚C.
e) ~95 µl of aqueous phase were mix with 300 µl 100% ethanol, 10 µl of sodium acetate (3M), pH 5.2 and 1 µl glycerol (5mg/ml) and incubated at -80˚C for 1 hour.
f) The tube was centrifuged at 15,000 rpm for 30 minutes at 4˚C.
g) The pellet was washed with 80% ethanol (twice).
h) Finally, the pellet was dissolved in 6 µl DEPC-H_2O.
i) cDNA synthesis and qRT-PCR analysis of decapped transcripts as in Chapter 2.10.3. The primer was designed to amplify the RNA adapter to an internal region of the specific transcript (Figure 2.2).

Figure 2.2. qRT-PCR analysis of decapped transcripts. For the native decapped transcripts, *primer 1.Fwd* (which located in the 5' adaptor) will be paired with the *primer 2.Rev* (specific genes). As a control, *primer 2.Fwd* (forward primer in a specific gene) will be paired with the *primer 2.Rev*.

CHAPTER 3: DECAPPING AND NMD

Introduction

Decapping is one of the major steps in mRNA decay (Franks and Lykke-Andersen, 2008; Parker and Song, 2004) which leads to the rapid 5' to 3' degradation and has been identified as a central rate limiting step in eukaryotic mRNA turnover (Fillman and Lykke-Andersen, 2005). The core component of the decapping complex is a Nudix family enzyme, Dcp2 (Chang et al., 2014; Coller and Parker, 2004; Dunckley and Parker, 1999) which is known to work together with Dcp1 (Valkov et al., 2016). Dcp1is non-catalytic but it plays an important role in activating Dcp2 (Chang et al., 2014).

NMD is an mRNA quality control pathway in eukaryotic cells, whereby transcripts with premature termination codons (PTC) are targeted for degradation (Durand et al., 2007; Karousis et al., 2016). This process prevents the build-up of potentially toxic, aberrant peptides that can arise from mRNA transcripts with a PTC. The half-life of affected transcripts is significantly reduced and in yeast NMD mediated degradation is initiated by mRNA decapping (Amrani et al., 2006). In *A. nidulans*, Upf1 and Upf2 (NmdA) have been shown to be required for NMD which is effective in significantly reducing the transcript levels of specific mutant alleles including *uaZ14*, a mutant allele of the urate oxidase-encoding gene and *hxA5*, a mutant allele of the xanthine dehydrogenase-encoding gene (Morozov et al., 2006; Morozov et al., 2012).

Preliminary evidence in *A. nidulans* suggested that disruption of Dcp2 did not disrupt NMD (Morozov and Caddick, unpublished data), unlike the yeast system (He and Jacobson, 2015; Swisher and Parker, 2011). Furthermore, cRT-PCR analysis indicated the presence of decapped transcripts in Dcp2 mutant (Figure 1.4). Additionally, the double deletion of Dcp2 and an exosome component, Rrp44 is not lethal in *A. nidulans* (Caddick, unpublished data) which

again distinguishes it from the situation in *S. cerevisiae* (Schneider et al., 2009). The various observations suggesting that potentially there are other decapping factors working together with Dcp2 in *A. nidulans*.

3.1. Deletion of the *A. nidulans dcp1* orthologue

In order to characterise the function of different components in decapping and RNA degradation, strains disrupted for the various activities were required. Dcp2 mutant was already available in our strains collection (Morozov and Caddick, unpublished data). The *A. nidulans* Dcp1 orthologue, AN7746 was identified previously and shown to localise to Processing (P) bodies (Morozov et al., 2010).

dcp1 (AN7746) was disrupted by transformation and homologous integration of deletion cassettes, produced by the Fungal Genetics Stock Centre. Strain validation was confirmed by PCR (Figure 3.1). Mutant strains bearing deletions which disrupted other components of the mRNA decapping and degradation mechanisms, Dhh1, Pat1, Lsm1 and Xrn1, were already available in our group. In order to assess the effect of disrupting the decapping factors, Dcp1 and Dcp2, and other components of the mRNA degradation machinery on NMD, the respective strains were crossed to introduce the *uaZ14* and *hxA5* alleles. Strain validation was conducted by growth tests for *uaZ14* and *hxA5* and the respective deletions were confirmed by PCR (Figure 3.1). Interestingly, in crosses both the Δ*dcp1* and Δ*dcp2* mutants co-segregate with a *fluffy* cotton-like morphology, which distinguishes them from WT (Figure 3.1 (c)).

a)

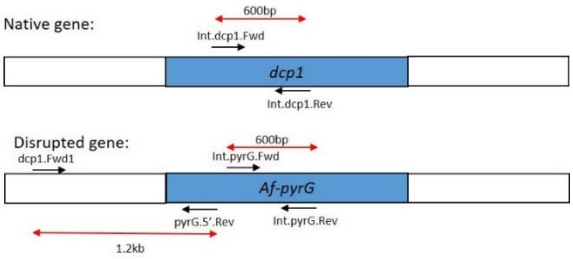

b)

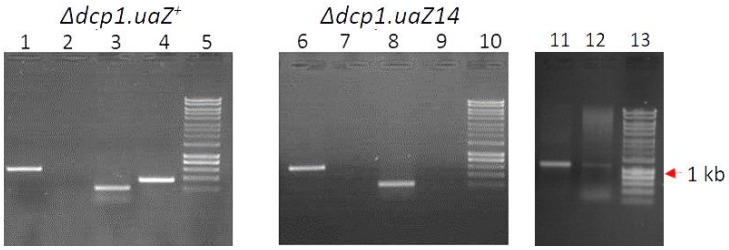

c)

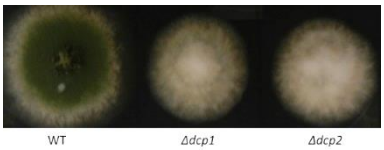

Figure 3.1. Disruption of *dcp1* and strain construction.

(a) A schematic diagram showing the location of primers (forward and reverse) used in the PCR validation of the native gene and disrupted allele. For example, there is no PCR product when internal *dcp1* primers (int.dcp1.for and int.dcp1.rev) were used in amplification of Δ*dcp1 uaZ*$^+$ but a PCR product was observed when internal *Af-pyrG* primers (int.pyrG.for and int.pyrG.rev) were used. Additionally, a 1.2kb PCR product using the primers (dcp1.Fwd1 and pyrG.5'.Rev) will validate the correct position of *Af-pyrG* marker in the genome. Primer sequences used in this experiment were listed in Table 2.1 (Chapter 2).
(b) PCR based validation of Δ*dcp1 uaZ*$^+$ and Δ*dcp1 uaZ14* strains using specific primer sets are given as an example. Based on the picture, a 600 bp band using Int_pyrG primers confirming the integration of *AfpyrG* gene into the *A. nidulans* genome (Lane 1,6), no product using Int_dcp1 primers is consistent with deletion of *dcp1* from the genome (Lane 2,7), a 300bp product using Int_dcp2 primers serves as a positive control (Lane 3,8), a 300bp product Int_nkuA confirmed the presence of *nkuA* (Lane 4,9), a deletion of which was also segregating in the cross, and DNA Ladder (Hyperladder1, Lane 5,10). Additionally, a 1.2kb PCR product using the primers (dcp1.Fwd1 and pyrG.5'.Rev) show that *Af-pyrG* marker insert at the correct location in the genomes of Δ*dcp1 uaZ*$^+$ (Lane 11) and Δ*dcp1 uaZ14* (Lane 12). DNA Ladder (Hyperladder1, Lane 13).
(c) Phenotypic differences between mutant strains used in this study (WT, Δ*dcp1* and Δ*dcp2*). The main difference is the *fluffy* cotton-like colony morphology of the Δ*dcp1* and Δ*dcp2* mutants as compared to the WT. All strains were grown on solid MM with required supplements for 3 days at 37ºC.

3.2. Localisation of decapping protein, Dcp2

Generally, decapping factors are found within the cytoplasm and can associate into microscopic foci known as the P-bodies, which have been identified across eukaryotes (Morozov et al., 2010; Parker and Sheth, 2007). In this study, Dcp2 was tagged at the C-terminus with either green or red fluorescent protein (GFP, RFP). This was achieved by homologous integration of linear constructs containing the tagging cassettes developed by Nayak et al. (2006). The resulting construct included either the GFP or RFP coding region and *Af-pyrG* as a selectable marker, positioned between the coding region and 3' UTR of *dcp2*. All GFP and RFP-tagged constructs were validated by PCR (Figure 3.2 (b)). Tagged proteins were visualised using confocal fluorescence microscopy. The samples were grown in MM for 16 hours at 30ºC with the addition of NH_4^+ which has been shown to increase the number of P-bodies in *A. nidulans* (Morozov et al., 2010). Nuclear staining was achieved by adding 4′,6-diamidino-2-phenylindole (DAPI) (Liu et al., 2009). As expected, Dcp2:GFP was found to aggregate into P-body-like structures (Figure 3.3 (a)). To monitor whether Dcp2 co-localises with Dcp1, we produced a *dcp2*:RFP *dcp1:*GFP double mutant by crossing the respective single mutants. Previously Dcp1:GFP was shown to localise to P-bodies (Morozov et al., 2010). Based on the confocal fluorescence microscopy, there is only limited co-localisation of Dcp2:RFP with Dcp1:GFP (Figure 3.4 (d)). Although both Dcp1:GFP and Dcp2:RFP localise into the expected P-body like structures these appear less predominant in the double mutant and it is possible that the tagging of both proteins has partially disrupted their association. However, these data would be consistent with significant proportions of Dcp2 and Dcp1 not forming a complex in *A. nidulans* at any one time.

a)

b)

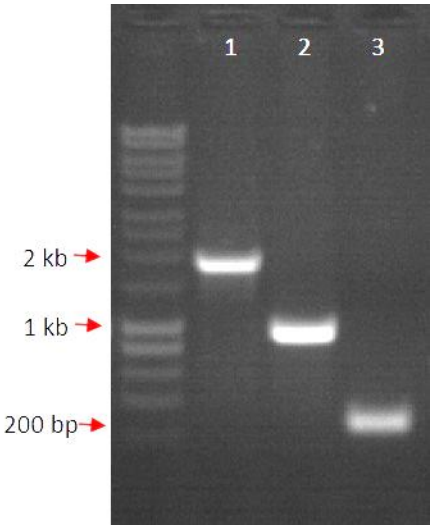

Figure 3.2. Construction of strains expressing Dcp2:GFP and Dcp2:RFP.

(a) A schematic diagram showing the location of primers (forward and reverse) used in the PCR validation of the dcp2:GFP and dcp2:RFP. For example, a 2 kb PCR product will be amplified using *dcp2.tagged.F1* and *Int.tag.R* primers and a 1 kb PCR product will be amplified using *3'.Tag.F* and *marker.R* primers and 200 bp of PCR product amplified using *Int.tag.F* and *Int.tag.R* primers were used. Successful transformants should give positive PCR products when amplified using such primer combination. Primer sequences used in this experiment are listed in Table 2.1 (Chapter 2).

(b) PCR based validation of *dcp2-tagged GFP* using specific primer sets are given as an example. Based on the picture, a 2 kb band using *dcp2.tagged.F1* and *Int.GFP.R* primers (Lane 1), a 1 kb band using *3'.Tag.F* and *Af-pyrG.R* primers (Lane 2) and finally 200 bp of PCR product amplified using *Int.GFP.F* and *Int.GFP.R* (Lane 3) confirming the integration of tagging cassette containing the GFP coding region and *Af-pyrG* gene into the coding region of *dcp2* in *A. nidulans* genome. Left lane is DNA Ladder (Hyperladder1).

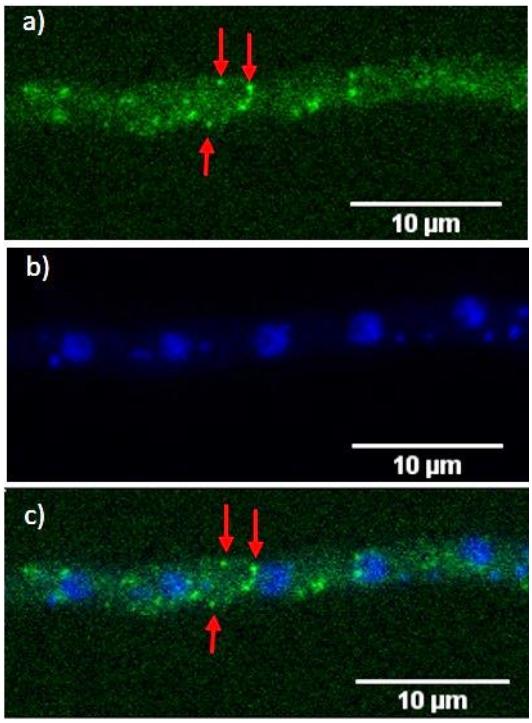

Figure 3.3. Fluorescence microscopy of GFP-tagged Dcp2. a) GFP; b) DAPI staining; c) merge images. GFP-tagged Dcp2 was observed in cytoplasm with a clear '*punctate*' formation indicative of Dcp2:GFP localising to the P-bodies (red arrow). DAPI was used as a control for nuclear staining. 10 µm scale is included (white line). Image was analyse using Fiji software from ImageJ (Schindelin et al., 2012).

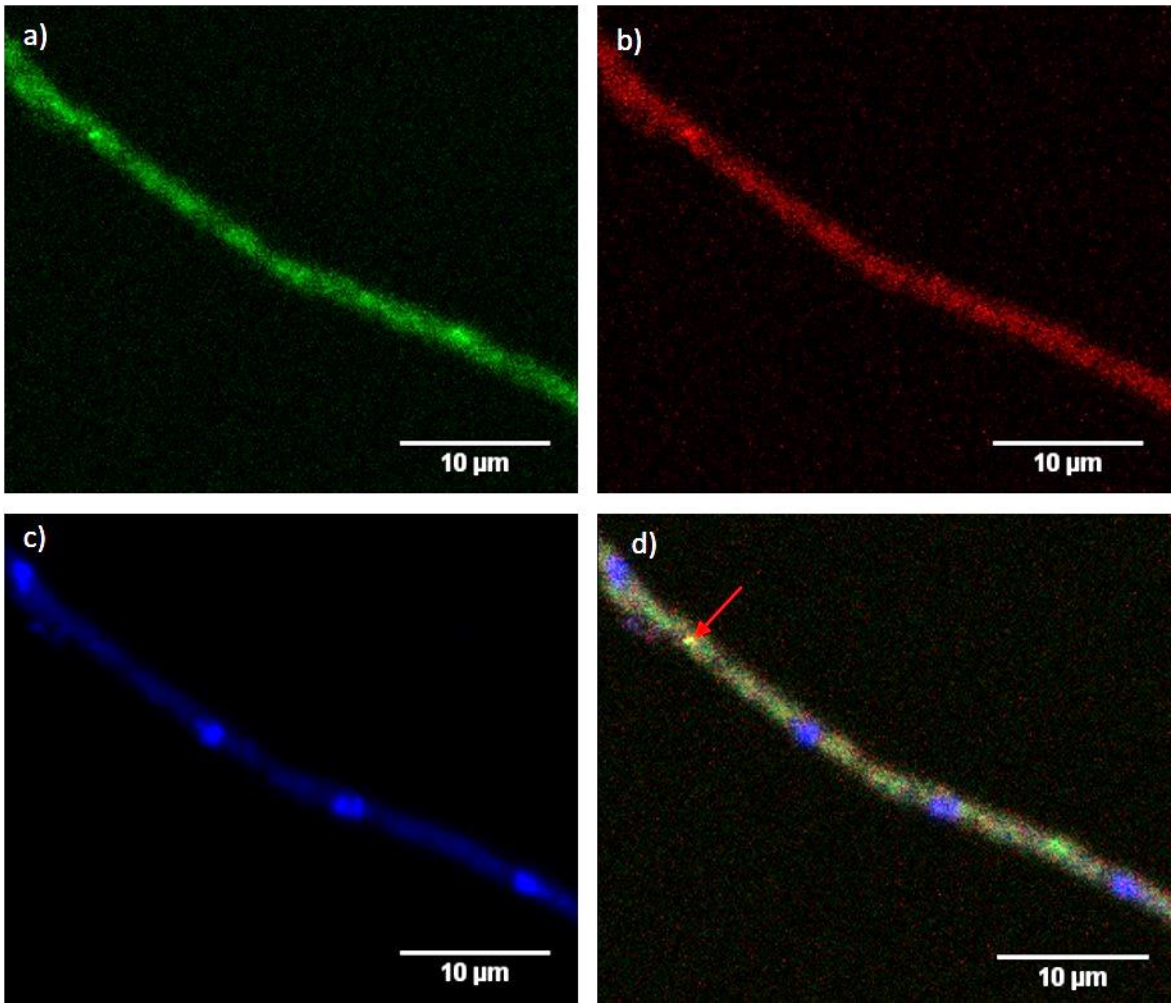

Figure 3.4. Fluorescence microscopy of RFP-tagged Dcp2 with GFP-tagged Dcp1. a) GFP-tagged Dcp1; b) RFP-tagged Dcp2; c) DAPI staining; d) merge images. A clear '*punctate*' formation observed indicated the Dcp2:RFP and Dcp1: GFP co-localised together (red arrow). However, a large proportion of the RFP signal is separated from the GFP signal, consistent with Dcp1 and Dcp2 not always associating in *A. nidulans*. DAPI was used as a control for nuclear staining. 10 µm scale is included (white line). The image was analyse using Fiji software from ImageJ (Schindelin et al., 2012).

3.3. Localisation of CutA and CutB

Previous study has shown that CutA and CutB act by adding the pyrimidine tags to partially degraded poly(A) tails (~A15). It is proposed that this promotes decapping by recruiting the Lsm-Pat1 complex, thus promoting decapping and the transcript degradation in *A. nidulans* (Morozov et al., 2012; Morozov et al., 2010). Thus, it was postulated that both proteins should co-localised in the cytoplasm. In this study, CutA and CutB were tagged at their C-termini with either GFP and RFP, respectively. Tagging was achieved as described for Dcp2 (See 3.2).

As expected, CutA was found to localise mainly in the cytoplasm (Figure 3.5 (i) & (iii)), with a diminished signal correlating with the position of the nuclei. Conversely, CutB was found mainly in the nucleus (Figure 3.5 (ii) & (iii)). To monitor if there is any changes of CutA when CutB is disrupted, *cutA*:GFP was crossed into the Δ*cutB* background. Interestingly, the relative proportion of CutA localised in the nucleus increased (Figure 3.6 (a)). Interestingly a number of factors associated with decapping, including Dcp1, Edc3 and Lsm1-7 components have been associated with P-bodies (Decker et al., 2007; Morozov et al., 2010). Additionally, deletion of *cutA* is known to disrupt P-bodies (Morozov et al., 2010). However, for both CutA and CutB there was no punctate distribution suggesting that neither is preferentially localised to P-bodies. The apparent requirement for CutA in P-body formation suggests that this relates to a process that occurs upstream from P-body formation.

i)

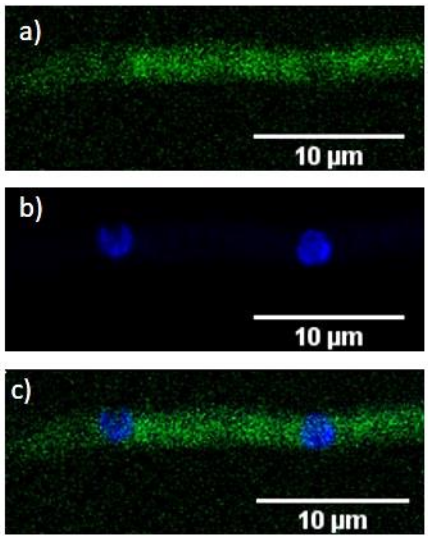

(% GFP-tagged in Nucleus) Percentage ± SE
9.24% ± 2.00

ii)

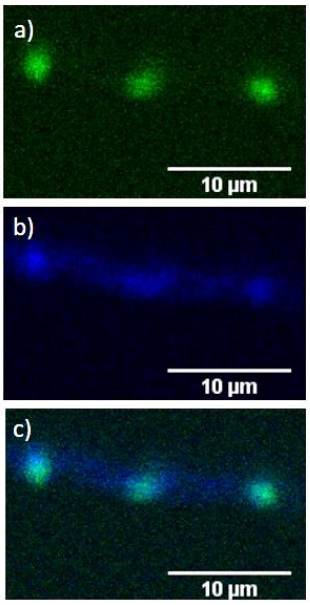

(% GFP-tagged in Nucleus) Percentage ± SE
36.02% ± 3.90

iii)

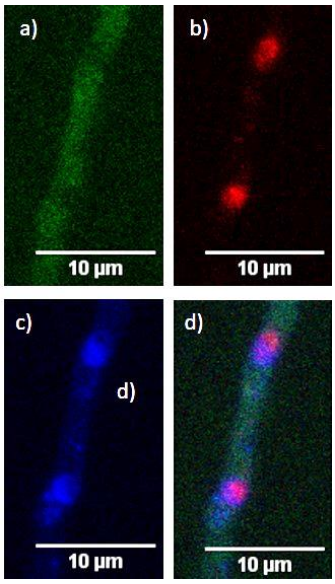

Figure 3.5. Confocal microscopy of fluorescently tagged CutA and CutB. Tagged strains: i) *cutA*:GFP; ii) *cutB*:GFP; iii) *cutA*:GFP *cutB*:RFP were analysed by confocal microscopy. Tagged CutA was observed mainly in cytoplasm whereas CutB localised primarily to the nuclei. DAPI was used as a control for nuclear staining (blue colour). 10 µm scale is included (white line). Image was analyse using Fiji software from ImageJ (Schindelin et al., 2012).

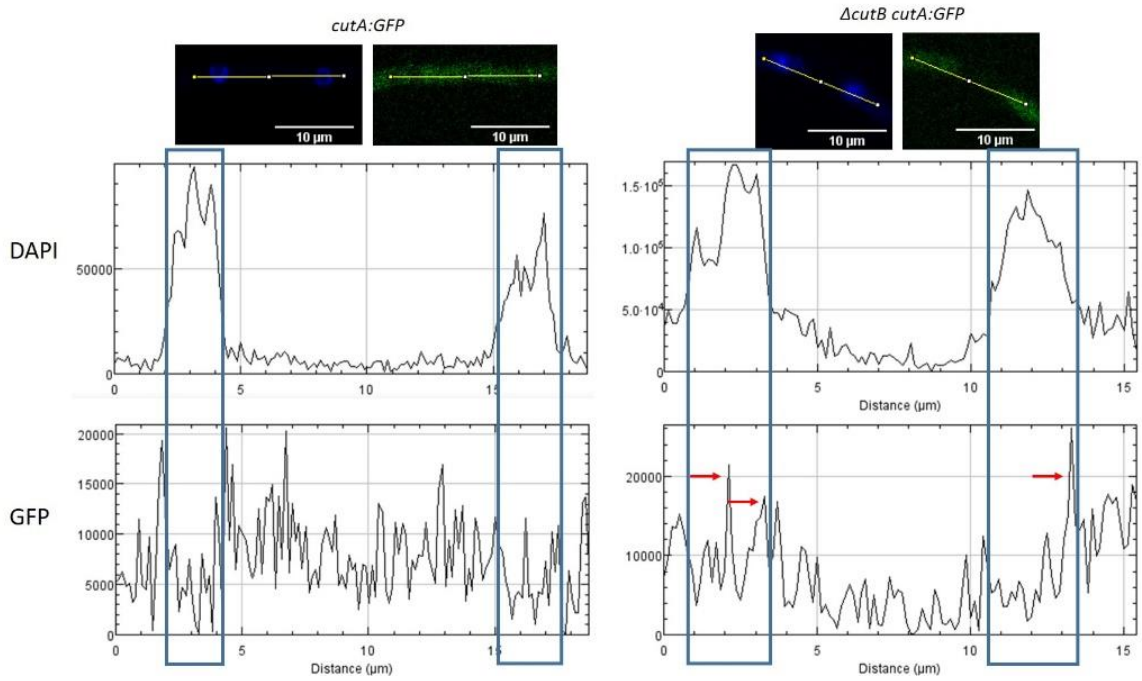

Figure 3.6. Fluorescence microscopy analysis comparing the signal intensity of DAPI and GFP in CutA:GFP and CutB:GFP with Δ*cutB* and Δ*cutA*, respectively.

In the *cutA*:GFP strain, the signal of GFP was primarily detected in cytoplasm which indicates that CutA was localised in cytoplasm. However, there are traces of GFP signal in nuclei (blue box), which indicates that a small amount of CutA also localised in nuclei. Interestingly, when CutB was disrupted, the GFP signal in nuclei increased proportionately (red arrow) which indicates that the amount of CutA in nuclei increased when CutB was disrupted. DAPI was used as a control for nuclear staining (blue colour). The signal reading was taken from yellow line using Fiji software from ImageJ (Schindelin et al., 2012). 10 µm scale is included (white line).

3.4. General transcript degradation and NMD

In eukaryotes, there are two main pathways for general mRNA degradation. The first pathways known as deadenylation-dependent decay pathway is initiated by shortening the poly(A) tail which triggers decapping, mediated by Dcp2/Dcp1, and subsequent 5' to 3' degradation mediated by the exonuclease Xrn1 (Parker, 2012; Sweet et al., 2012). The second pathways involves the 3′ degradation activity provided by the exosome complex (Houseley and Tollervey, 2009; Schneider et al., 2009). Here, we focusing on factors known to be involved in the first pathway: Dcp1, Dcp2, Dhh1, Xrn1, Lsm1 and Pat1.

To monitor the expression level of transcripts subject to NMD in strains lacking specific factors involved in general transcripts degradation, we utilised the qRT-PCR analysis. All strains were grown overnight in MM in the presence of nitrate as sole nitrogen source. Uric acid was added two hours prior to harvesting to induce expression of *uaZ* and *hxA* (Morozov et al., 2012). Total RNA were extracted from each mutant and converted to cDNA for qRT-PCR analysis. Analysis of the PTC-containing transcript, *uaZ14*, in the wild type background, revealed an 80% reduction compared to the uaZ^{+} (Figure 3.7). Similar results were observed for a second PTC-containing transcript, *hxA5* (Figure 3.8). These results demonstrated the effect of NMD for these alleles where the PTC-containing transcript was rapidly degraded. The equivalent experiment in the Δ*dcp1,* Δ*dcp2* and Δ*lsm1* mutant backgrounds show that although the level of PTC containing transcripts is still reduced there was a significantly higher proportions than in the WT background (Figure 3.7 & 3.8). This is consistent with increased stability of NMD substrates in these mutant backgrounds. These data demonstrate that NMD occurs in these mutants but not as drastically as in the WT background. Previous analysis of two highly conserved components of the NMD machinery, Upf1 and NmdA (Upf2), showed NMD was fully supressed in strains disrupting these activities (Morozov et al., 2012; Morozov et al., 2006). The partial suppression of NMD observed in strains disrupted for Dcp1, Dcp2 and Lsm1

is consistent with these proteins functioning in the same decapping mechanism but only playing a minor role in NMD. In the cytoplasm, Lsm1 forms a large complex with six other Lsm proteins, known as Lsm1-7 (Fillman and Lykke-Andersen, 2005), and this has been shown to recruit the decapping complex to deadenylated mRNAs (Tharun et al., 2000). These data would be consistent with the *A. nidulans* Lsm1-7 complex having a similar role in promoting decapping in response to NMD.

Disruption of Pat1, Dhh1 and Xrn1 did not affect the relative levels of *uaZ*$^{+}$ and *uaZ14* transcript when compared to the WT backgound, which is consistent with these proteins not playing a signficant role in NMD (Figure 3.7). The difference in NMD phenotype between disruption of Lsm1 and Pat1 was suprising, as Pat1 is known to form a complex with the Lsm1-7 complex and has been implicated in promoting mRNA decapping (Chowdhury et al., 2014). However, these data may indicate that Pat1's activity is limited to deadenylation dependent decapping, whereas Lsm1-7 appears to have a wider function. It was discovered recently that Pat1 was bound to Lsm2 and Lsm3 in the complex and not with the Lsm1 (Wu et al., 2014) and therefore it is possible that Pat1's function is retained in Δ*lsm1* mutants. Dhh1 is known as a decapping activator which works in a complex with Pat1 and Xrn1 in the deadenylation-dependent decay pathway. Previous studies in *S. cerevisiae* showed that disruption of Dhh1 did not have an effect on the degradation of nonsense-containing mRNAs (Fischer and Weis, 2002). Disruption of Xrn1 showed a surprising phenotype, as it did not affect NMD. In eukaryotes there is another exonuclease known as Rat1, which is typically localised primarily in the nucleus but may also be cytoplasmic (Johnson, 1997; Parker, 2012). In *A. nidulans* there is a Rat1 orthologue (AN0707) and it is possible that this activity can replace Xrn1 to facilitate NMD. A mutant deleted for *rat1* has been constructed, however it is very sick strain making it impossible to include in this analysis (Caddick, unpublished data).

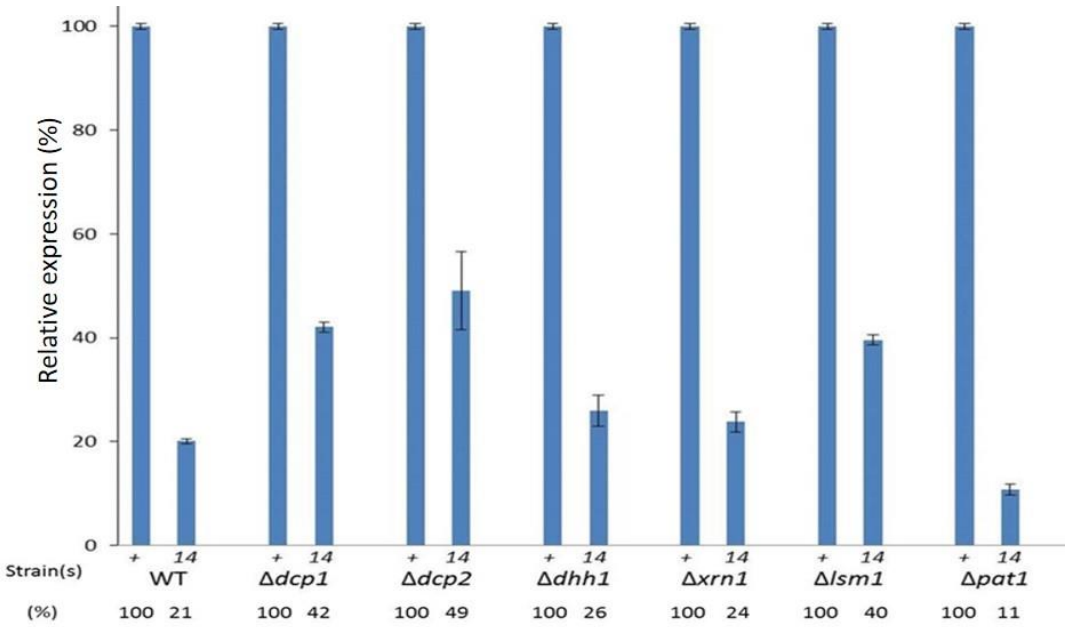

Figure 3.7. NMD of *uaZ14* in different mutant backgrounds. qRT-PCR analysis of total RNA samples was conducted to monitor the level of *uaZ*$^+$ (+) and *uaZ14* (*14*) transcripts in different genetic backgrounds: the wild type (WT), Δ*dcp1*, Δ*dcp2,* Δ*dhh1,* Δ*xrn1,* Δ*lsm1* and Δ*pat1*. 18S rRNA was used as endogenous control to monitor the expression of *uaZ* transcripts. The average level of *uaZ14* expression, relative to *uaZ*$^+$, is indicated for each strain (%). Results are representative of three independent experiments with the standard error (error bar).

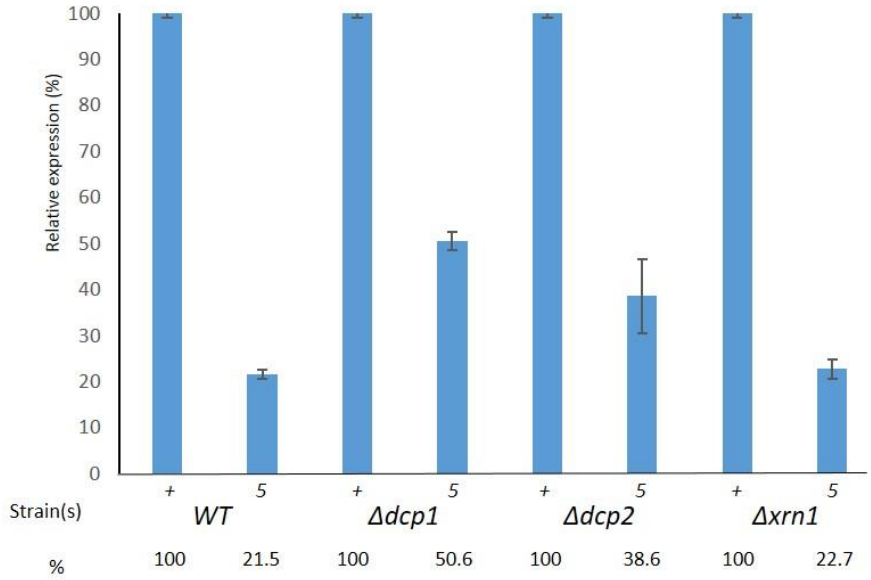

Figure 3.8. NMD of *hxA5* in different mutant backgrounds. qRT-PCR analysis of total RNA samples was conducted to monitor the level of *hxA*$^+$ (+) and *hxA5* (*5*) transcripts in different genetic backgrounds: the wild type (WT), Δ*dcp1*, Δ*dcp2*, and Δ*xrn1*. 18S rRNA was used as endogenous controls to monitor the expression of *hxA* transcripts. The average level of *hxA5* expression, relative to *hxA*$^+$, is indicated for each strain (%). Results are representative of three independent experiments with the standard error (error bar).

3.5. Translation and mRNA decapping

A previous study has shown that the transcripts subject to NMD were enriched within the polysome and monosome fractions in Δ*cutA* and Δ*cutB* mutants. CutA and CutB are terminal transferases which add pyrimidine tags to the poly(A) tails and are thought to promote decapping but are not required for NMD (Morozov et al., 2012). If Δ*dcp1* and Δ*dcp2* are required for decapping it is possible that their disruption would also lead to retention of NMD substrates within the polysome and monosome fractions. So an experiment was conducted to determine if decapping mutants (Δ*dcp1* and Δ*dcp2*) have a similar phenotype.

Ribosome profiling was conducted using differential centrifugation (Morozov et al., 2012) for *uaZ*$^{+}$ and *uaZ14* strains with either a Δ*dcp1*, Δ*dcp2* or WT background. Based on the absorbance profile at $A_{254,}$ four pooled fractions were prepared: polysome, disome & monosome (80S), subunits (60S and 40S) and ribonucleoproteins (RNPs). The RNA from each fraction was purified and reverse transcribed to produce cDNA. qRT-PCR was used to quantify the relative level of *uaZ* transcripts in each fraction and the resulting data is presented in Figure 3.9. Compared to the enrichment of NMD substrates in the polysome and monosome fraction observed for Δ*cutA* and Δ*cutB* mutants (Morozov *et al.,* 2012) no similar effect was observed for either Δ*dcp1* and Δ*dcp2* strains. This would suggest that this aspect of the Δ*cutA* and Δ*cutB* phenotype is not specifically associated with failure to activate *Dcp2* mediated decapping. In the WT background, there was an increase in the proportion of *uaZ14* transcripts in the RNP fraction, as compared to *uaZ*$^{+}$ (Figure 3.9). However, this was not observed for either Δ*dcp1* or Δ*dcp2* strains. Similarly, in *S. cerevisiae* transcripts subject to NMD were detected mainly in the lighter fractions (RNPs) but in a Δ*dcp2* strain a higher percentage of the PTC-containing transcripts bound to polysome and monosome. It was argued, this indicates that decapping of NMD transcripts occurs while the transcripts are bound to the ribosomes and that translational repression is a component of NMD (Hu et al., 2010). Interestingly, irrespective of which *uaZ*

allele is being tested, the transcripts bound to the polysome fractions increased in both the Δ*dcp1* and Δ*dcp2* strains, which is also in agreement with the results observed for *S. cerevisiae*. Interestingly, the ribosomal profile of WT, Δ*dcp1* and Δ*dcp2* strains varied significantly and this is explored further in Chapter 6.

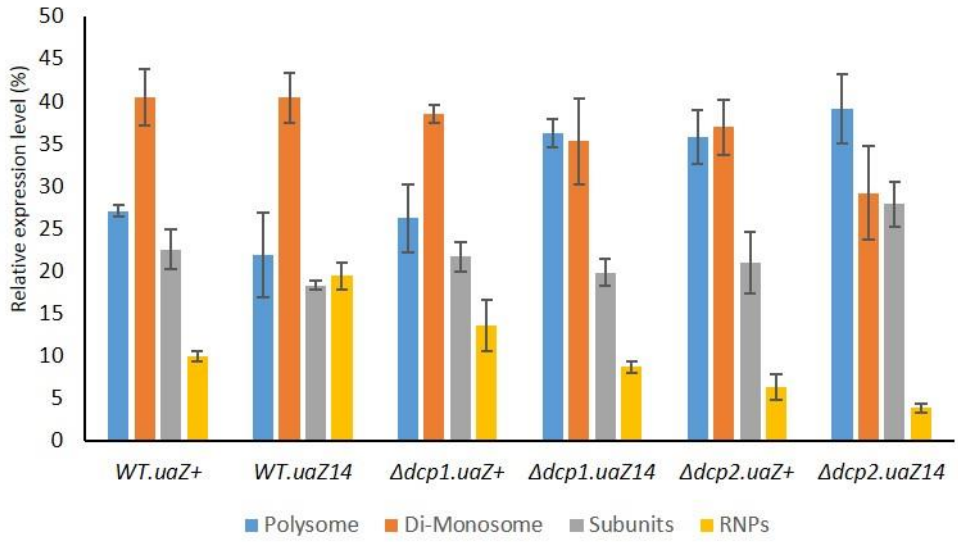

Figure 3.9. *uaZ* transcript distribution relative to the ribosome profile. qRT-PCR analysis from the pooled polysome fractionation was conducted to monitor the level of *uaZ*$^{+}$ and *uaZ14* transcripts in different ribosomal fractions, comparing WT, Δ*dcp1* and Δ*dcp2* strains. Fractions were pooled according to polysome, disome and monosome (80S), subunits (60S and 40S) and ribonucleoproteins (RNPs) after monitoring the absorbance at A_{254}. Results are representative of three independently performed experiments with the standard errors (error bars).

3.6. Transcript stability in the mutant strains

Based on other systems, mRNA decapping is a key transition point in mRNA degradation, facilitating rapid 5'-3' degradation which is the major degradation mechanism (Parker, 2012). In a wide range of organisms, extending from *S. cerevisiae* to mammalian systems, Dcp1 and Dcp2 are the primary decapping proteins and it has been shown that disruption of these leads to mRNA stabilisation. To investigate this in *A. nidulans* we undertook Northern hybridisation analysis to monitor transcript levels after the chemical inhibition of transcription by proflavine. This method has been used previously to quantify the degradation rate of mRNA in *A. nidulans* (Morozov et al., 2012; Morozov et al., 2006; Platt et al., 1996) and similar approaches has been applied to a variety of other organisms including bacteria (Luciano et al., 2012), yeast (Coller, 2008) and mammalian cells (Streit et al., 2008). Utilising this approach we inhibited transcription and monitored *uaZ*$^{+}$ transcript levels in WT, Δ*dcp1* and Δ*dcp2* strains over a 30 minute time-course. Deletion of *dcp2* leads to a significant stabilisation of the transcripts (Figure 3.10 (b)), while deletion of *dcp1* did not have a significant effect on the transcript stability (Figure 3.10 (a)) (regression analysis; WT: 18.89 ± 2.79; Δ*dcp1*: 19.51 ± 3.61; Δ*dcp2*: 33.40 ± 1.29). This indicated that Dcp2 is involved in the maintaining the stability of the transcript, which supported the function of this protein in decapping. However, it was surprising that deletion of *dcp1* did not mirror the effect of deleting *dcp2* as the respective proteins have been shown to form a complex, with Dcp1 activating Dcp2 activity. However, it has been shown in *S. cerevisiae* that deletion of *dcp1* can be suppressed by overexpression of *dcp2*, demonstrating that the Dcp2 function is not fully dependent on Dcp1 (Dunckley and Parker, 1999). It is, therefore, possible that in *A. nidulans* disruption of *dcp1* only partially inactivates Dcp2 activity and that the resulting phenotype is less severe.

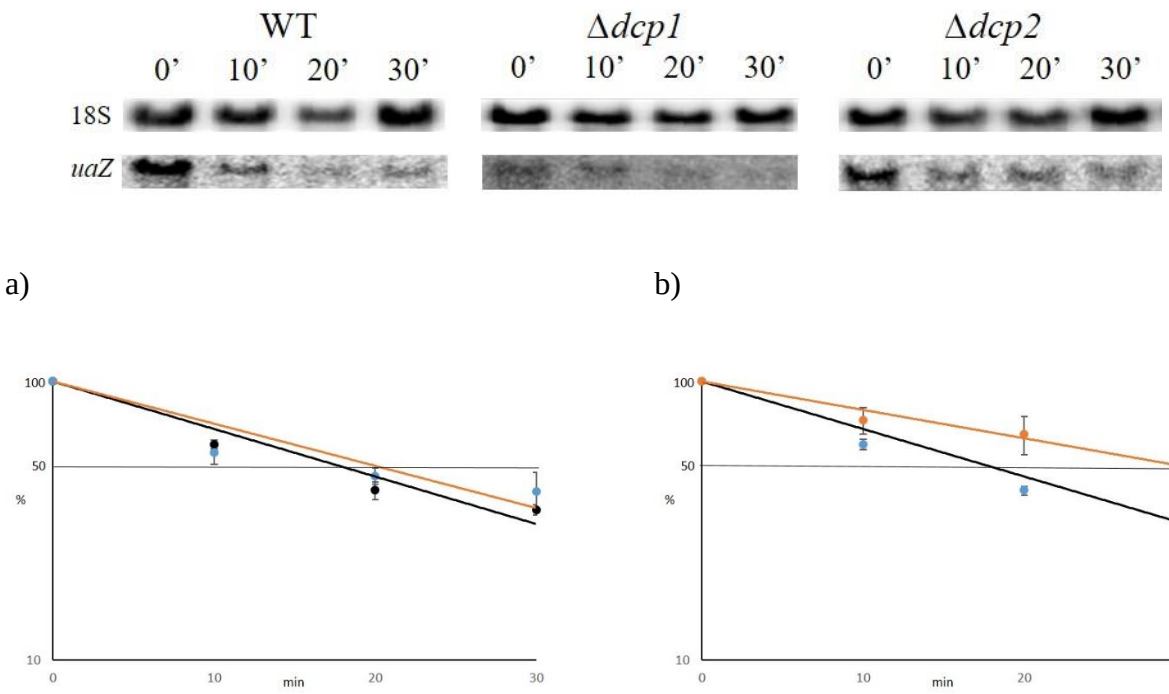

Figure 3.10. Stability of the *uaZ*$^+$ transcripts in WT and selected mutants. Representative images of northern blots for *uaZ*$^+$ and 18S rRNA are shown for the wild-type, Δ*dcp1*, and Δ*dcp2* strains as indicated. Quantitative data comparing *uaZ*$^+$ mRNA levels for the WT with a) Δ*dcp1* and b) Δ*dcp2* are given. 18S rRNA was used as a loading control. Transcript degradation was monitored over a 30 minutes time-course at 30º C after the addition of 10 mM NH_4^+ at t_0. Transcription was inhibited by the addition of proflavine to cultures at 10 min before the time-course began. The results represent mean values from three independent replicates. WT (black line) and mutant (orange line).

3.7. Summary

The main objective of this part of the study was to determine whether the disruption of decapping factors, Dcp2 and Dcp1 have an effect on NMD. Δ*dcp2* mutant strains were available in our strains collection, while the Δ*dcp1* mutant was constructed as part of this work. Morphologically, the two mutant strains, Δ*dcp1* and Δ*dcp2*, were very similar with a distinctive *fluffy* cotton-like colony morphology and poor conidiation (Figure 3.1 (c)). In *A. nidulans*, the appearance of the *fluffy* phenotype has been associated with genes involved in the conidiation process where mutations in genes such as *fluG* and *brlA*, a well-characterized transcriptional regulator, produce *fluffy* colonies (Chang et al., 2012; Wieser et al., 1994). The appearance of a *fluffy* morphology in strains disrupted for Dcp1 and Dcp2 indicate that these two proteins may be required for this complex developmental process to function appropriately in *A. nidulans* (Wieser et al., 1994). The similarity in appearance of the two mutants is also consistent with the respective proteins being functionally related.

Based on the qRT-PCR analysis of total RNA in the WT background, the PTC-containing transcripts for *uaZ14* and *hxA5* had an 80% reduction in the transcript levels compared to the wild-type transcripts. These results confirm the effect of NMD on the expression of the *uaZ14* and *hxA5* alleles and are consistent with previous studies (Morozov et al., 2012; Morozov et al., 2006). For the Δ*dcp1* and Δ*dcp2* mutant strains, the level of *uaZ14* mRNA, compared to the respective wild-type transcripts, was reduced by only 50% to 60%, respectively. Similar results were also observed for the *hxA5* mRNA. These data indicate that NMD occurs in these mutants but the severity of the effect is diminished (Figure 3.7 and Figure 3.8). Based on work in *S. cerevisiae*, PTC-containing transcripts will be degraded via decapping and 5'-3' exoribonuclease activity (Hu et al., 2010), these data show that the situation in *A. nidulans* is more complex with disruption of both *dcp1* and *dcp2* leading to only partial suppression of the NMD response. This indicates that other mechanisms are probably involved, which is

consistent with animal systems where an endonuclease, SMG6, is also implicated (Eberle et al., 2009). Another possibility is that there are other decapping factors in *A. nidulans* such as other Nudix family proteins, as has been observed in other eukaryotes (Song et al., 2013).

Disruption of Pat1 and Dhh1, factors that are required for promoting decapping in response to deadenylation, did not stabilise the *uaZ14* transcript in *A. nidulans*, which shows that neither of these factors is required for NMD (Figure 3.7). Our results are consistent with the results observed in yeast (Swisher and Parker, 2011). In *S. cerevisiae*, Pat1 is known to form a complex with Lsm1-7 complex (Chowdhury et al., 2014) and interact with both the decapping activator, Dhh1 and the 5'-3' exonuclease, Xrn1, as part of the deadenylation-dependent decay pathway in eukaryotes. Disruption of Dhh1 in yeast showed accumulated of deadenylated transcripts and stabilisation of transcripts, thus supporting the idea that it works as decapping activator in response to deadenylation (Coller et al., 2001). However, previous studies have shown that Dhh1 and Pat1 do not have an effect on the degradation of nonsense-containing mRNAs (Fischer and Weis, 2002).

Similar observation w observed when the exonuclease, Xrn1, was disrupted. In yeast, there are two major 5'-3' exonucleases, Xrn1 and Rat1/Xrn2. Xrn1 is primarily localised in cytoplasmic P-bodies (Parker and Sheth, 2007) whereas Rat1 is primarily nuclear (Xiang et al., 2009) and may also be cytoplasmic (Johnson, 1997; Parker, 2012). In mammalian system, Rat1 has been shown to associated with other NMD factors such as Upf1, Upf2, Upf3X, Dcp2, Xrn1, and exosome components PM/Scl100, Rrp4, and Rrp41 (Lejeune et al., 2003). Therefore it is possible that Xrn1 is not the primary 5'-3' exonuclease involved in NMD in *A. nidulans*. Rat1 has been successfully deleted from the *A. nidulans* genome, however, deleted strains show very poor growth and could not be cultured (Caddick, unpublished data) making it difficult to test.

Polysome profiling of the Dcp2 and Dcp1 (~37%) mutants indicates that nearly 50% increase of the *uaZ14* transcripts bind to the polysome fractions as compared to the WT (~21%) (Figure 3.9). Our results have no similar effect as compared to the enrichment of NMD substrates in the polysome and monosome fraction observed for Δ*cutA* and Δ*cutB* mutants (Morozov *et al.,* 2012). CutA and CutB are ribonucleotidyltransferases involved in 3'-tagging and associated with NMD-induced poly(A)-independent decapping (Morozov et al., 2012). This would suggest that this aspect of the Δ*cutA* and Δ*cutB* phenotype is not specifically associated with failure to activate *Dcp2* mediated decapping. Moreover, a previous study in *S. cerevisiae* demonstrated that degradation of NMD transcripts occurs while the transcripts are bound to the ribosome and in a Δ*dcp2* strain it has been shown that 70% of *CHY2* and GFP^{PTC67} (harbouring PTCs) were bound to polysome and monosome, whereas about 50% in the WT. Interestingly, a higher portion of transcripts w detected in the lighter fractions (RNPs) in WT as compared to the Δ*dcp2* stain (Hu et al., 2010). Similar results were obtained in *A. nidulans* which indicate translational repression is a component of NMD in this fungus.

Based on the RNA degradation experiment, it has been shown that disruption of Dcp2 leads to a partial stabilisation of transcripts in *A. nidulans* (Figure 3.10 (b)). This indicated that Dcp2 is involved in transcript degradation, consistent with its function in decapping. Surprisingly, deletion of *dcp1* only have a little effect on the stabilising the *uaZ* transcripts. In other systems, Dcp1 is required for the activation of Dcp2 and both mutation have a similar phenotype. Additionally, the fluorescence microscopy of both Dcp1:GFP and Dcp2:RFP shows that both proteins localise into the expected P-body-like structures. However, the significant proportion of Dcp2:RFP and Dcp1:GFP did not localise and were not, therefore, forming a complex in *A. nidulans*. The data suggest that the Dcp2 activity is not dependent solely on Dcp1, suggesting a divergence between *A. nidulans* and *S. cerevisiae*.

CutA was shown to be localised in the cytoplasm while CutB localised primarily to the nuclei. However, based on the GFP signal analysis, it shows that there a small traces of CutA presence in nuclei and CutB presence in the cytoplasm. Both proteins are involved in 3'pyrimidine-tagging of transcripts which are proposed to promote decapping in *A. nidulans* (Morozov et al., 2012). However, for both CutA and CutB, there was no punctate distribution suggesting that neither is preferentially localised to P-bodies. The apparent requirement for CutA in P-body formation suggests that this relates to a process that occurs upstream from P-body formation. Interestingly, the proportion of CutA in nuclei increased when CutB was disrupted (Figure 3.5 (a)).

CHAPTER 4: ADDITIONAL DECAPPING ACTIVITIES IN *A. nidulans*

Introduction

Decapping is one of the major steps in mRNA decay, which leads to rapid 5' to 3' degradation (Franks and Lykke-Andersen, 2008; Parker and Song, 2004). Dcp2 has been identified as the main decapping enzyme in *S. cerevisiae* (Coller and Parker, 2004).

In *S. cerevisiae*, Dcp2 has been shown to be required for NMD (Swisher and Parker, 2011).However, in *A. nidulans* only partial suppression of NMD was observed in strains deleted for *dcp1* or *dcp2* (as in Chapter 3.3) cRT-PCR analysis revealed the presence of decapped transcripts in Δdcp2 mutant strains (Morozov and Caddick, unpublished data) and deletion of *dcp2* and the gene encoding the exosome component, Rrp44, is not lethal in *A. nidulans (*Caddick, personal communication*).* In these respects, *A. nidulans* appears to differ from *S. cerevisiae.* One possible explanation would be that in *A. nidulans* an additional decapping activity is present.

Recent studies showed that Nucleoside Diphosphate linked to X (Nudix) family proteins other than Dcp2 also possess mRNA decapping activity (Song et al., 2013). The Nudix family proteins contain phosphohydrolases which cleave a phosphate bond in their substrate to create two products. Studies have shown that Nudt2, Nudt3, Nudt12, Nudt15, Nudt17 and Nudt19 from mice, are all able to effect decapping, although their relative activity varies significantly (Song et al., 2013). The Nudix superfamily is widespread in bacteria, archaea, viruses, fungi and higher eukaryotes (McLennan, 2006). They are mainly pyrophosphohydrolases which act upon substrates of general structure, **nu**cleoside **di**phosphate linked to another moiety, **X** (NDPX), to yield NMP and P-X (Bessman et al., 1996). There are a variety of Nudix substrates such as (d)NTPs (both canonical and oxidised derivatives), nucleotide sugars and alcohols,

dinucleoside polyphosphates (NpnN), dinucleotide coenzymes and capped RNAs (McLennan, 2006).

Nudix proteins have a conserved 23-amino acid domain which is known as the Nudix motif or Nudix box, Gx5Ex5[UA]xREx2EExGU, where U is an aliphatic, hydrophobic residue. This sequence is located in a loop-helix-loop structural motif and the glutamic acid (E) residues in the core of the motif, REx2EE, plays an important role in binding essential divalent cations. In most cases, Mg^{2+} is likely to be the most physiologically relevant. Several studies have found that each individual residue in the Nudix box play's an important role in catalysis (Mildvan et al., 2005).

The laboratory strains of *E. coli* have 13 Nudix hydrolase-encoding genes (McLennan, 2006) with diverse functions in the cell. Nudix A (NudA) from the *E. coli* has the ability to efficiently convert the mutagenic, oxidised nucleotide 8-OH-dGTP [a product of reactive oxygen species (ROS) attack on dGTP]. Additionally, recent studies showed that one Nudix protein (RppH) from bacteria has decapping activity (Song et al., 2013). RppH, which was formally known as NudH/YgdP, is a pyrophosphohydrolase that hydrolyzes the 5′- triphosphate of prokaryotic RNAs to remove the terminal diphosphate, thus leaving a 5′-end monophosphate RNA (Deana et al., 2008). This is analogous to the RNA product generated by both Dcp2 and Nudt16 decapping enzymes in eukaryotes.

S. cerevisiae has been shown to have six Nudix proteins, known as Npy1p, Ddp1p, Pcd1p, Ysa1p, YJR142w and Dcp2 (Song et al., 2013). Previous studies in yeast have shown that Dcp2 is the main decapping enzyme (Chang et al., 2014; Coller and Parker, 2004; Steiger et al., 2003), and recently it has been shown that Ddp1p has decapping activity *in vitro* (Song et al., 2013). Furthermore, it has been shown that decapping activity was inhibited when the Nudix domain of Ddp1p was mutated (Song et al., 2013). Interestingly, Ddp1p appear to be the

homolog of Nudt3, which suggests that these two proteins were evolutionarily conserved decapping enzymes.

In mammalian system, Dcp2 and Nudt16 were known to have decapping activity. Recently, another six Nudix proteins, Nudt2, Nudt3, Nudt12, Nudt15, Nudt17, and Nudt19, were identified. All these proteins were shown to have varying degrees of decapping activity *in vitro* on both monomethylated and unmethylated capped RNAs (Song et al., 2013). In general, Dcp2 generates m^7GDP as its hydrolysis product, which is similar to the product generated by Nudt17 and Nudt19. However, Nudt2, Nudt3, Nudt12 and Nudt15 produced both m^7GMP and m^7GDP (Song et al., 2013).

Previous study on Nudix proteins in *A. nidulans* led to the identification of five candidates, including Dcp1, and showed that NdxA controls the level of NAD+/NADH in the cell by hydrolysing cellular NAD+/NADH (Shimizu and Takaya, 2013). Additionally, it was shown that NdxA is involved in the negative regulation of sirtuin function and chromatin structure by decreasing the level of the secondary metabolites sterigmatocystin and penicillin G. These two metabolites were important in maintaining the level of acetylation of histone H4, thus explaining the functional link between NdxA and chromatin structure (Shimizu et al., 2012). Furthermore, when the NdxA mutant was grown under the oxygen limited condition, glucose consumption, ethanol and lactate production and cellular ATP levels were all reduced, as compared to the WT (Shimizu and Takaya, 2013).

4.1. Analysis of NUDIX protein sequences.

In order to identify additional potential decapping activities, the NUDIX protein sequences from *A. nidulans* were retrieved from the *Aspergillus* genome database (http://www.aspgd.org/). These were *ndxA* (AN1202), *ndxB* (AN7711), *ndxC* (AN8204), *ndxD* (AN6251) and *dcp2* (AN10010). NUDIX sequences from other fungal species with similarity to the *A. nidulans* NUDIX proteins were identified through a GenBank BLASTp search using

the NUDIX protein sequences of *A. nidulans* (AN1202, AN7711, AN8204 and AN6251). Protein sequences from different fungi species which have an E-value above $10e^{-5}$ and more than 60% coverage from the query were extracted and inserted into the file for alignment. NUDIX protein sequences from higher eukaryotes (*Mus musculus* and *Homo sapiens*) were identified through searches in NCBI database (http://www.ncbi.nlm.nih.gov/). The list of the protein sequences used in constructing the phylogenetic tree is listed in Table 4.1.

4.2. Phylogenetic analysis

All NUDIX proteins, including Dcp2, shared the conserved motif, GXXXXXEXXXXXXXREUXEEXGU, where U is Isoleucine, Leucine, or Valine and X is any amino acid (McLennan, 2006). An alignment was therefore made using partial sequences, including 30 amino acid upstream and downstream from the NUDIX motif (Figure 4.1).

Phylogenetic analysis was carried out from the alignment generated as in Figure 4.1 with 1000 replicates were performed. From the analysis, it shows that Dcp2 and Nudt16 were together in a large group, consistent with the idea that both proteins have a similar function (Song et al., 2013). Additionally, all Dcp2 proteins group together in the same clade (Figure 4.2), indicative of a high level of conservation between species. Interestingly, all four *Aspergillus* Dcp2 orthologues examined segregated together as a sub-clade, indicating divergence from both human and yeast Dcp2 which grouped together.

NdxA (AN1202), which is known to control the cellular level of NAD+/NADH in the cell by catalysing their hydrolysis, is closely related to the mammalian Nudt15 (Figure 4.2). Nudt15 contained nucleoside diphosphatase activity which can hydrolyse m^7Gpp to m^7Gp (Song et al., 2013). Although it was shown that NdxA has a function other than decapping, based on the phylogenetic analysis, NdxA was chosen for further analysis to determine whether it has a role in decapping or not. NdxB (AN7711), which has ADP-ribose pyrophosphatase activity (Shimizu et al., 2012), was grouped together with the ADP-ribose pyrophosphatase and YSA1

protein (Figure 4.2). This clade grouped near to the Nudt15/NdxA clade, therefore, it is also possible that NdxB possesses decapping activity.

NdxD (AN6251) was in the same clade as the fungal MutT proteins and shares the root with the Ddp1p clade from yeast (Figure 4.2). Ddp1p proteins are known to possess a decapping activity by producing m^7GDP and m^7GMP hydrolysis products *in vitro*. Mutations within the Nudix motif in Ddp1p significantly inhibit this decapping activity (Song et al., 2013). Interestingly, these two clades appear to have diverged from the mammalian Nudt3 clade, which has also been shown to have decapping activity (Song et al., 2013). NdxC (AN8204) was grouped with the NADH pyrophosphatase and has diverged significantly away from the other NUDIX and Dcp2 clades.

Based on the phylogenetic analysis, it was postulated that NdxA, NdxB and NdxD are likely to possess decapping activity. Therefore, mutant strains disrupted for the three respective genes were constructed in order to assess if they contribute to decapping and RNA degradation.

Table 4.1. List of NUDIX and Decapping proteins used in the phylogenetic analysis.

Protein	Nomenclature Species	Accession No
Dcp2	*Aspergillus nidulans*	AN10010
Dcp2	*Aspergillus flavus*	XP_002381167
Dcp2	*Aspergillus oryzae*	XP_001824083
Dcp2	*Aspergillus niger*	XP_001401303
Dcp2	*Saccharomyces cerevisiae*	ABN58602
Dcp2	*Saccharomyces arboricola*	XP_011105221
Dcp2h1	*Homo sapiens*	NP_689837
Dcp2h2	*Homo sapiens*	NP_001229306
ndxA	*Aspergillus nidulans*	AN1202
ndxB	*Aspergillus nidulans*	AN7711
ndxC	*Aspergillus nidulans*	AN8204
ndxD	*Aspergillus nidulans*	AN6251
ADP-ribose	*Aspergillus niger*	XP_001390332
ADP-ribose	*Penicillium roqueforti*	CDM36048
NUDIX2	*Aspergillus flavus*	XP_002376712
NUDIX2	*Aspergillus fumigatus*	XP_751032
Nudix/MutT	*Aspergillus niger*	XP_001399320
Nudix/MutT	*Aspergillus clavatus*	XP_001275583
Nudix/MutT	*Aspergillus fumigatus*	XP_753812
NADH.pyro	*Aspergillus flavus*	XP_002382813
NADH.pyro	*Aspergillus oryzae*	XP_001822696
Ysa1p	*Saccharomyces cerevisiae*	NP_009669
Ysa1p	*Saccharomyces kudriavzevii*	EJT41751
Ddp1p	*Saccharomyces cerevisiae*	AHY77454
Ddp1p	*Saccharomyces kudriavzevii*	EHN00180
Pcd1p	*Saccharomyces cerevisiae*	NP_013252
Pcd1p	*Saccharomyces kudriavzevii*	EHN01215
Nudt3	*Homo sapiens*	O95989
Nudt16	*Homo sapiens*	AAH31215
Nudt3	*Mus musculus*	AAH16534
Nudt15	*Mus musculus*	NP_766115
Nudt16	*Mus musculus*	XP_001471808
Nudt16	*Rattus norvegicus*	AAI66915
Nudix2	*Brassica rapa*	XP_009128986

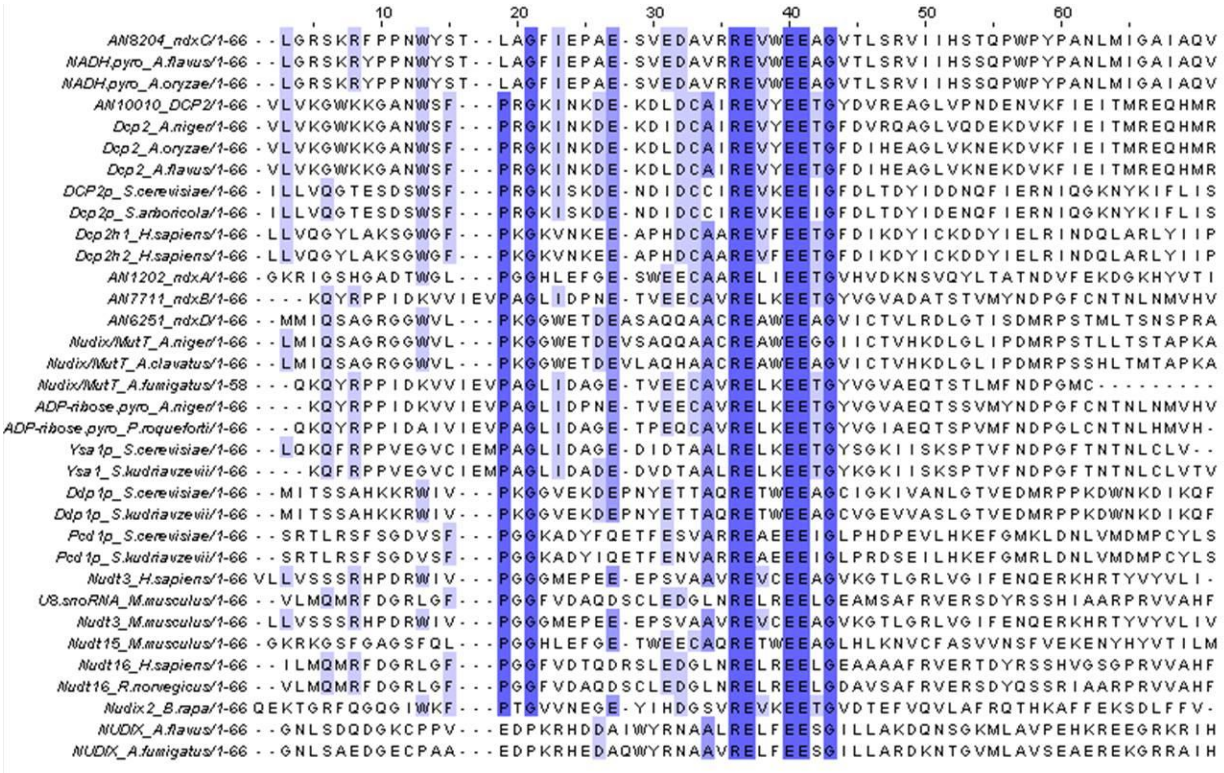

Figure 4.1. Amino acid alignment of NUDIX proteins. Partial (30 amino acids upstream/downstream) sequence alignment for Dcp2 (AN10010), NdxA (AN1202), NdxB (AN7711), NdxC (AN8204) and NdxD (AN6251) were performed using Muscle (Edgar, 2004) program. Identical amino acids are shaded in purple using Jalview software (Waterhouse et al., 2009).

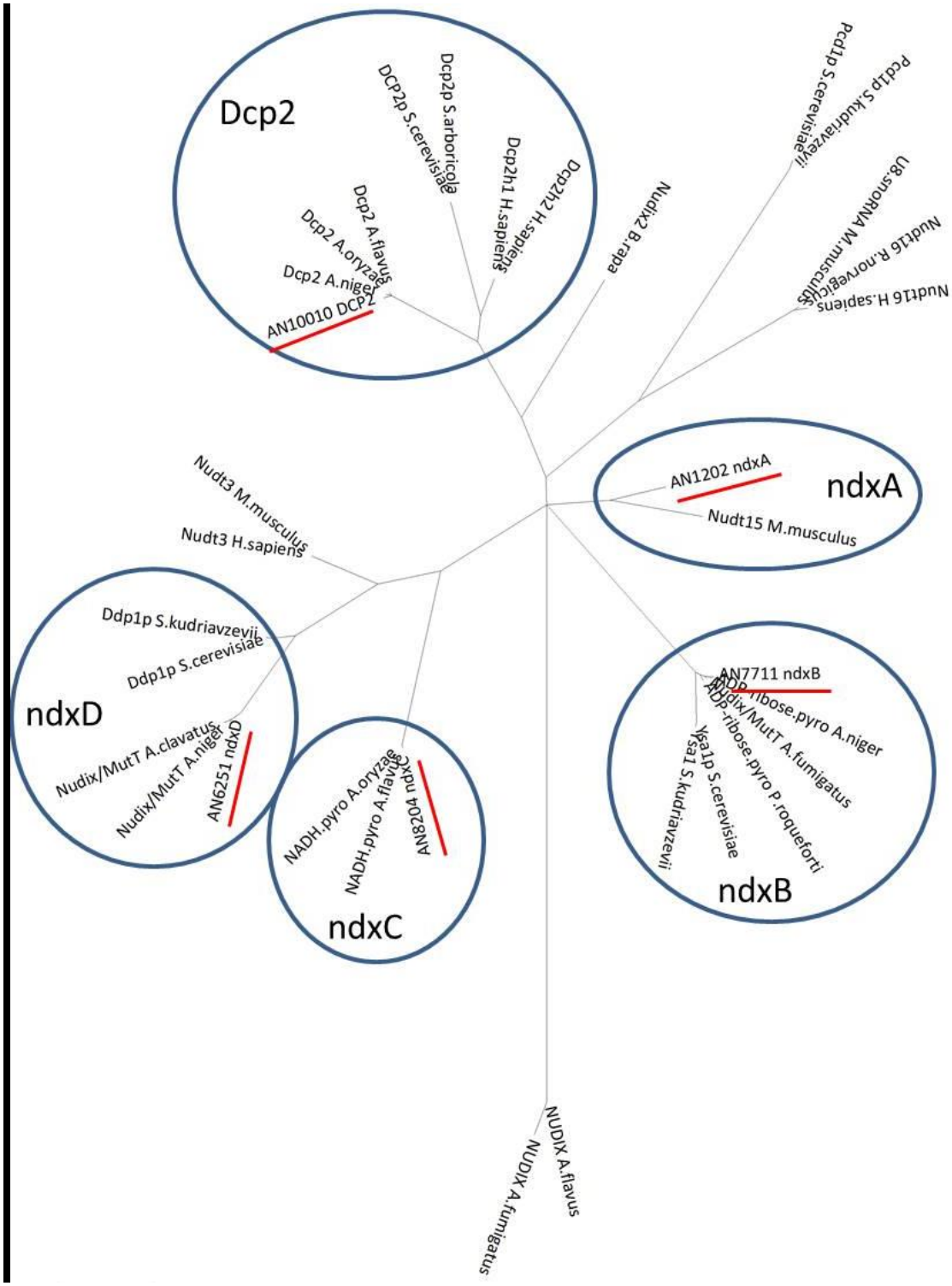

Figure 4.2. Phylogenetic tree of all Dcp2 and NUDIX proteins from different organisms including yeast, fungi, mice and human. The tree was constructed using the partial sequences (30 amino acid upstream and downstream the NUDIX motif (GXXXXXEXXXXXXXREUXEEXGU)). All *A. nidulans* sequences are underline in red. Analysis was carried out using MEGA6 software with Maximum likelihood with 1000 replicates.

4.3. Strain construction

In order to characterise the function of different components in decapping and RNA degradation, strains disrupted for the various activities were required. *ndxA* (AN1202), *ndxB* (AN7711) and *ndxD* (AN6251) were disrupted by transformation and homologous integration of deletion cassettes, produced by the Fungal Genetics Stock Centre. Strain validation was conducted by PCR. An example of this, the validation of *Δ*ndxA alleles, is illustrated in Figure 4.3 where there is no PCR product when internal *ndxA* primers (forward and reverse) were used in amplification of DNA from putative Δ*ndxA* strains but a 600bp PCR product was observed when internal *Af_pyrG* primers (forward and reverse) were used. A schematic diagram showing the location of internal primers (forward and reverse) used in the PCR validation of the native gene and disrupted allele were shown in Figure 4.3 (a). Sequences of all primer used in this experiment were listed in Table 2.1 and the strains constructed are listed as in Table 2.2.

These strains, deleted for genes putatively encoding key components involved in mRNA degradation, were crossed to *uaZ14* strains. *uaZ14* is a mutant allele of the urate oxidase-encoding gene which contains a premature termination codon and is subject to NMD (Morozov et al., 2012).

a)

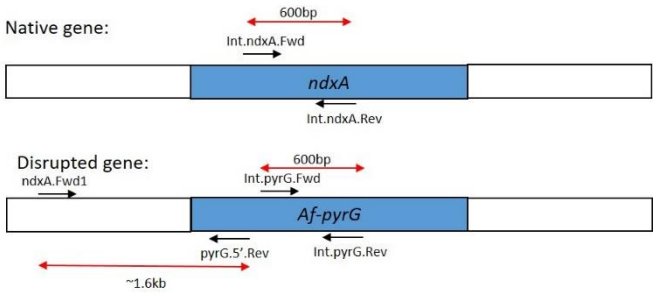

b)

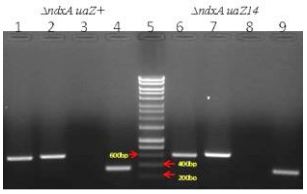

c)

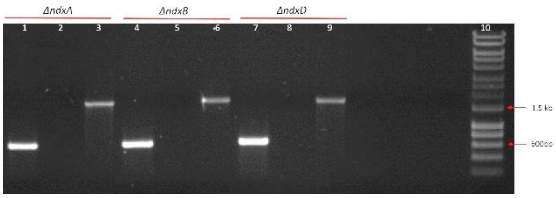

d)

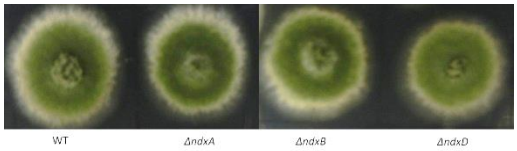

Figure 4.3. Disruption of Nudix (*ndxA*, *ndxB* and *ndxD*) and strain construction.
(a) A schematic diagram showing the location of internal primers (forward and reverse) used in the PCR validation of the native gene and disrupted allele. For example, there is no PCR product when internal *ndxA* primers (forward and reverse) were used in amplification of Δ*ndxA uaZ*$^{+}$ but a PCR product was observed when internal *Af_pyrG* primers (forward and reverse) were used. Primer sequences used in this experiment were listed in Table 2.1 (Chapter 2).
(b) PCR based validation of Δ*ndxA uaZ*$^{+}$ and Δ*ndxA uaZ14* strains using specific primer sets. Based on the picture, a 600 bp band using Int_pyrG primers confirming the introduction of *AfpyrG* gene into the *A. nidulans* genome via homologous recombination (Lane 1,6), a 650bp product Int_ndxB (as positive control) (Lane 2,7), no product using Int_ndxA confirmed deletion of *ndxA* gene from the genome (Lane 3,8) and a 300bp product Int_nkuA (as positive control)(Lane 4,9) and DNA Ladder (Hyperladder1)(Lane 5).
c) PCR based validation of Δ*ndxA*, Δ*ndxB* and Δ*ndxD* strains using specific primer sets. Based on the picture, a 600 bp band using Int_pyrG primers confirming the introduction of *Af-pyrG* gene into the *A. nidulans* genome via homologous recombination (Lane 1,4,7), no band observed when PCR using specific Internal primer (ndxA, ndxB, ndxD) confirmed deletion of respective gene from the genome (Lane 2,5,8), and a band size ~1.6 kb when using specific primer at the 5'UTR of respective gene with pyrG.5'.Rev will confirm the insertion of *Af-pyrG* marker at the correct position in the genome (Lane 3,6,9) and DNA Ladder (Hyperladder1)(Lane 10).
d) Phenotypic observation between Nudix mutants (Δ*ndxA*, Δ*ndxB* and Δ*ndxD*) as compared to WT. There is no *fluffy* cotton-like appearance, unlike in Δ*dcp1* and Δ*dcp2* mutants (Figure 3.1 (c)). All strains were grown on solid MM with required supplements for 3 days at 37ºC.

4.4. Localisation of Nudix proteins

Our initial postulation is that if the Nudix protein involved in the mRNA decay may be localised in the P-bodies. In this study, NdxA, NdxB and NdxD were tagged with either green or red fluorescent protein (GFP or RFP) as described for Dcp2 (Chapter 3.2) and the tagged proteins were visualised using confocal fluorescence microscopy. As expected, all Nudix-tagged GFP were found to localise in cytoplasm (Figure 4.4). To monitor whether NdxA, NdxB and NdxD are localised in P-bodies, all Nudix-tagged RFP were crossed with Dcp1 tagged-GFP, which was shown to localised in P-bodies (Morozov et al., 2010). Based on the confocal fluorescence microscopy, none of the Nudix proteins co-localised with Dcp1 based on the merged images (Figure 4.4 i), ii), iii) (d)). The role of P-bodies and the function of Dcp1 and Dcp2 within them is not well understood, particularly as decapping is known to occur primarily on the ribosomes prior to transcript localisation to P-bodies. Therefore, it remains possible that NdxA, NdxB and NdxD are directly involved in the mRNA decay in *A. nidulans* but that they act separately from Dcp1.

i)

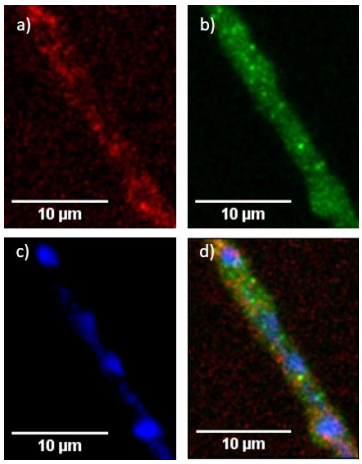

ii)

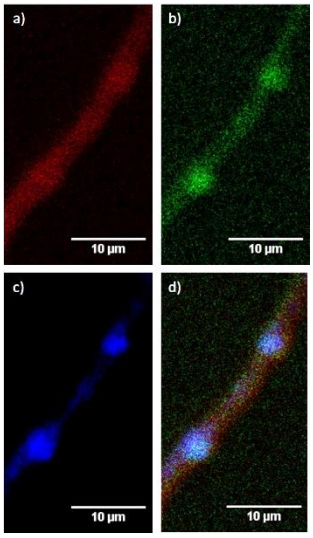

iii)

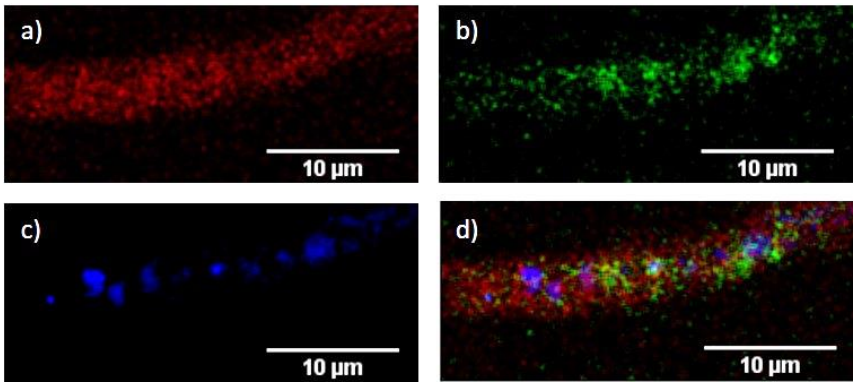

Figure 4.4. Fluorescence microscopy of RFP-tagged Nudix with the GFP-tagged Dcp1. i) NdxA:RFP with Dcp1:GFP; ii) NdxB:RFP with Dcp1:GFP; iii) NdxD:RFP with Dcp1:GFP. A clear '*punctate*' formation observed consistent with the Dcp1-tagged GFP were localised in P-bodies. However, all the Nudix-tagged RFP did not overlap with the GFP signal which indicate that the neither NdxA, NdxB or NdxD were co-localised with Dcp1 in the P-bodies in *A. nidulans*. However, both NdxA and NdxD produces a putnctated distribution. DAPI were used as a control for nuclear staining. 10 µm scale is included (white line). Strains were grown in liquid MM for 16 hours at 30ºC with the addition of NH_4^+ which has been shown to increase the number of P-bodies in *A. nidulans* (Morozov et al., 2010). Nuclear staining was done by adding the 4′,6-diamidino-2-phenylindole (DAPI) (Liu et al., 2009). Image was analysed using Fiji software from ImageJ (Schindelin et al., 2012).

4.5. Nudix and NMD in *A. nidulans*

To study the involvement of the *A. nidulans* Nudix proteins in NMD, the transcript levels for both *uaZ*$^{+}$ and *uaZ14* were monitored in both the wild type background and appropriate Nudix mutant strains (Δ*ndxA*, Δ*ndxA uaZ14*, Δ*ndxB*, Δ*ndxB uaZ14*, Δ*ndxD* and Δ*ndxD uaZ14).* *uaZ14* contains a premature termination codon and is subjected NMD (Morozov et al., 2006). Transcript levels were determined by qRT-PCR analysis using the total RNA from each strain. Based on this analysis, the relative expression levels of *uaZ* and *uaZ14* in Δ*ndxA* and Δ*ndxB* are similar to the that observed for the WT background, which indicates that NdxA and NdxB do not affect the NMD response and are unlikely to be involved in NMD induced transcripts degradation. Interestingly, disruption of NdxD (Figure 4.5) produced similar results to Δ*dcp1* and Δ*dcp2* mutants (see Figure 3.5), with partial suppression of the *uaZ14* NMD response, consistent with NdxD playing a minor but significant role in NMD induced transcripts degradation.

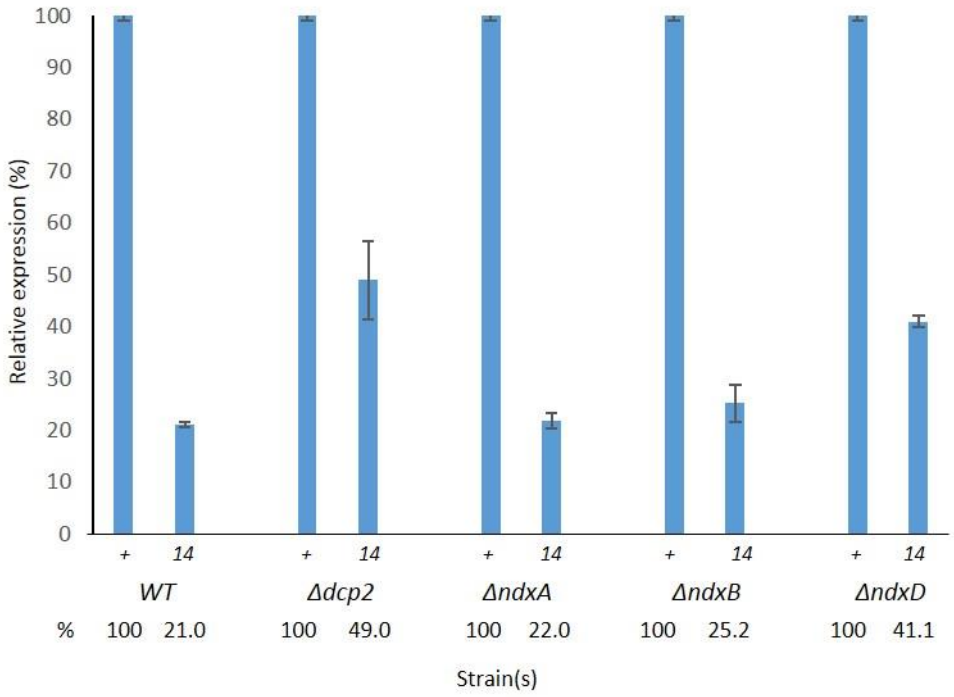

Figure 4.5. Analysis of NMD in different single Nudix mutant backgrounds. qRT-PCR analysis of total RNA samples was conducted to monitor the level of *uaZ*$^{+}$ and *uaZ14* in different genetic backgrounds: the wild type (WT), Δ*dcp2*, Δ*ndxA*, Δ*ndxB* and Δ*ndxD*. 18S rRNA was used as endogenous controls to monitor the expression of the *uaZ* transcript. Relative transcript levels for *uaZ*$^{+}$ and *uaZ14* in the Δ*ndxA* and Δ*ndxB* strains were similar to that observed for the corresponding strains with a wild type background. However, in Δ*ndxD* the proportion of *uaZ14* was 20% higher. The relative transcript levels are indicated for each strain (%). Results are representative of three independent experiments the with the standard error (error bar).

To investigate whether disruption of both the Nudix proteins and Dcp2 will enhance the stabilisation of the transcripts, all three Nudix mutants were crossed with Δ*dcp2* and the respective double mutants isolated. These strain were validated by PCR to confirm that the respective loci were deleted (Figure 4.6 (a)). In all cases the fluffy morphology associated with Δ*dcp2* was displayed by the double mutants (Figure 4.6 (b)).

To assess the impacted on NMD, qRT-PCR analysis of *uaZ*$^{+}$ and *uaZ14* transcript levels was conducted as described previously. Based on the qRT-PCR analysis, the relative transcript levels for *uaZ*$^{+}$ and *uaZ14* in the double mutants, Δ*dcp2* Δ*ndxA*, Δ*dcp2* Δ*ndxB* and Δ*dcp2* Δ*ndxD* were all similar to that of the WT (Figure 4.7). These results indicate that NMD mediated transcript degradation does not involve either the NdxA, NdxB, NdxD or Dcp2. Most suprisiingly, disruption of both NdxD and Dcp2 contrasts with that of the respective single mutants, both of which partially supressed NMD (see Figure 4.5). Interpreting this is not straight forward as the ratio observed is a product of more that one degradation rate; both degradation of wild type transcripts, probably mediated by deadenylation-dependent decapping, and separately NMD dependent degradation of *uaZ14* mRNA. Therefore, dramatic stabilisation of the wild type transcript would result in an apparent increase in NMD. There is also the additional issue, not addressed here, that degradation rates and the associated machinery can influence transcription rates (Braun and Young, 2014; Sun et al., 2013). Consequently the disruption of two factors potentially involved in RNA degradation may have complex interplay that may have impacted on these data.

a)

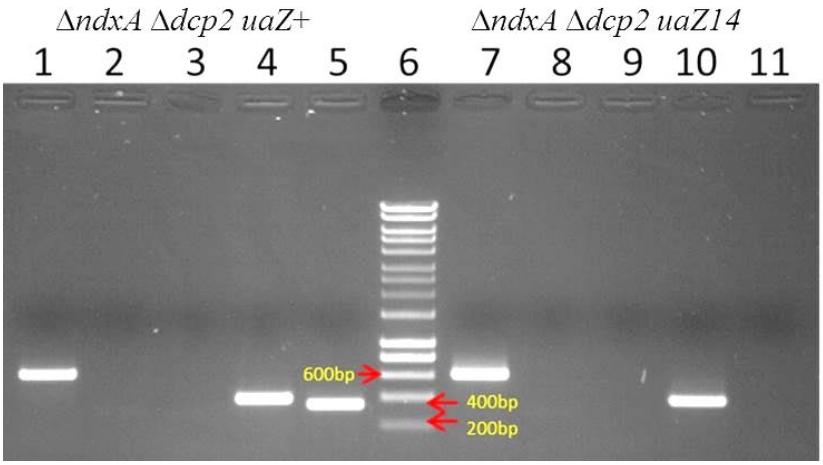

b)

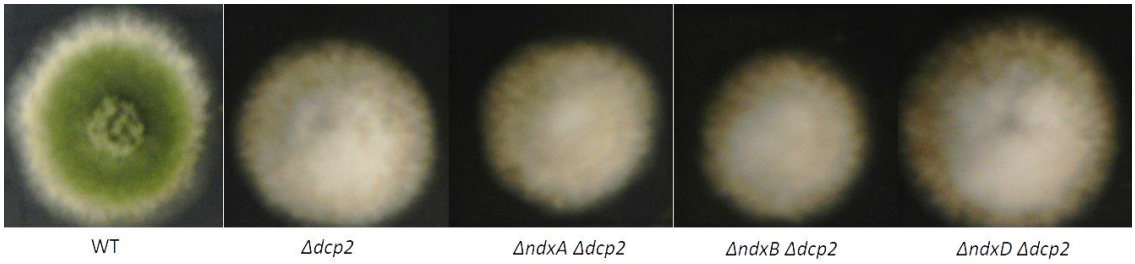

Figure 4.6. Characterisation of Δ*ndx* Δ*dcp2* double mutants. a) PCR based validation of double mutant Δ*ndxA* Δ*dcp2 uaZ*$^{+}$ and Δ*ndxA* Δ*dcp2 uaZ14* using specific primer sets. Based on the picture, a 600bp band using the Int_pyrG primers confirmed the introduction of *Af_pyrG* gene into the *A. nidulans* genome (Lane 1,7) no product using the Int_ndxA primers is consistent with deletion of *ndxA* from the genome (Lane 2,8), no product using Int_dcp2 primers is consistent with deletion of *dcp2* from the genome (Lane 3,9), a 400bp product Int_dcp1 (as positive control)(Lane 4,10), a 300bp product Int_nkuA (as positive control)(Lane 5,11) and DNA Ladder (Hyperladder1)(Lane 6).

b) Phenotypic observation of Nudix double mutants (crossed with Δ*dcp2*) and WT. The *fluffy* cotton-like appeared in double mutants, unlike in all Nudix single mutants where there is no *fluffy* cotton-like appearance. This indicates that the Δ*dcp2* mutants phenotype is epistatic. All strains were grown on solid MM with required supplements for 3 days at 37ºC.

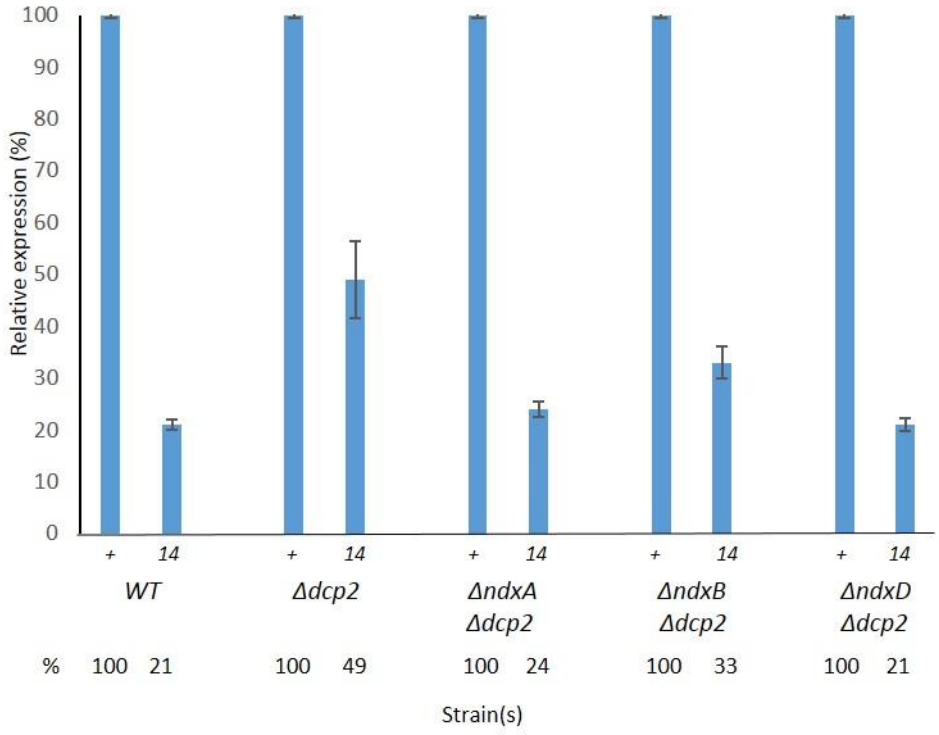

Figure 4.7. Analysis of NMD in Δ*ndx dcp2* double mutants. qRT-PCR analysis of total RNA samples was conducted to monitor the level of *uaZ*$^{+}$ and *uaZ14* in different genetic backgrounds: the wild type (WT), Δ*dcp2*, Δ*ndxA* Δ*dcp2*, Δ*ndxB* Δ*dcp2* and Δ*ndxD* Δ*dcp2*. 18S rRNA was used as endogenous controls to monitor the expression of *uaZ* transcript. Relative transcript levels for *uaZ*$^{+}$ and *uaZ14 in the* Δ*ndxA*, Δ*ndxB* and Δ*ndxD* strains were similar to that observed in the WT background. The relative transcript levels are indicated for each strain (%). Results are representative of three independent experiments with the standard error (error bar).

4.6. Transcript stability in the mutant strains

In order to determine whether disruption of Nudix proteins; NdxA, NdxB and NdxD stabilised wild type transcripts, *uaZ*$^{+}$ was used to monitor the degradation rates. This was investigated using quantitative Northern analysis based on previous studies in *A. nidulans* in which transcription was inhibited using proflavin and transcript degradation monitored over a 30 min timecourse using quantitative Northern hybridisation (Jacobson and Peltz, 1999; Morozov et al., 2012). Preliminary results indicate that the RNA half-life in Δ*ndxA* and Δ*ndxB* were not significantly different from the WT (regression analysis WT:18.53; Δ*ndxA*:19.31; Δ*ndxB*:20.09). However, Δ*ndxD* have a significantly longer half-life as compared to the WT (regression analysis: Δ*ndxD*: 24.57). Based on these results, disruption of NdxA and NdxB did not alter the transcripts stability (Figure 4.8 (a) and (b)). However, disruption of NdxD stabilised the *uaZ* transcript (Figure 4.8 (c)), although significant, this is not a marked as was observed for Dcp2. This result is consistent with NdxD playing a role in transcript degradation.

To further investigate the relationship between the Nudix proteins and transcript stability, the respective Δ*dcp2* Δ*ndx* double mutants were also tested. From the resulting data it is apparent that that the respective double mutants stabilised the *uaZ*$^{+}$ transcripts significantly as compared to the wild type (regression analysis WT:18.53; Δ*ndxA* Δ*dcp2*:25.83; Δ*ndxB* Δ*dcp2*:25.87; Δ*ndxD* Δ*dcp2*:32.78) (Figure 4.9). However, Δ*ndxA* Δ*dcp2* and Δ*ndxB* Δ*dcp2* have a shorter half-life than the Δ*dcp2* single mutant (regression analysis Δ*dcp2*:31.52). For the *uaZ*$^{+}$ transcript half live in Δ*ndxD* Δ*dcp2* and Δ*dcp2* strain are not significantly different and therefore there is not apparent additivity. As such this does not provide any supporting evidence that NdxD acts to decap transcripts via a mechanism that is distinct from Dcp2

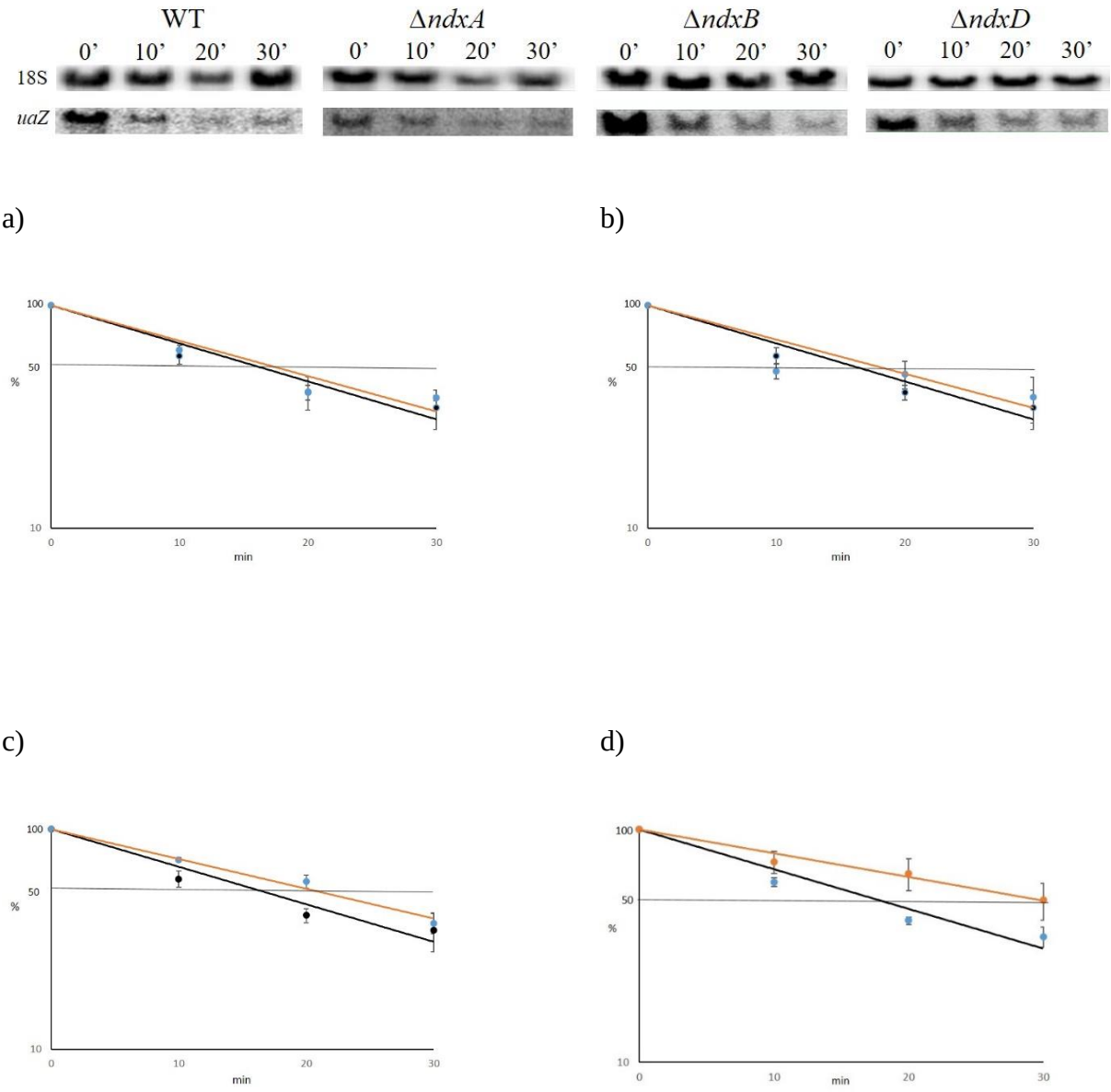

Figure 4.8. Stability of *uaZ* transcripts in WT and single Nudix mutants. a) Δ*ndxA*; b) Δ*ndxB*; c) Δ*ndxD*; d) Δ*dcp2*. Transcript degradation was monitored over a 30 minutes time-course at 30ºC after the addition of 10mM NH_4^+ at t_0. 18S rRNA was used as a loading control. Transcription was inhibited by the addition of proflavin to cultures 10 min before the time-course began. The results represent mean values from two independent replicates. WT (Black line) and mutant (orange line).

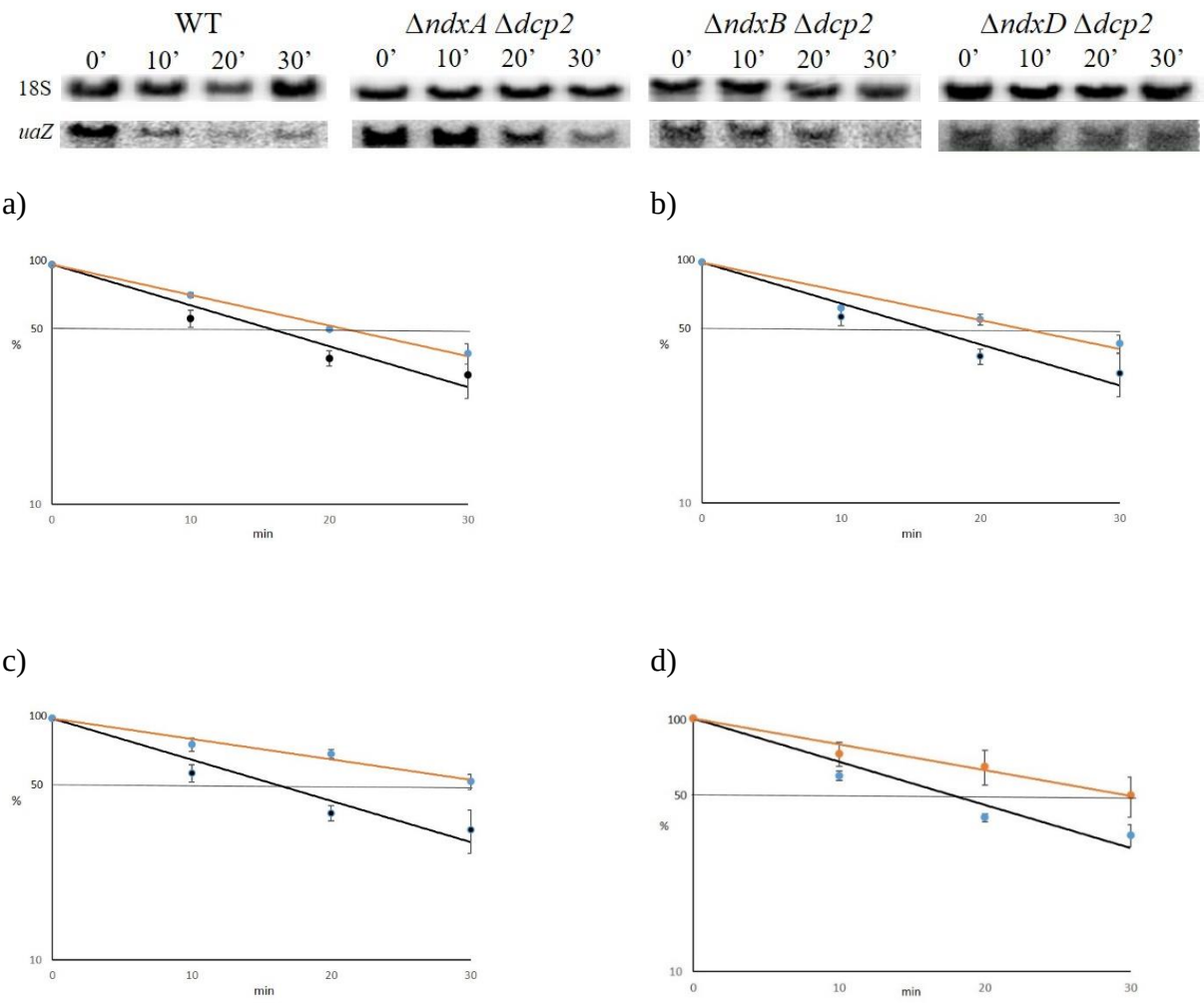

Figure 4.9. Stability of *uaZ* transcripts in WT and Nudix double mutants. a) Δ*ndxA* Δ*dcp2*; b) Δ*ndxB* Δ*dcp2*; c) Δ*ndxD* Δ*dcp2*; d) Δ*dcp2*. Transcript degradation was monitored over a 30 minutes time-course at 30ºC after the addition of 10mM NH_4^+ at t_0. 18S rRNA was used as a loading control. Transcription was inhibited by the addition of proflavin to cultures 10 min before the time-course began. The results represent mean values from two independent replicates. WT (Black line) and mutant (orange line).

4.7. Summary

Decapping is one of the major steps in mRNA decay, which leads to rapid 5' to 3' degradation (Franks and Lykke-Andersen, 2008; Parker and Song, 2004). Dcp2 has been identified as the main decapping enzyme in *S. cerevisiae* (Coller and Parker, 2004). Recent studies showed that other Nucleoside Diphosphate linked to X (Nudix) family proteins also possess mRNA decapping activity (Song et al., 2013). In this chapter, we tried to test whether *A. nidulans* has any additional decapping factors, as in mammalian systems.

To investigate this, bioinformatics analysis was carried out to determine possible decapping proteins from *A. nidulans*. Four Nudix proteins (ndxA, ndxB, ndxC and ndxD) were selected for phylogenetic analysis with the Nudix proteins from other Aspergilli, yeast and mammals. Based on the phylogenetic analysis, Dcp2 and Nudt16 were together in a large group, consistent with the idea that both have a similar function (Song et al., 2013). Additionally, all Dcp2 proteins group together in a same clade (Figure 4.2), which shows that Dcp2 orthologues are relatively well conserved between these species. Interestingly, *Aspergillus* Dcp2 proteins appear to have diverged from human and yeast Dcp2 which appear more closely related.
Additionally, three Nudix proteins in *A. nidulans* (NdxA, NdxB and NdxD) were found to be closely related to proteins from other organisms which posses a decapping activity. NdxA (AN1202) is closely related to the mammalian Nudt15 (Figure 4.2), a protein contained nucleoside diphosphatase activity which can hydrolyse m7Gpp to m7Gp (Song et al., 2013). NdxB (AN7711), which has ADP-ribose pyrophosphatase activity (Shimizu et al., 2012), was grouped together with the ADP-ribose pyrophosphatase and YSA1 protein (Figure 4.2). NdxD (AN6251) was in the same clade as the fungal MutT proteins and it also shares the root with the Ddp1p clade from yeast (Figure 4.2). Ddp1p proteins are known to possess a decapping activity by producing m^7GDP and m^7GMP in its hydrolysis products *in vitro* (Song et al.,

2013). Based on this phylogenetic analysis, it was postulated that NdxA, NdxB and NdxD may possess decapping activity.

Strains disrupted for the three respective Nudix genes were constructed in order to assess if they contribute to NMD and RNA degradation. To study the involvement of Nudix proteins in *A. nidulans* NMD, the Nudix mutants the relative transcript levels of *uaZ14*, which contains a premature termination codon and is subject to NMD, and uaZ^+ were determined. NMD response in Δ*ndxA* and Δ*ndxB* strains was indistinguishable from the WT, consistent with neither NdxA and NdxB being involved in NMD. Interestingly, disruption of NdxD produced similar results to that of Δ*dcp1* and Δ*dcp2*, where the NdxD response was partially supressed (Figure 4.5). However, in the *Δndx D Δdcp2* double mutant NMD appeared to be fully restored to the WT level (Figure 4.7). This result appears to contradict the analysis of the respective single mutants..

General transcript stability in the *Δndx* strains was conducted by utilising Northern hybridisation. In this study, uaZ^+ transcript degradation was monitored over a 30 min time course. Preliminary results showed that disruption of NdxA and NdxB did not alter transcript stability. However, our preliminary observation shows that disruption of NdxD appeared to stabilise the uaZ^+ transcript, although not as dramatically as Dcp2. Again, this result is consistent with NdxD playing a role in transcript degradation. For the transcript degradation rate for the Δ*ndx* Δ*dcp2* double mutants have a shorter half-lives as compared to the Δ*dcp2* single mutant, except for Δ*ndxD* Δ*dcp2* which showed a marginally longer half life (Figure 4.9). These data are not sufficient to demonstrate additivity but are consistent with NdxD having decapping activity. NdxD is closely related to the MutT, a protein which has been shown posses decapping activity in other organism (Parrish et al., 2007). The vaccinia virus D10 protein, which contains of the Nudix/MutT motif,, has been shown to release m^7GDP from

capped RNA substrates. Furthermore, point mutations in the Nudix/MutT motif of D10 proteins abolished decapping activity *in vitro* (Parrish et al., 2007). Yeast Dcp2 also contains a Nudix/MutT motif, and mutational analyses indicates that the region of Dcp2 containing the MutT motif is necessary and sufficient for Dcp2's function in mRNA decapping (Dunckley and Parker, 1999). These observations are all consistent with NdxD playing a role in *A. nidulans* decapping.

CHAPTER 5: DEVELOPMENT OF DECAPPING ASSAY

Introduction

Decapping is one of the major steps in controlling the fate of transcripts in the cell. It would be useful if we can determine the proportion of the transcripts decapped and being degraded. Currently, there are various reported methods to quantify capped transcripts, such as immunoprecipitation of the capped RNA (Abdelhamid et al., 2014) and using Xrn1 treatment to eliminate decapped transcript prior to quantification (Kiss et al., 2016; Mukherjee et al., 2012). However, there are no reliable and sensitive methods that specifically detect and allow quantification of the mRNA in the decapped form. In order to achieve this goal, we tried to develop a simple and fast methods to quantify the proportion of decapped transcripts in a sample.

5.1. Terminator™ 5′-Phosphate-Dependent Exonuclease method

In order to specifically identify the decapped transcripts, we tried several methods. Firstly, we utilised Terminator™ 5′-Phosphate-Dependent Exonuclease treatment. Total RNA was treated with alkaline phosphatase to dephosphorylate the 5′ ends of RNA. This step should specifically dephosphorylate decapped transcripts and block their degradation by the 5′-Phosphate-Dependent Exonuclease. Subsequently, tobacco acid pyrophosphatase (TAP) treatment was applied to de-cap the remaining transcripts. Finally, the samples were treated with the Terminator™ 5′-Phosphate-Dependent Exonuclease which will specifically degrade the phosphorylated decapped transcripts arising from TAP treatment and not the natively decapped, dephosphorylated transcripts in the sample. A schematic diagram of this method is shown in Figure 5.1. However, we failed to get the end product from this method after several attempts.

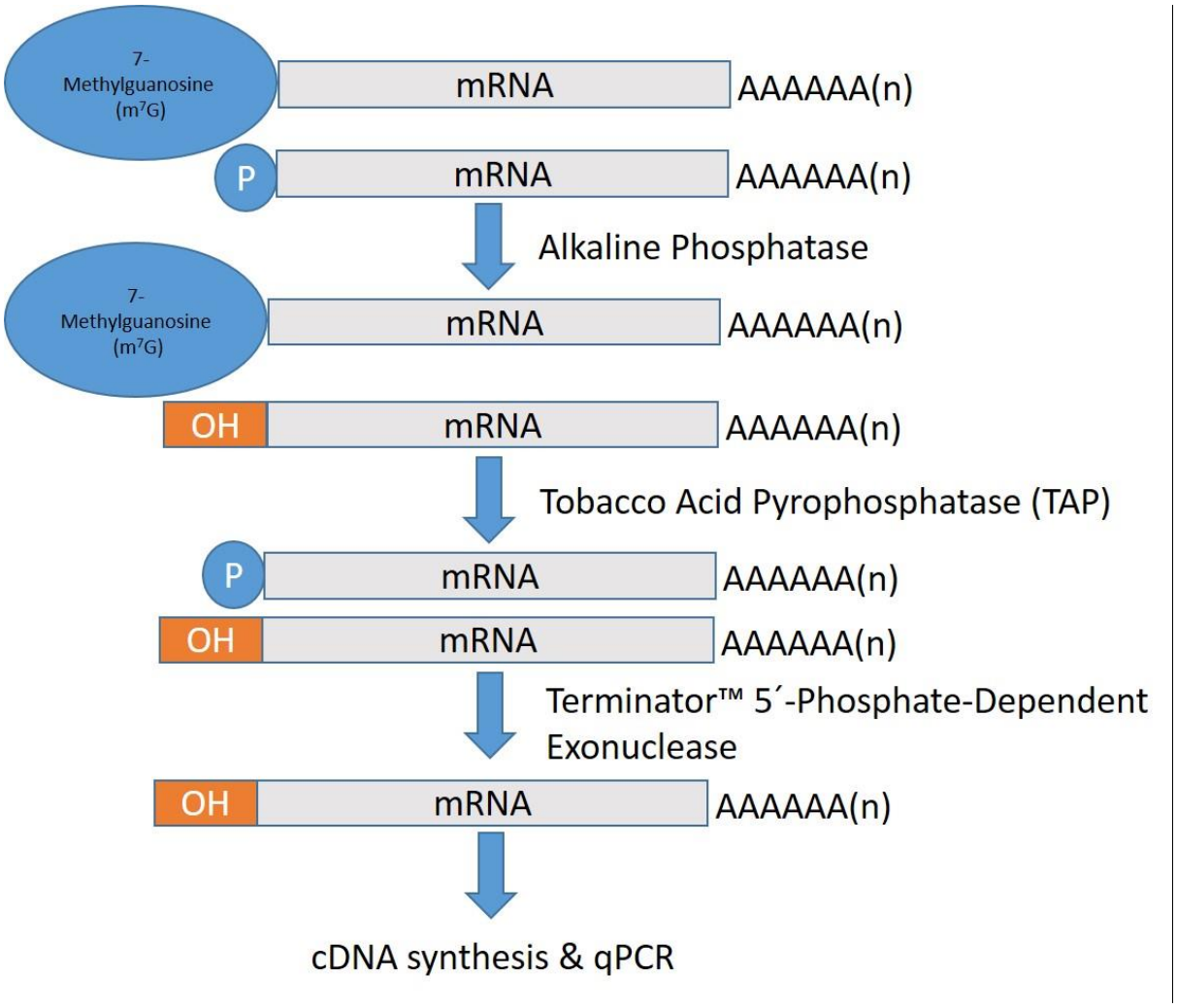

Figure 5.1. Schematic diagram of the Terminator™ 5´-Phosphate-Dependent Exonuclease treatment. Dephosphorylation of the 5´ ends of RNA which substitute the phosphate group (-P) with the hydroxyl group (-OH) was carried out using the alkaline phosphatase. Then, TAP treatment was carried out to remove the 7-methylguanosine (m^7G) from the 5'end mRNA. Finally, the sample was treated with the Terminator™ 5´-Phosphate-Dependent Exonuclease which will specifically degrade the phosphorylated decapped transcripts arising from TAP treatment and not the natively decapped dephosphorylated transcripts in the sample.

5.2. Splinted-primer ligation method

An alternative approach was to specifically tag decapped mRNA with an oligonucleotide, in order to facilitate subsequent qRT-PCR amplification of the primer ligated mRNA. We attempted to ligate a DNA-RNA primer to the decapped transcripts using the single-stranded RNA ligase, RNA Ligase 1. However, we consistently failed to get the final PCR product. The most likely reasons were the low proportion of decapped mRNA and the inefficiency of the ligation reaction.

As an alternative approach, we attempted to utilise a splinted-ligation method in which a DNA-primer is used to enhance the ligation of an RNA adapter to the 5'-end of all decapped transcripts. A splinted-ligation method has been used before to quantify specific transcripts, *RPL41A* and *YLR084C* from the *S. cerevisiae* (Blewett et al., 2011). However, this method is limited as it requires a specific splinted-primer for each transcript and will only be effective for one specific 5' end. Here, we tried to use the same principle, but with a universal splinted-primer having random nucleotides (N_4, N_6, N_8) at it's 5' end so that it can potentially hybridise with any RNA sequence and facilitate the ligation of the RNA primer (Figure5.2).

In this study, a 49 nucleotide RNA adapter (5'-UUU GGA UUU GCU GGU GCA GUA CAA CUA GGC UUA AUA CUC GAG UCC GAC G-3') was used. This was derived from the published sequence of a primer used in a large-scale sequencing project to characterise the sequence diversity of transcription start sites (Gowda et al., 2007). The adapter was synthesised by Integrated DNA Technologies (IDT).

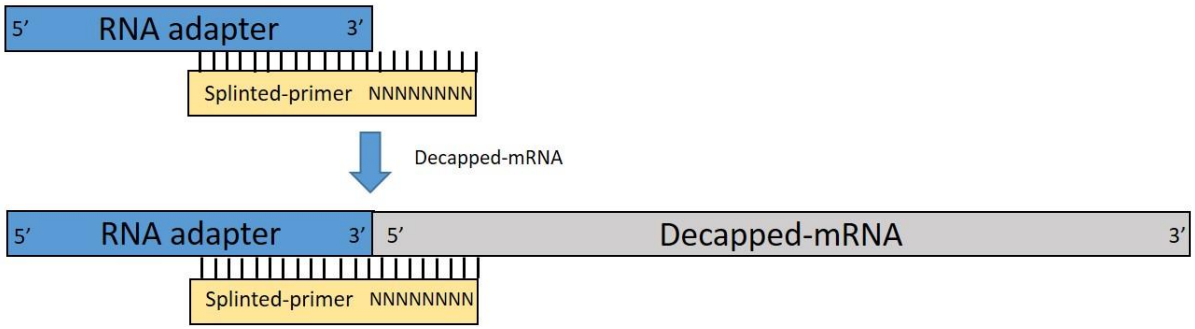

Figure 5.2. Splinted-primer ligation strategy. A DNA splinted-primer was designed which included 14 nucleotides complementary to the 3'-end of the RNA adapter and extended with random nucleotide (N_4, N_6 or N_8) at the 5'-end. The DNA primer was hybridised to a 49 nucleotides RNA primer. This was then added to an RNA sample, potentially allowing it to hybridise with any 5'-ends of decapped transcripts. The aim being to produce a good substrate for the ligase, facilitating efficient addition to the 49 nucleotides RNA primer to decapped mRNA irrespective of the transcripts 5' sequence.

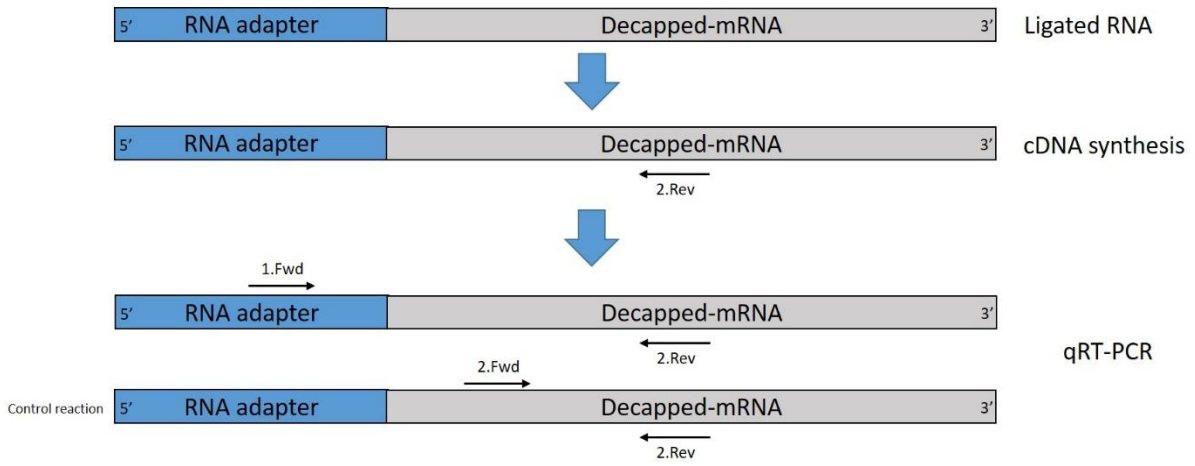

Figure 5.3. qRT- PCR analysis of decapped transcripts. Prior to PCR, the RNA primer was ligated to native decapped transcripts. The transcript was then reverse transcribed for cDNA synthesis. The resulting cDNA, depicted above, was then used for qRT-PCR using two specific PCR reactions. cDNA derived from decapped mRNA ligated to the RNA primer was specifically amplified using primer *1. Fwd* (which located within the 5' adaptor specified sequence) and primer *2.Rev*.As a control, to amplify all cDNA, derived from both the capped and uncapped mRNA, primer *2.Fwd* and primer *2.Rev* were used.

5.3. Optimisation of the ligation method

To develop the decapped RNA assay, optimisation of various components and steps was required. The first step was to choose the best ligase to be used in the assay. In this experiment, three ligases (DNA Ligase 1 (NEB), RNA Ligase 1 (NEB) and RNA Ligase 2 (NEB)) were tested to see which gave the best results.

To test the system RNA was pre-treated with the tobacco acid pyrophosphatase (TAP) to remove the 5' cap (Schaefer, 1995) so that the RNA adapter can be ligated to the decapped transcripts. TAP-treated RNA was used, as the proportion of natively decapped transcripts in the mRNA population was expected to be very low. To test if the ligation had been successful qRT-PCR was conducted to detect two transcripts *uaZ* and *gdhA*. This included a PCR with two transcript specific primers as a positive control and separately a test PCR, which involved the same transcript specific reverse primer and a forward primer specific for the ligated RNA oligo sequence (Figure 5.3). The splinted-ligation step was regarded as successfull when a product from the test PCR of the expected size appeared on the gel after qRT-PCR.

Based on the gel picture (Figure 5.4), successful ligation was achieved with RNA Ligase 1 (sample B), RNA Ligase 2 (sample C) and DNA Ligase 1 with the commercially DNA Ligase buffer (NEB) (Sample D:Lane 1 and 3), where products for both *uaZ* and *gdhA* were visible on the gel. Based on the intensity of the bands RNA Ligase 1 appeared to give the best results. However, for DNA Ligase 1 using the published ligation buffer (Nilsen, 2013) developed for the 5' RNA sequencing analysis, no products were observed (Sample A: Lane 1 and 3). There is only one difference between this ligation mixture and the commercially available DNA ligase 1 buffer (NEB), which is the presence of polyethylene glycol (PEG) in the ligation mixture (as in Step 2.13). RNA Ligase 1 was chosen for the subsequent

experiments because it gave the most end product (*uaZ* and *gdhA*) based on the gel picture (Figure 5.4). Additionally, from multiple experiments, more consistent results were achieved using RNA Ligase 1 compared to other ligases tested.

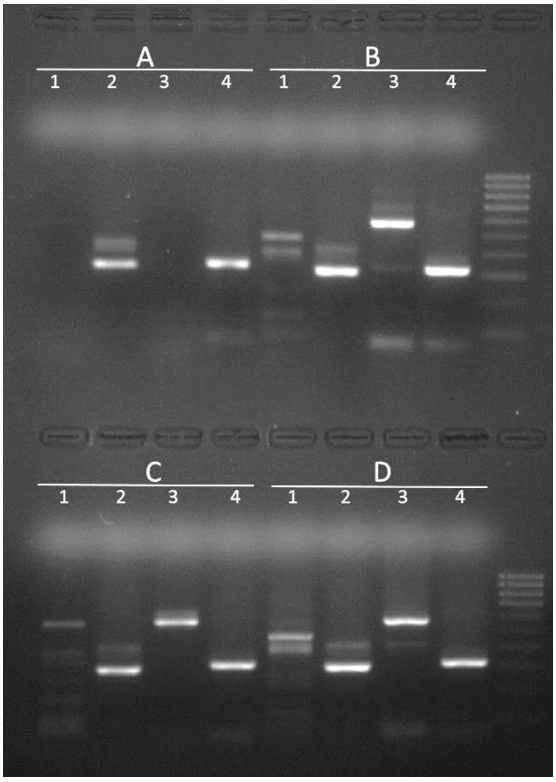

Figure 5.4. Optimisation of primer ligation to mRNA 5' ends. Ligation of 5' RNA adapter was undertaken using (A) DNA Ligase 1 (NEB), (B) RNA Ligase 1 (NEB), **(C)** RNA Ligase 2 (NEB)and (D) DNA Ligase 1 (NEB) with the commercial DNA ligase buffer (NEB). Lane 1: *uaZ* gene (1.Fwd/2.Rev), Lane 2: Internal *uaZ* (2.Fwd/2.Rev), Lane 3*: gdhA* gene (1.Fwd/2.Rev), Lane 4: internal *gdhA* (2.Fwd/2.Rev). Based on the gel picture, RNA Ligase 1 and RNA Ligase 2 were good candidates. However, DNA Ligase 1 only worked when used together with the commercial DNA Ligase buffer (NEB).

5.4. Quantification of decapped transcripts in different *A. nidulans* single mutants

In order to test whether the methods developed above can be used to quantify levels of decapped mRNA in different samples, several *A. nidulans* mutant strains which might have altered RNA degradation processes were analysed. There was no decapped RNA specific amplification product detected, for any of the strains used. One possibility is that decapped transcripts are rapidly degraded by Xrn1, an exoribonuclease which is known to hydrolyzes RNA in the 5' to 3' direction (Blewett et al., 2011; Mullen and Marzluff, 2008) and consequently, decapped mRNA is at too low a concentration to be detected. To test this hypothesis, we undertook analysis of RNA samples from a number of strains, including Δ*xrn1* (Figure 5.5). From this only the RNA sample derived from the Δ*xrn1* strain produced visible PCR product. This is consistent with Xrn1 being the major exonuclease responsible for degradation of the *uaZ*$^{+}$ mRNA in *A. nidulans*, the decapped transcripts being stabilised in the Δ*xrn1* strain allowing them to be detected.

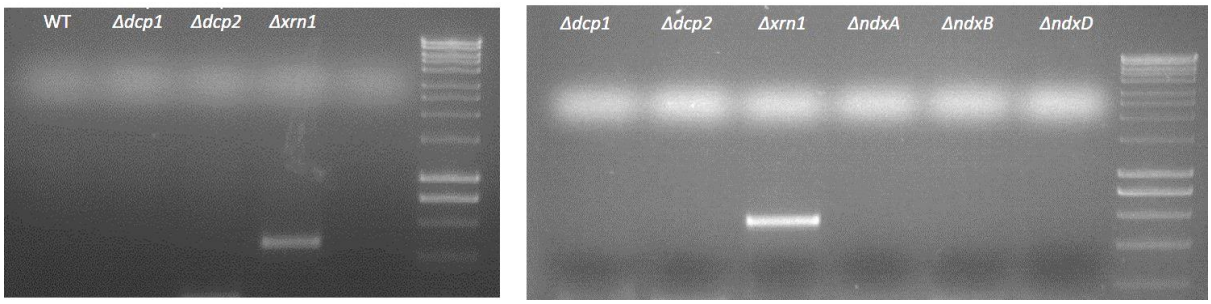

Figure 5.5. Amplification of decapped *uaZ* mRNA in different *A. nidulans* mutant strains. Primer ligation-mediated RT-PCR was conducted using total RNA extracted from WT and mutant strains (as indicated) to detect decapped *uaZ* mRNA. No PCR products were produced for the WT or mutants tested with the exception of Δ*xrn1*. The identity of the PCR product produced was similar to the expected size.

5.5. Quantification of decapped transcripts

5.5.1 Strain construction

To take into account the requirement for Δ*xrn1* in order to detect the decapped mRNA, all mutants to be tested in this study were crossed into the Δ*xrn1* background so that the decapped transcripts will be stabilised and not degraded by Xrn1. Δ*dcp2*, Δ*ndxA*, Δ*ndxB* and Δ*ndxD* were successfully crossed with Δ*xrn1*, and the respective double mutants produced. However, multiple attempts to crosses Δ*dcp1* with Δ*xrn1* failed to give a positive double mutant from over 20 mutants tested. It seems like the crosses did work because we got the re-assortment of the markers, however, failure to get the double mutant might indicate the double mutant is lethal.

5.5.2 Quantification of decapping

In order to determine if mutations in the nudix proteins affected decapping, total RNA was extracted from Δ*xrn1* strains disrupted for the putative decapping activities: Dcp2, NdxA, NdxB and NdxD. Primer ligation-mediated qRT-PCR was conducted for each of the double mutants and compared to the Δ*xrn1* single mutant. Based on the qRT-PCR analysis, the proportion of decapped *uaZ* transcripts was reduced by 20% in the in Δ*dcp2* Δ*xrn1* strain (Figure 5.6). These data supported the hypothesis that Dcp2 is a major decapping activity in *A.nidulans*. However, there does appear to be a significant amount of decapped *uaZ* mRNA in Δ*dcp2* Δ*xrn1,* which is consistent with our hypothesis that there is another protein involved in decapping mRNA.

The qRT-PCR analysis also indicated that the proportion of decapped *uaZ* mRNA in Δ*ndxA* Δ*xrn1* and Δ*ndxB* Δ*xrn1* was marginally reduced (about 5%) as compared to Δ*xrn1*. With respect to ndxA, this result is surprising because a previous study showed that NdxA was involved in controlling the total levels of NAD^+/NADH and negatively regulates sirtuin

function and chromatin structure (Shimizu et al., 2012). It is possible but perhaps surprising if NdxA also has a minor decapping function.

Interestingly, the relative proportion of decapped *uaZ* transcripts in Δ*ndxD* Δ*xrn1* strain is similar to that of the Δ*dcp2* Δ*xrn1* strain and distinct from the relatively minor reduction observed in both Δ*ndxA* Δ*xrn1* and Δ*ndxB* Δ*xrn1* strains. These data suggest that NdxD may play a significant role in decapping.

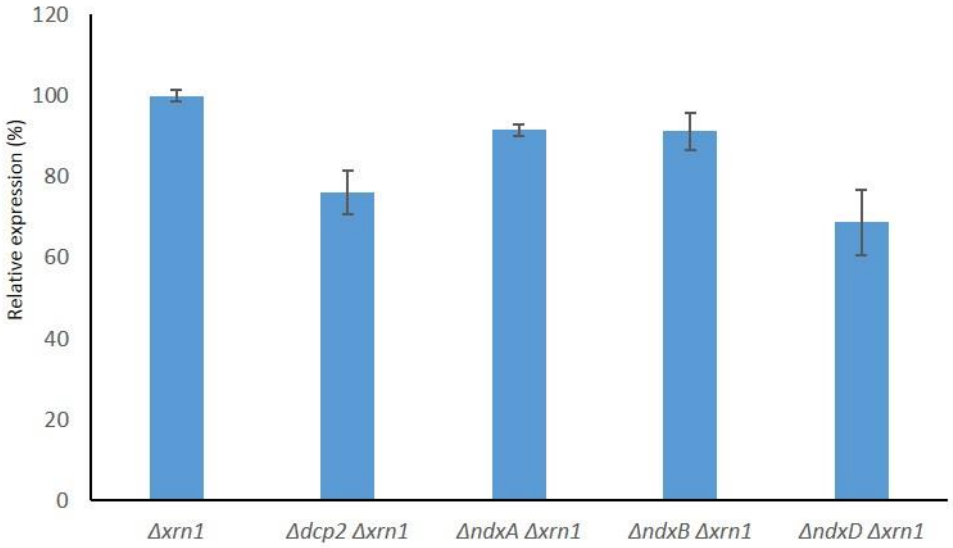

Figure 5.6. qRT-PCR analysis of decapped *uaZ* transcripts from different *A. nidulans* strains. The relative amount of decapped *uaZ* RNA was calculated after normalisation against the Δ*xrn1* using the ΔΔCt method (Livak and Schmittgen, 2001). Internal *uaZ* (2.Fwd/2.Rev) was used as endogenous controls to compare the expression of the decapped *uaZ* transcript (1.Fwd/2.Rev). qRT-PCR in the mutant strains showed a significant amount of decapped transcripts of *uaZ* in the Δ*dcp2* Δ*xrn1* (unpaired t-test, t=4.8377, P=0.0084), Δ*ndxA* Δ*xrn1* (unpaired t-test, t=4.9863, P=0.0076), Δ*ndxB* Δ*xrn1* (unpaired t-test, t=5.8704, P=0.0042), Δ*ndxD* Δ*xrn1* (unpaired t-test, t=4.6110, P=0.0099) with respect to the Δ*xrn1*. Results are representative of three independent experiments with the standard error (error bar).

The amplification products from the qRT-PCR were subjected to agarose gel electrophoresis. Surprisingly, the size of the final product obtained from primer ligation-mediated PCR were smaller than the internal control (Figure 5.7-Lane 1 and 2 as compared to Lane 3). This was unexpected and contradicts the preliminary work in developing the assay. To confirm the identity of the PCR products they were purified and sequenced. The presence of the full 38 bp sequence equivalent to the RNA adaptor sequence (Figure 5.8) at the 5'-end of the decapped transcript confirmed successful ligation between the RNA adapter and 5'-end of the decapped transcript using the splinted-ligation process. However, in all four cases the transcript was truncated with respect to the expected 5' end, the primer ligating at a sequence within the putative *uaZ* coding region.

Interpreting these data is, therefore, problematic. The control PCR indicates that transcripts extend beyond the 5' end defined by primer ligation-dependent PCR and that these are a major form as smaller. This is also consistent with the putative gene structure and previously identified 5' UTR based on cRT-PCR (Morozov et al., 2006). One possibility is that aberrant decapped transcripts accumulate in *Δxrn1*. For example, these could be transcriptional artefacts normally removed by Xrn1. However, this calls into question any conclusions arising from these assays which will require further characterisation and development.

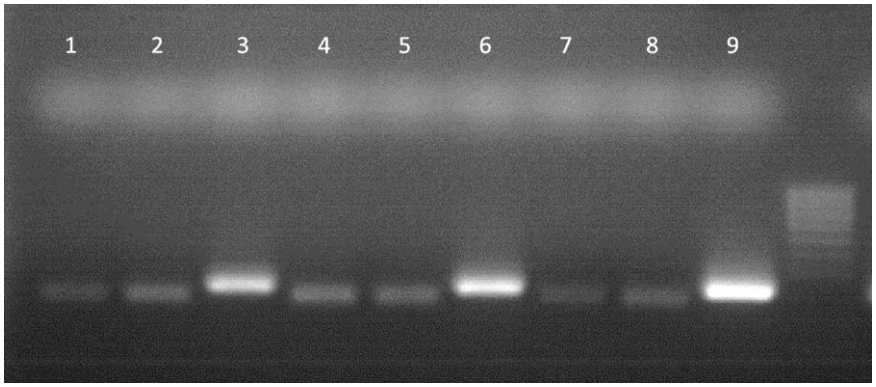

Figure 5.7. Amplification of *uaZ* in different *A. nidulans* double mutant strains. There are PCR products in all mutants tested; decapped uaZ (*primer 1.Fwd* and *2.Rev*) Δ*dcp2* Δ*xrn1* (Lane 1 & 2), Δ*ndxA* Δ*xrn1* (Lane 4 & 5), Δ*xrn1* (Lane 7 & 8). Internal *uaZ* (primer 2.Fwd and 2.Rev) was used as a control (Lane 3,6 and 9). However, the size of the final product of *uaZ* obtained from the ligation between RNA adapter and decapped transcripts were smaller than the internal control (i.e Lane 1 and 2) as compared to Lane 3. The identity of the PCR product produced was confirmed by sequencing.

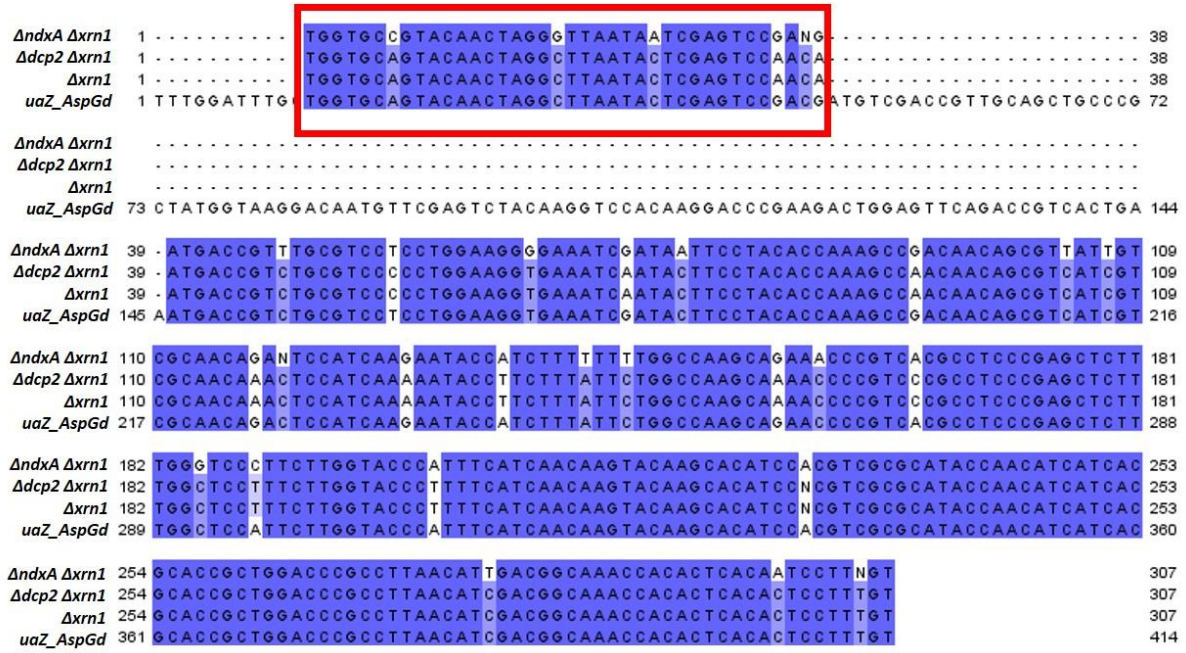

Figure 5.8. Sequence alignment of *uaZ* from the PCR product arising from primer ligation. The presence of 38 bp from the RNA adaptor sequence at the 5'-end of the transcript (Red box). cDNA confirms that the splinted-ligation process was successful. Interestingly, the *uaZ* sequence from the qRT-PCR starts 96 bp downstream from the start codon of *uaZ* (*uaZ_AspGd*–retrieved from the *Aspergillus* genome database) in three different strains (Δ*ndxA* Δ*xrn1*, Δ*dcp2* Δ*xrn1* and Δ*xrn1*)contrary to the expected 5' UTR. Sequence alignment was performed using Muscle (Edgar, 2004) program. Identical nucleotide is shaded in purple using Jalview software (Waterhouse et al., 2009).

5.6. Summary

In this chapter, work aimed at the development of an easy and fast method to quantify the amount of decapped transcripts in RNA population have been described. After several trials of different methods and protocol has been developed which utilised the use of splinted-ligation process. In this method an RNA adaptor is ligated to the 'free' 5'-end of decapped mRNA by the help of splinted-primer. RNA Ligase 1 was chosen as the most efficient and most robust enzyme for performing this task.

After successfully developing the method, several mutant strain were selected for the assay to determine the relative level of decapped to capped transcripts. Unfortunately, failure to get PCR products using single mutants led us to cross the single mutants of interest with the Δ*xrn1* disrupted for an exoribonuclease which hydrolyses decapped transcripts (Mullen and Marzluff, 2008). Inactivation of Xrn1 has been shown to stabilise decapped transcripts and inhibit the 5′ decay in other systems (Blewett et al., 2011). After successfully generating the double mutants, the full assay was performed to quantify decapped transcripts using the primer ligation method developed. Theoretically, the assay developed will only ligate the RNA adapter with the 'free' decapped transcripts and not to the capped transcripts because of the presence of cap at it's 5'-end. In yeast, Dcp2 is known as the main protein that removes the cap from the mature transcripts, thus our working hypothesis was that the same situation pertains to *A. nidulans*. In Δ*dcp2* it was expected that primer ligated to mRNA could not occur since the decapping activity would be absent. Contrary to this, in Δ*dcp2* primer ligation-mediated PCR product was detected which suggests that there is another decapping activity in addition to Dcp2. This result verified the initial findings from the cRT-PCR analysis, where decapped transcripts were found in Δ*dcp2* (Morozov and Caddick, unpublished data). This result is consistent with *A. nidulans* being similar to mammalian systems which have two main decapping enzymes, Dcp2 and Nudt16 (Song et al., 2013).

Quantification of the proportion of decapped mRNA indicated that disruption of either dcp2 or ndxD had a similarly significant effect. Based on these data which suggest Dcp2 and NdxD are the primary decapping activities in *A.nidulans*. We attempted to make the triple mutant Δ*ndxD* Δ*dcp2* Δ*xrn1*, which may indicate the full loss of decapping, however, we were unable to achieve this. One possibility is that this strain is inviable.

A major concern as to the validity of this approach relates to the finding that the size of final products from the qRT-PCR is smaller than expected size. One possibility is that the adaptor preferentially ligates to the smaller decapped/degraded transcript. Further optimisation steps are required to develop a robust assay. However, the assay developed in this chapter provides a good basis for further development.

CHAPTER 6: POLYSOME ANALYSIS

Introduction

A previous study has shown that in *A. nidulans* Δ*cutA* and Δ*cutB* mutant strains, NMD is functional but that transcript subject to NMD are disproportionately retained within the polysome fractions (Morozov et al., 2012). Transcript 3' pyrimidine tagging, which is mediated by CutA and CutB,is proposed to promote the recruitment of Lsm1-7 protein complex and thus activate decapping by Dcp2 (Morozov et al., 2012). To investigate whether disruption of the decapping factors, Dcp1 and Dcp2, also lead to a similar effect we undertook polysome profiling and the distribution of transcripts was monitored (see 3.4). This work uncovered an unusual pattern in the ribosome profile of Δ*dcp1* mutant strains. This suggested that Dcp1 and/or Dcp2 may play a role in ribosome degradation and this chapter describes the analysis undertaken to investigate this.

6.1. Polysome profiles in *A. nidulans*

Polysome profiling is one of the methods widely used to study the translation process. This utilises sucrose density gradient centrifugation, which separates mRNAs bound to multiple ribosomes, known as polyribosomes (polysomes), from single ribosomes (monosomes) and the large and small ribosomal subunits (Esposito et al., 2010). Normally, taking samples from the bottom of the sucrose gradient (highest density) the first two or three peaks of RNA (as determined by UV spectrophotometry) that appear on the polysome profile represent the polysomes. These peaks correlate to the fractions with the highest density and consist of more than one ribosome attached to a single transcript. The largest peak is generally the monosome peak (80S) which represents single ribosomes, followed by a large subunit peak (60S) and small subunit peak (40S). Examples of polysome profiles from *A. nidulans* are given in Figure 6.1.

The methods for polysome profiling from *A. nidulans* has been developed and optimised previously (Morozov et al., 2012). This utilises the antibiotic cycloheximide, which binds to the 60S ribosomal subunit and blocks translation elongation (Xu et al., 2006) by preventing the release of deacylated tRNA from the ribosome E site after translocation (Pestova and Hellen, 2003), thus stalling the translating ribosomes on the mRNA and stabilising the polysomes (Mašek et al., 2011).

6.2. Assess different profile in *dcp1* mutant

The polysome profiles of strains disrupted for either *dcp1* or *dcp2* were compared to wild type (Figure 6.1). One of the decapping mutant strains (Δ*dcp1*) appeared to have a relatively large 60S peak which distinguished it from WT (Figure 6.1 (c)). Disruption of *dcp2* (Figure 6.1 (d)) did not result in the same aberrant profile, although the respective proteins are known to act together in decapping mRNA (Chang et al., 2014; Valkov et al., 2016). To confirm that this difference is associated with disruption of *dcp1* and does not relate to an unidentified background allele several additional Δ*dcp1* mutant strains, obtained by outcrossing the original Δ*dcp1* strain, were also subjected to polysome profiling. In all three cases, a similar aberrant polysome profile was observed consistent with the higher 60S peak being a consequence of *dcp1* deletion (Figure 6.2).

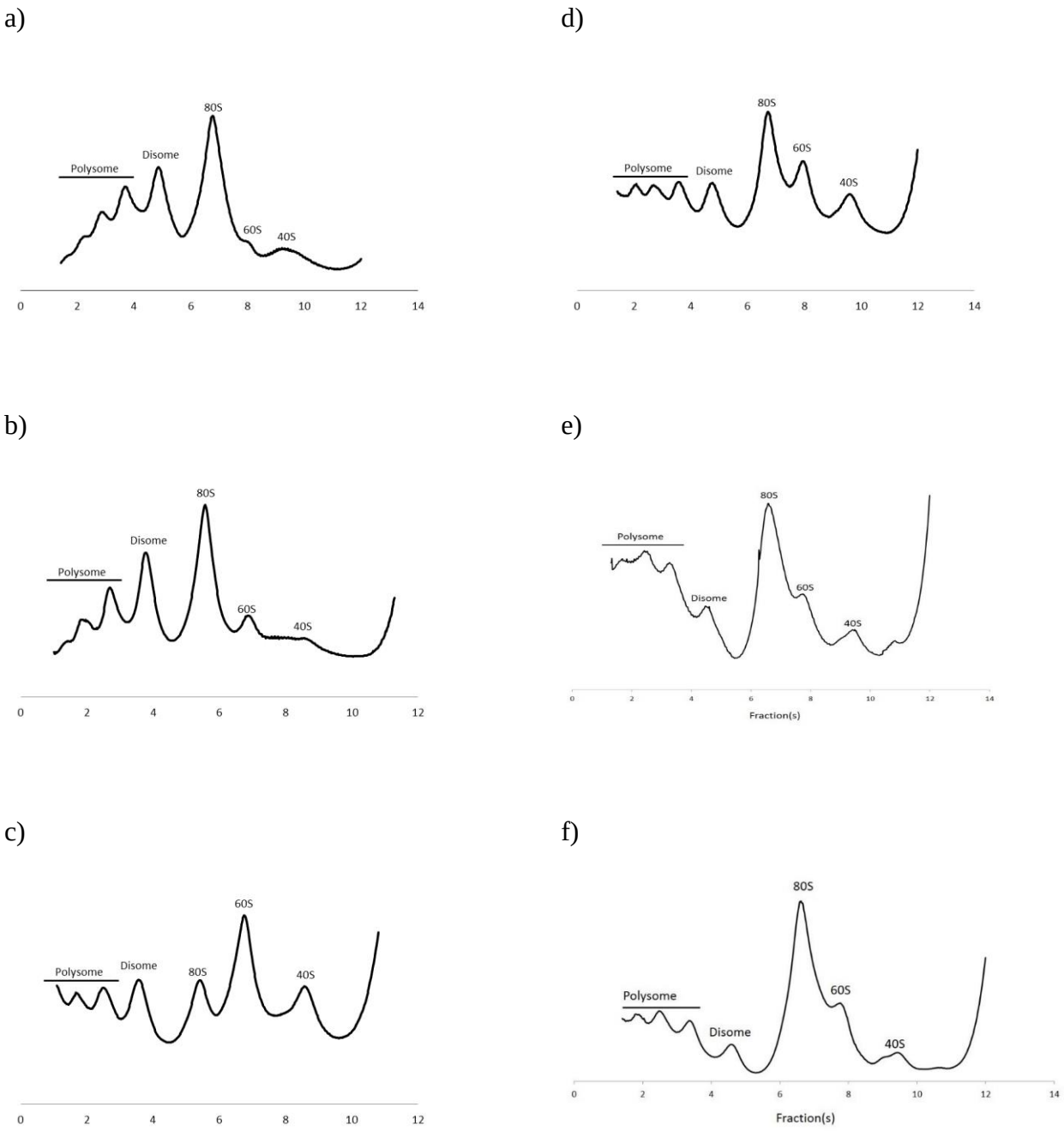

Figure 6.1. Polysome profiles from different *A. nidulans* strain. Cell-free extracts derived from three strains (a) WT; (b) *uaZ14* (c) Δ*dcp1 uaZ14*; (d) Δ*dcp2 uaZ14; e)* Δ*dcp1* Δ*dcp2; f)* Δ*dcp1 dcp2*^{E148Q} were subject to ribosome profiling using sucrose density centrifugation. Cell lysates were separated on a 10-50% sucrose gradient and the absorbance at 254 nM along the gradient was monitored. The sedimentation position of ribosomal complexes (40S, 60S, 80S, disome and polysomes) is indicated on each panel. Results are representative of multiple (≥ 3) independent experiments.

a)

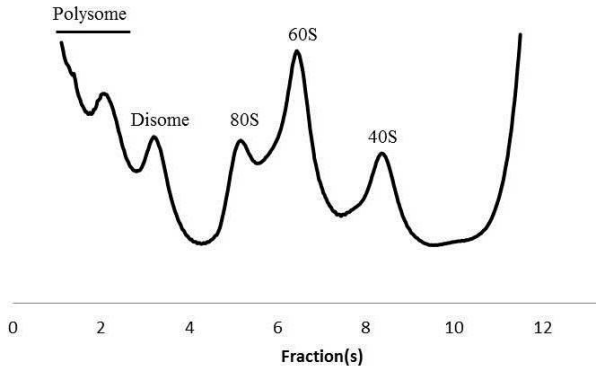

b)

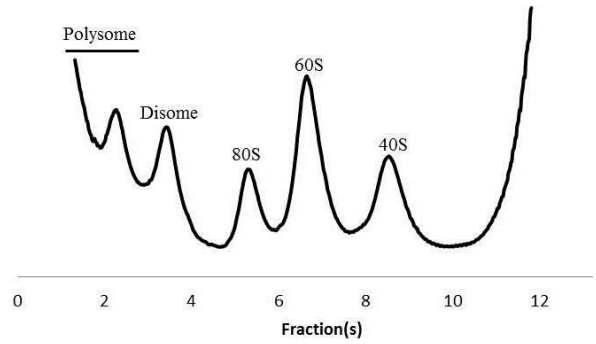

Figure 6.2. Polysome profile from two additional Δ*dcp1* strains. Two additional strains, (a) Δ*dcp1*; (b) Δ*dcp1.hxA5*. Cell lysates were separated on a 10-50% sucrose gradient and the A254 along the gradient was monitored. The sedimentation position of ribosomal complexes (40S, 60S, 80S, disome and polysomes) is indicated on each panel. Results are representative of three independently performed experiments.

6.3. Ribosome degradation on 60S rRNA

Purified RNA from the polysome profiling was subjected to agarose gel electrophoresis under non-denaturing conditions. The resulting gel revealed a distinct difference in the 60S fractions of the WT and Δ*dcp1* mutant strain. Interestingly, in the Δ*dcp1* strain, an additional band appeared which migrated marginally more slowly than 18S rRNA. One possibility is that it represented a degradation product derived from the 28S rRNA (Figure 6. 3). The same aberrant profile was also found in the two other *dcp1* mutants tested. It was therefore postulated that a ribosome degradation product was produced and accumulated specifically as a consequence of the disruption of *dcp1*.

a)

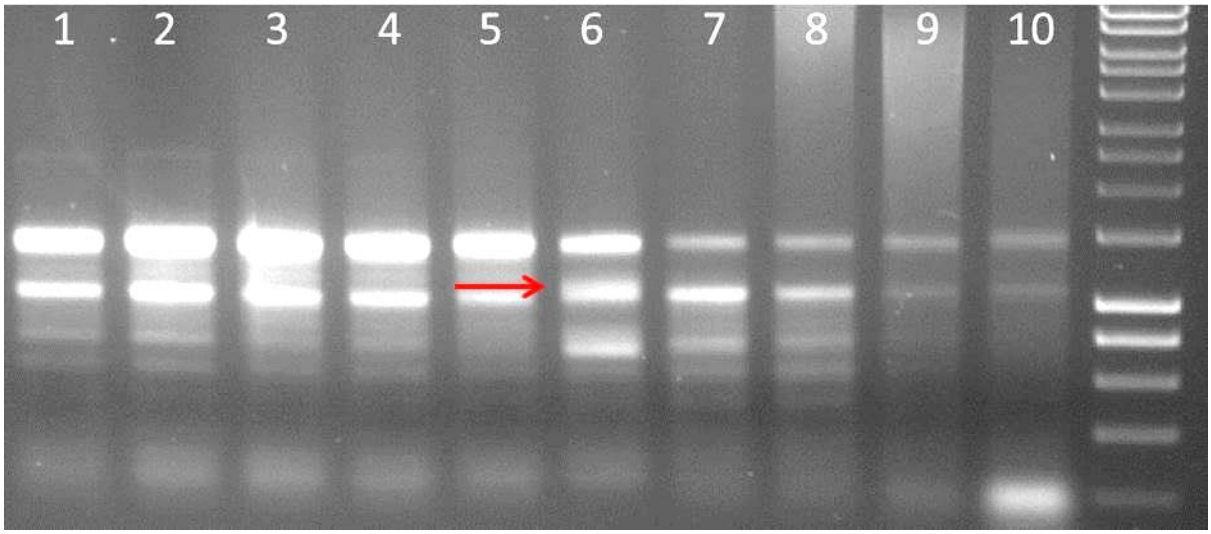

b)

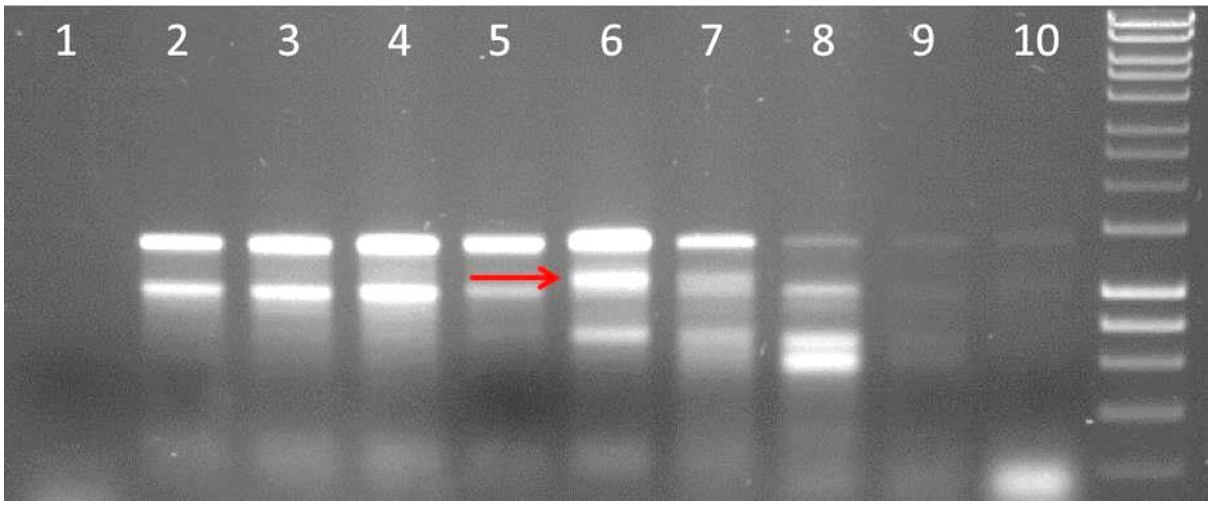

Figure 6.3. Purified RNA from the polysome fractionation of WT and Δ*dcp1* strains. (a) Gel picture of purified RNA from the WT strain. Based on the picture, we can see a clear 18S and 28S rRNA bands in the polysome peaks and monosome peak (Lane 1,2,3,4,5,6). DNA Ladder (Hyperladder1)(Lane 11). (b) Gel picture of purified RNA from the Δ*dcp1* strain. Based on the picture, we can see a clear 18S and 28S rRNA bands in the polysome peaks and monosome peak (Lane 1,2,3,4,5), However, there is a clear extra band above the 18S rRNA band in 60S fraction (Red arrow, Lane 6) and DNA Ladder (Hyperladder1)(Lane 11).

6.4. Sequencing of ribosomal repeat in *A. nidulans*

Since there was no complete sequence of *A. nidulans* rRNA in any available database, we undertook to clone and fully sequence the ribosomal repeat. This was important because in order to characterise the putative rRNA degradation product we needed to design primers and probes for PCR and Northern analysis, respectively. To achieve this, divergent primers complementary to the available partial sequence of 18S rRNA (Accession No: U77377) were synthesised. Using these primers a PCR product with the size of ~6 kb was amplified, which approximates to the expected size of ribosomal repeats (18S rRNA, ITS-1, 5.8S rRNA, ITS-2 and 28S rRNA). The PCR product was then cloned into pGEMT-Easy vector and sequenced. The complete sequence of *A. nidulans* ribosomal repeat is given in Figure 6.4. Based on the sequencing result, the full length of *A .nidulans* 18S rRNA is 1908 bp and it was 139 bp longer as compared to the sequence of 18S rRNA available in NCBI database (Accession No: U77377), suggesting that the sequence available in NCBI is not full 18S. Ribosomal sequences from the available databases were used as a reference to determine the junctions between 18S, ITS-1, 5.8S, ITS-2 and 28S rRNA (Borsuk et al., 1982; Henry et al., 2000).

The structure and sequence of the ribosomal repeat are highly conserved between Aspergillus species. The size of ITS-1 in *A. nidulans* is 165bp, 5.8S is 156bp and ITS-2 is 168bp, respectively (Figure 6.5). From the sequencing results, the full length of the 28S rRNA in *A. nidulans* is 3262 bp. The partial sequence of 28S rRNA from *A. niger* was used as a reference because it is closely related to *A. nidulans* the only near full-length 28S rRNA sequence available in the *Aspergillus* genome database (http://www.aspergillusgenome.org/). Based on the sequence alignment analysis, the 28S rRNA sequence from *A. nidulans* extends 291 bp at the 3'-end (Figure 6.5). The *A. nidulans* rRNA sequence from this study has been submitted to the GenBank (Accession No. KY074656 , KY074657 and KY074658) (NCBI).

GCCCCTCCAGAGTGAATACCTACGTGCTTTCTGCCCCTCCGGGGGCTTTCGGGCGCCGGGGGTGCCGGGTAAAACCGCGCCTCCGGGTTACGTC
CGGGAGGAACAAGGTATCTGGTTGATTCTGCCAGTAGTCATATGCTTGTCTCAAAGATTAAGCCATGCATGTCTAAGTATAAGCAATCTATACT
GTGAAACTGCGAATGGCTCATTAAATCAGTTATCGTTTATTTGATAGTACCTTACTACATGGATACCTGTGGTAATTCTAGAGCTAATACATGC
TAAAAACCCCGACTTCGGGAGGGGTGTATTTATTAGATAAAAAACCAATGCCCCTCGGGGCTCCTTGGTGATTCATAATAACTTAACGAATCGC
ATGGCCTTGCGCCGGCGATGGTTCATTCAAATTTCTGCCCTATCAACTTTCGATGGTAGGATAGTGGCCTACCATGGTGGCAACGGGTAACGGG
GAATTAGGGTTCGATTCCGGAGAGGGAGCCTGAGAAACGGCTACCACATCCAAGGAAGGCAGCAGGCGCGCAAATTACCCAATCCCGACACGGG
GAGGTAGTGACAATAAATACTGATACGGGGCTCTTTTGGGTCTCGTAATTGGAATGAGAACAATTTAAATCCCTTAACGAGGAACAATTGGAGG
GCAAGTCTGGTGCCAGCAGCCGCGGTAATTCCAGCTCCAATAGCGTATATTAAAGTTGTTGCAGTTAAAAAGCTCGTAGTTGAACCTTGGGTCT
GGCTGGCCGGTCCGCCTCACCGCGAGTACTGGTCCGGCTGGACCTTTCCTTCTGGGGAACCCCATGGCCTTCACTGGCTGTGGGGGGAACCAGG
ACTTTTACTGTGAAAAAATTAGAGTGTTCAAAGCAGGCCTTTGCTCGGATACATTAGCATGGAATAATAGAATAGGACGTGCGGTTCTATTTTG
TTGGTTTCTAGGACCGCCGTAATGATTAATAGGGATAGTCGGGGGCGTCAGTATTCAGCTGTCAGAGGTGAAATTCTTGGATTTGCTGAAGACT
AACTACTGCGAAAGCATTCGCCAAGGATGTTTTCATTAATCAGGGAACGAAAGTTAGGGGATCGAAGACGATCAGATACCGTCGTAGTCTTAAC
CATAAACTATGCCGACTAGGGATCGGGCGGCGTTTCTTTTATGACCCGCTCGGCACCTTACGAGAAATCAAAGTTTTTGGGTTCTGGGGGGAGT
ATGGTCGCAAGGCTGAAACTTAAAGAAATTGACGGAAGGGCACCACAAGGCGTGGAGCCTGCGGCTTAATTTGACTCAACACGGGGAAACTCAC
CAGGTCCAGACAAAATAAGGATTGACAGATTGAGAGCTCTTTCTTGATCTTTTGGATGGTGGTGCATGGCCGTTCTTAGTTGGTGGAGTGATTT
GTCTGCTTAATTGCGATAACGAACGAGACCTCGGCCCTTAAATAGCCCGGTCCGCGTCCGCGGGCCGCTGGCTTCTTAGGGGGACTATCGCCTC
AAGCCGATGGAAGTGCGCGGCAATAACAGGTCTGTGATGCCCTTAGATGTTCTGGGCCGCACGCGCGCTACACTGACAGGGGCAGCGAGTACAT
CACCTTGGTCCGAGAGGCCCGGGTAATCTTGTTAAACCCTGTCGTGCTGGGGATAGAGCATTGCAATTATTGCTCTTCAACGAGGAATGCCTAG
TAGGCACGAGTCATCAGCTGCTGCCGATTACGTCCCTGCCCTTTGTACACACCGCCCTGTCGCTACTACCGATTGAATGGCTCGGTGAGGCCTCC
GGACTGGCTCAGGAGGGTTGGCAACGACCCCCCAGAGCCGGAAAGCTGGTCAAACCCGGTCATTTAGAGGAAGTAAAAGTCGTAACAAGGTTTC
CGTAGGTGAACCTGCGGAAGGATCATTACCGAGCAGGTCCAGACTGCGGGCTGCCTCCGGGCGCCCAACCTCCCACCCGTGACTACCTAACACT
GTTGCTTCGGCGGGGAGCCCCCCAGGGGCGAGCCGCCGGGGACCACTGAACTTCATGCCTGAGAGTGATGCAGTCTGAGCCTGAATACAAATCA
GTCAAAACTTTCAACAATGGATCTCTTGGTTCCGGCATCGATGAAGAACGCAGCGAACTGCGATAAGTAATGTGAATTGCAGAATTCAGTGAAT
CATCGAGTCTTTGAACGCACATTGCGCCCCCTGGCATTCCGGGGGGCATGCCTGTCCGAGCGTCATTGCTGCCCTCAAGCCCGGCTTGTGTGTT
GGGTCGTCGTCCCCCCCGGGGGACGGGCCCGAAAGGCAGCGGCGGCACCGTGTCCGGTCCTCGAGCGTATGGGGCTTTGTCACCCGCTCGATTA
GGGCCGGCCGGGCGCCAGCCGGCGTCTCCAACCTTATTTTTCTCAGGTTGACCTCGGATCAGGTAGGGATACCCGCTGAACTTAAGCATATCAA
TAAGCGGAGGAAAAGAAACCAACCGGGATTGCCTCAGTAACGGCGAGTGAAGCGGCAAGAGCTCAAATTTGAAAGCTGGCCCCTTCGGGGTCCG
CGTTGTAATTTGCAGAGGATGCTTCGGGTGCGGCCCCTGTCTAAGTGCCCTGAACGGGCCGTCAGAGAGGGTGAGAATCCCGTCTTGGGCAGGG
TGCCCGTGCCCGTGTGAAGCTCCTTCGACGAGTCGAGTTGTTTGGGAATGCAGCTCTAAATGGGTGGTAAATTTCATCTAAAGCTAAATACCGG
GCCGGAGACCGATAGCGCACAAGTAGAGTGATCGAAAGATGAAAAGCACTTTGAAAAGAGAGTTAAACAGCACGTGAAATTGTTGAAAGGGAAG
CGCTTGCGACCAGACTCGGCCCCGGGGTTCAGCCAGCACTCGTGCTGGTGTACTTCCCCGGGGGCGGGCCAGCGTCGGTTTGGGCGGCCGGTCA
AAGGCCCCAGGAATGTATCGCCCTCCGGGGTTGTCTTATAGCCTGGGGTGCAATGCGGCCAGCCCGGACCGAGGAACGCGCTTCGGCACGGACG
CTGGCGTAATGGTCGCAAACGACCCGTCTTGAAACACGGACCAAGGAGTCTAACATCTACGCGAGTGTTCGGGTGTCAAACCCGTACGCGCAGT
GAAAGCGAACGGAGGTGGGAGCCCCCCCGGGGCGCACCATCGACCGATCCTGATGTCTTCGGATGGATTTGAGTAAGAGCGTAGCTGTGGGGAC
CCGAAAGATGGTGAACTATGCCTGAATAGGGCGAAGCCAGAGGAAACTCTGGTGGAGGCTCGCAGCGGTTCTGACGTGCAAATCGATCGTCAAA
TTTGGGTATAGGGGCGAAAGACTAATCGAACCATCTGGTAGCTGGTTCCTGCCGAAGTTTCCCTCAGGATAGCAGTAACGCGGATCAGTTTTAT
GAGGTAAAGCGAATGATTAGAGGCATTGGGGTTGAAACAACCTTAACCTATTCTCAAACTTTAAATATGTAAGAAGCCCTTGTTGCTTAGTTGA
ACGTGGGCATTAGAATGGAGCGTTACTAGTGGGCCATTTTTGGTAAGCAGAACTGGCGATGCGGGATGAACCGAACGCGAGGTTAAGGTGCCGG
AATACACGCTCATCAGACACCACAAAAGGTGTTAGTTCATCTAGACAGCCCGACGGTGGCCATGGAAGTCGGAATCCGCTAAGGAGTGTGTAAC
AACTCACGGGCCGAATGAACTAGCCCTGAAAATGGATGGCGCTCAAGCGTGTTACCCATACCTCGCCGTCGGGGTAGAAACGATGCCCCGACGA
GTAGGCAGGCGTGGGGGTCCGTGACGAAGCCTTGGGCGTGAGCCCGGGTCGAACGGCCCCTAGTGCAGATCTTGGTGGTAGTAGCAAATACTCA
AATGAGAACTTTGAGGACTGAAGTGGGGAAAGGTTCCATGTGAACAGCAGTTGGACATGGGTTAGTCGATCCTAAGGCATAGGGAAGTTCCGTT
TGAAAGGCGCCCTCGTGCGCCGTGTGCCGAAAGGGAAGCCGGTTAATATTCCGGCACCTGGATGTGGATTCTCCACGGTAACGTAACTGAACGC
GGAGACGTCGGCGGGGGTCCTGGGAAGAGTTCTCTTTTCTTCTTGACGGCCTATCACCCTGAAATCGGTTTGTCCGGAGCTAGGGTTCAATGGC
CGGCAGAGCCCTGCACCTTTGCAGGGTCCGGTGCGCCCCCGACGACCCTTGAAAATCCGCGGGAAGGAATAGTTTTCACGCCAGGTCGTACTCA
TAACCGCAGCAGGTCTCCAAGGTGAACAGCCTCTAGTTGATAGAACAATGTAGATAAGGGAAGTCGGCAAAATGGATCCGTAACTTCGGGATAA
GGATTGGCTCTAAGGGTCGGGCTCGCTGGGCCTTGGGGGGAACCCCCTGGAGCAGGGGGGCACTAGCCGGGCAACCGGCCGGCGCCCCCCAGCA
CCGGGGTGGGGACGCCCTTGGCAGGCTTCGGCCGTCCGGCGGGCGCTTAACGACCAACTTAGAACTGGTACGGACAAGGGGAATCTGACTGTCT
AATTAAAACATAGCATTGCGATGGCCAGAAAGTGGTGTTGACGCAATGTGATTTCTGCCCAGTGCTCTGAATGTCAAAGTGAAGAAATTCAACC
AAGCGCGGGTAAACGGCGGGAGTAACTATGACTCTCTTAAGGTAGCCAAATGCCTCGTCATCTAATTAGTGACGCGCATGAATGGATTAACGAG
ATTCCCACTGTCCCTATCTACTATCTAGCGAAACCACAGCCAAGGGAACGGGCTTGGCAGAATCAGCGGGGAAAGAAGACCCTGTTGAGCTTGA
CTCTAGTTTGACATTGTGAAAAGACATATGGGGTGTAGAATAGGTGGGAGCTTCGGCGCCAGTGAAATACCACTACCTTTATCGTTTTTTTACT
TATTCAATGAAGCGGAACTGGGCTTCACCGCCCATCTTCTGGCGTTAAGGTCCTTCGCGGGCCGATCCGGGTTGAAGACATTGTCAGGTGGGGA
GTTTGGCTGGGGCGGCACATCTGTTAAACCACAACGCAGGTGTCCTAAGGGGGGCTCATGGAGAACAGAAATCTCCAGTGGAACAAAAGGGTAA
AAGCCCCCTTGATTTTGATTTTCAGTGTGAATACAAACCATGAAAGTGTGGCCTATCGATCCTTTAGTCCCTCGAAATTTGAGGCTAGAGGTGC
CAGAAAAGTTACCACAGGGATAACTGGCTTGTGGCAGCCAAGCGTTCATAGCGACGTTGCTTTTTGATCCTTCGATGTCGGCTCTTCCTATCAT
ACCGAAGCAGAATTCGGTAAGCGTTGGATTGTTCACCCACTAATAGGGAACGTGAGCTGGGTTTAGACCGTCGTGAGACAGGTTAGTTTTACCC
TACTGATGAAGGTCGCCGCAACGGTAATTCAATTTAGTACGAGAGGAACCGTTGATTCAGATAATTGGTTTTTGCGGCTGTCTGACCAGGCAGT
GCCGCGACGCTACCATCTGCCGGATAATGGCTGAACGCCTCTAAGTCAGAATCCGTGCCGGAACGCGGCGATGTTGCCCCGCACGTCGTAGTTG
GATACGAATAGGCCTCCGGGCCCTGTACCTCAGCAGGCTGGCGACGGCCCCGGGGAGAAGCCCTCGGGAGCCGGCTGGCGGATTGCAATGTCAC
CTCGCGCGGGGATGAATCC

Figure 6.4. Complete sequence of ribosomal repeats in *A. nidulans*. 18S rRNA sequence (grey), Internal Transcribe Spacer 1, ITS-1 (yellow), 5.8S rRNA (cyan), Internal Transcribe Spacer 2, ITS-2 (green) and 28S rRNA (pink).

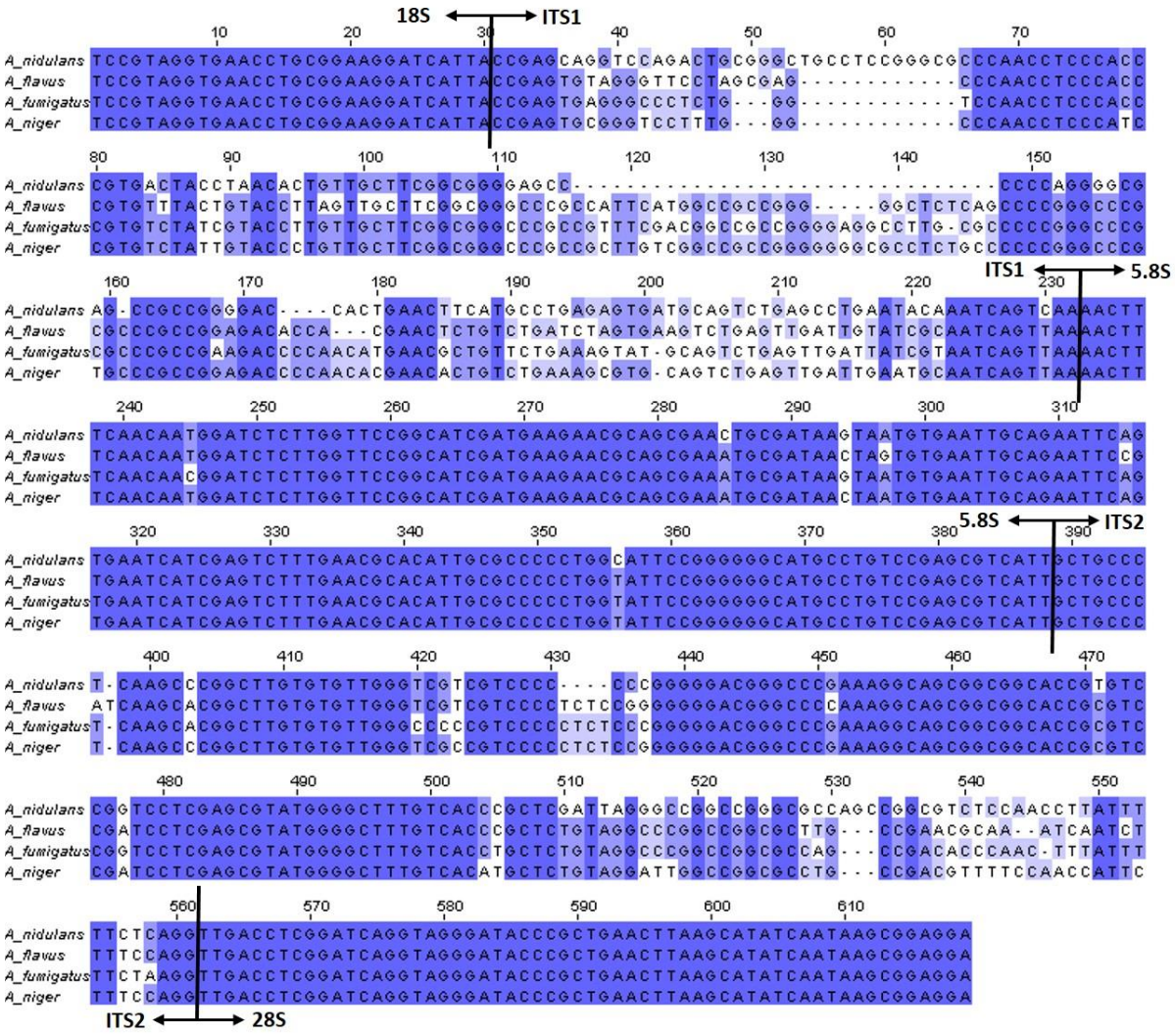

Figure 6.5. Multiple sequence alignment of ribosomal repeats of *A. nidulans* (this study), *A. falvus* (Accession No: KC621105), *A. fumigatus* (Accession No: FJ478096) and *A. niger* (Accession No: FJ878650). The alignment consists of the 3' end of the 18S ribosomal DNA (rDNA) gene, the complete ITS 1 region, the complete 5.8S region, the complete ITS 2 region, and the 5' end of the 28S rDNA gene. Sequence alignment was performed using Muscle (Edgar, 2004). Identical nucleotide are shaded in purple using Jalview software (Waterhouse et al., 2009).

6.5. Northern hybridisation analysis of rRNA fractions

To investigate whether the putative degradation product was in fact derived from the 28S rRNA, we utilised Northern blot analysis utilising the 28S rDNA sequence as a probe (Figure 6.8). Non-denaturing agarose gels had been used for the initial analysis of samples from polysome fractionation (Figure 6.6 (a)). For Northern analysis we used both non-denaturing (TAE) and denaturing (MOPS/formaldehyde) gels, to assess the effect of RNA structure on the relative migration of fragments (Figure 6.6 (b)). Based on the Northern hybridisation, as expected a major band appeared in the Δ*dcp1* 60S sample, migrating further than the full-length 28S band. Interestingly, a week band with similar migration was also observed in both the WT and Δ*dcp2* samples. Hybridisation of the 28S probe demonstrates that this putative degradation product is derived from 28S rRNA. Similar results were observed using both types of gel (Figure 6.6 (b) and (c)) and subsequent experiment were conducted using denaturing gels.

To characterise the 28S rRNA degradation product further the membrane was probed separately using sequences specific to the 5'-end, an internal region and the 3' end of the 28S rDNA, as depicted in Figure 6.7 (a). Based on the Northern hybridisation, there are several bands which are postulated to be the degradation products of 28S rRNA appeared in the 60S fraction of WT, Δ*dcp1* and Δ*dcp2* (Figure 6.7 (b)). However, their relative intensity varies, being dramatically higher in Δ*dcp1* derived sample (Figure 6.7 (b)). Based on these results, it gives an indication that the cleavage occurs in several positions of the 28S rRNA. Interestingly, we observed the dramatic loss of 18S rRNA signal (up to 50% relative to the 80S signal) in Δ*dcp1* 60S fraction and not in WT and Δ*dcp2*.

a)

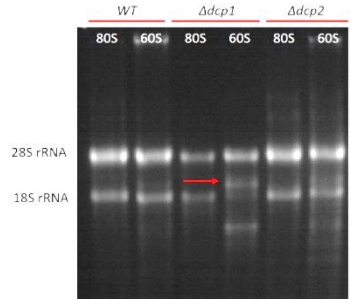

b)

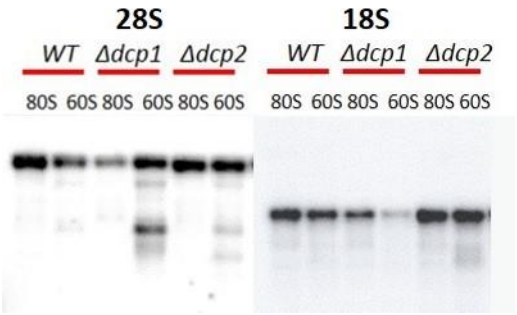

c)

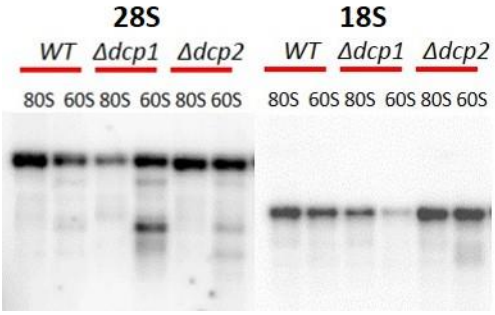

Figure 6.6. Northern of rRNA fractions, comparing denaturing and non-denaturing gel electrophoresis. The 80S and 60S rRNA fractions from sucrose density centrifugation of cell extracts from WT, Δ*dcp1* and Δ*dcp2* strains were run on non-denaturing agarose (TAE) (Figure (a). Northern hybridisation analysis comparison after probed with a DNA sequence complementary to the full-length 18S and 3'-end 28S rRNA on b) non-denaturing agarose (TAE) and c) denatured (formaldehyde/MOPS) gel electrophoresis.

a)

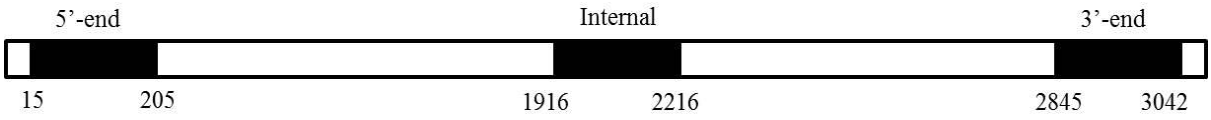

b)

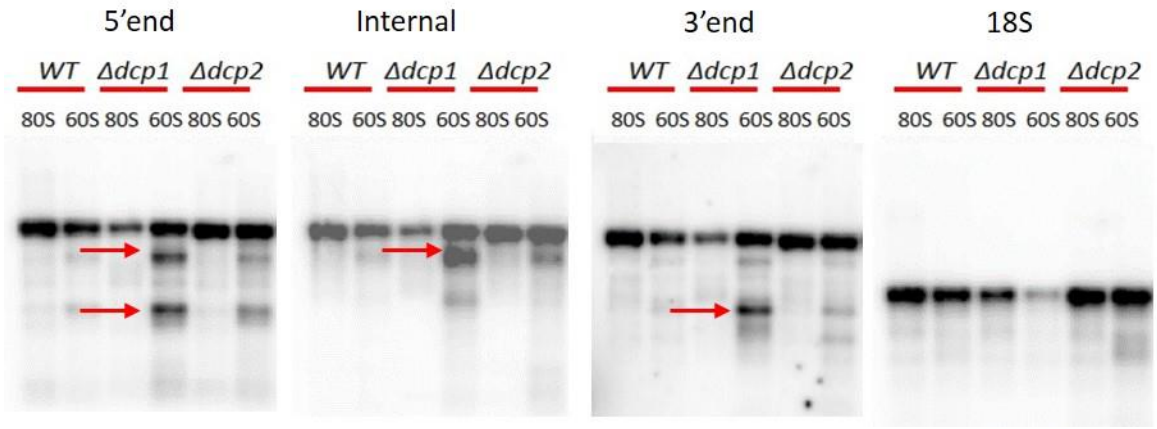

Figure 6.7. a) **A schematic diagram showing the location of probes used in Northern blot analysis for the 28S rRNA in *A. nidulans*.** Three different regions of 28S rRNA were selected for probing (name as 5'-end, internal and 3'-end.

b) Northern blot analysis of 28S rRNA from the polysome fractionation. Purified RNA of monosome (80S) and large subunit (60S) from three different strains; WT, Δ*dcp1* and Δ*dcp2*. a) 28S_5'-end probing; b) 28S_internal probing; c) 28S_3'-end probing and d) 18S_full. Interestingly, we observed the dramatic loss of 18S rRNA signal in Δ*dcp1* 60S fraction. Red arrow indicates the distinctive fragments which appeared in Δ*dcp1* and Δ*dcp2*.

6.6 Sequencing of 28S degradation products.

Based on the Northern blotting, it seems that the Δ*dcp1* strain produces a major 28S rRNA degradation product. To further investigate this, we undertook to clone and sequence the 'degradation' product.

Non-denaturing agarose gel electrophoresis was used to isolate major "degradation" product derived from the Δ*dcp1* strain. This was extracted from the gel and purified prior to cloning using the NEB Next® Multiplex Small RNA Library Prep Set for Illumina® (Set 1 from NEB). This method successfully sequences complementary to 28S rRNA. As expected the cloned sequences derived from the 5' end and central region of the 28S rRNA. However, the products were approximately 350 bp, shorter than expected based on the migration of the sequence relative to 18S rRNA which suggested a size in excess of 1.5 kb. Of the 15 clones sequenced 14 derived from the 5'-end of 28S rRNA (Figure 6.8 (a)). One was derived from the central region of the 28S rRNA (Figure 6.8 (b)). This suggests that in spite of using formaldehyde gels the degradation product observed is in fact composed of multiple small fragments that have not been fully denatured. This is consistent with polyacrylamide gel electrophoresis analysis of the rRNA fractions (Appendix 5). Based on this, a complex banding pattern was observed which did not reflect that observed by agarose gel electrophoresis (Figure 6.3 (a), (b) and Figure 6.6 (a)). The strong cloning bias towards 5' end fragments suggests that internal fragments present may be poor cloning substrates. One possibility is that the phosphorylation state is not optimal. This may reflect the cleavage reaction that produced them and may be overcome with pre-treatment of the extracted RNA with phosphatase and polynucleotide kinase ensure that the fragments are mono-phosphorylated.

a)

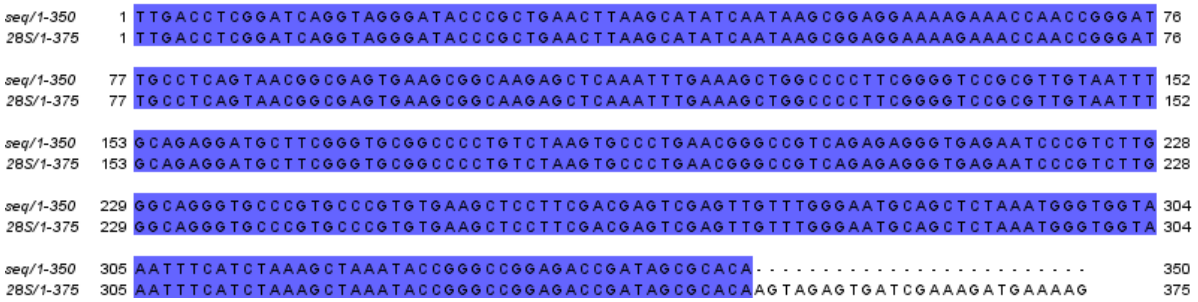

b)

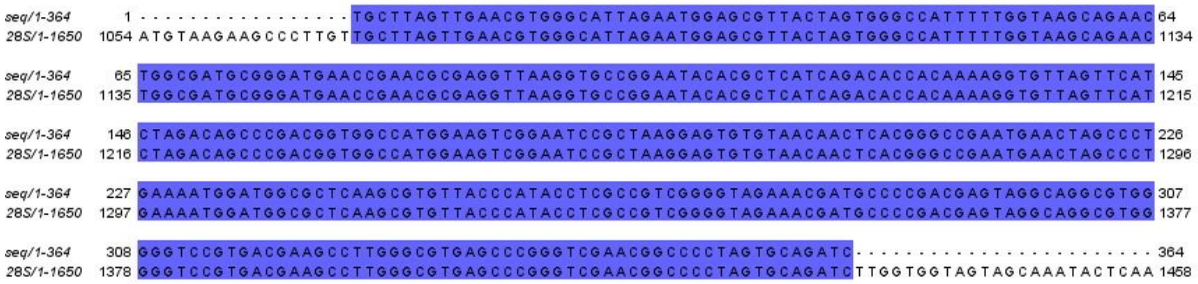

Figure 6.8. Sequence alignment of the degradation products of 28S rRNA. Alignment was performed using Muscle (Edgar, 2004) program. Identical nucleotides are shaded in purple using Jalview software (Waterhouse et al., 2009). (a) The sequence obtained is similar to the Northern blotting observation in the 5'-end region. (b) The sequence obtained is slightly different to the Northern blotting observation in the internal region of 28S rRNA.

6.7. Characterising the role of Dcp2 in 28S rRNA degradation.

Dcp1 and Dcp2 are known to work together in the decapping complex (Coller and Parker, 2004; Valkov et al., 2016). So, to study whether the aberrant ribosomal profile and high level of 28S rRNA degradation products produced by Δ*dcp1* strains are *dcp2*-dependent, Δ*dcp1* was crossed with Δ*dcp2,* producing the double mutant for polysome analysis. Strain validation was confirmed by PCR (Figure 6.9).

The polysome profiles of the double mutant, Δ*dcp1* Δ*dcp2,* had a relatively low 60S peak (Figure 6.1 (e)) distinguishing it from the Δ*dcp1* single mutant (Figure 6.1 (c)). The purified RNA from the polysome fractions was subjected to agarose gel electrophoresis and only a weak band located in the region of the Δ*dcp1* degradation product was observed in the 60S fraction (Appendix 2). Suppression of this aspect of the Δ*dcp1* phenotype by deletion of *dcp2* would be consistent with this predominant degradation product resulting from Dcp2 mediated cleavage in the absence of Dcp1.

To test whether the Nudix domain in Dcp2 is important for rRNA cleavage in Δ*dcp1* strains, a single amino acid substitution was introduced to disrupt the catalytic site of Nudix domain of Dcp2. The mutation was a guanine (G) to cytosine (C) substitution resulting in the glutamic acid (E) at position 148 being replaced by a glutamine (Q) (Figure 6.10). The equivalent mutation is known to disrupt the decapping activity of *S. cerevisiae* Dcp2 (Song et al., 2013). The $dcp2^{E148Q}$ mutant allele was "knocked in" to the original Δ*dcp2* strain (Δ*dcp2:AfpyrG, pyrG89, pyroA4,* Δ*nkuA:argB)* as a linear DNA construct, replacing *AfpyrG* and resulting in resistance to 5-fluoroorotic acid. Putative transformants were screened by PCR to confirm reintegration of *dcp2* and the point mutation confirmed by sequencing (Appendix 3). The resulting mutant strain was morphologically very similar to Δ*dcp2* (Figure 6.11(b)).

a)

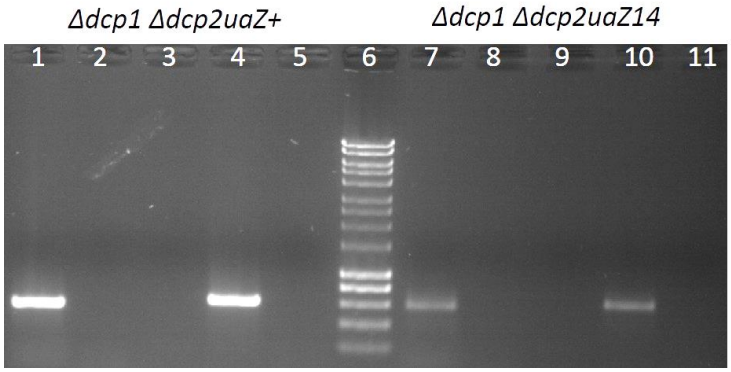

b)

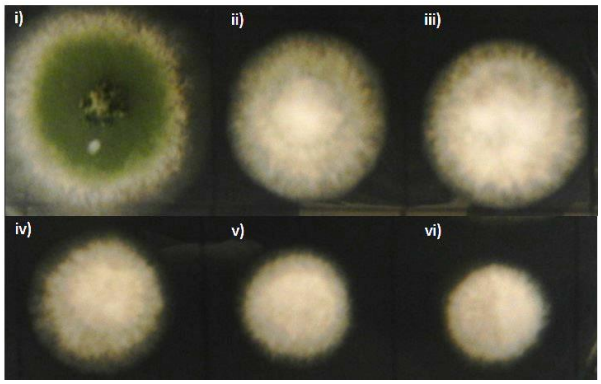

Figure 6.9. Double mutant construction of decapping in *A. nidulans*.

a) PCR-based validation of Δ*dcp1* Δ*dcp2 uaZ+* and Δ*dcp1* Δ*dcp2 uaZ14* strains using specific primer sets is given as an example. Based on the picture, a 600bp band in Int_pyrG confirming the introduction of *AfpyrG* gene into the *A. nidulans* genome via homologous recombination (Lane 1,7), a 650bp product Int_ndxB (as positive control) (Lane 4,10), no product using Int_dcp1 confirmed deletion of *dcp1* gene (Lane 2,8) and Int_dcp2 confirmed deletion of *dcp2* gene (Lane 3,9) from the genome. A 300bp product of Int_nkuA (as control)(Lane 5,11) and DNA Ladder (Hyperladder1)(Lane 6).

b) Phenotypic differences with the *fluffy* cotton-like appearance in all decapping mutants; i)WT; ii) Δ*dcp1*; iii) Δ*dcp2*; iv) Δ*dcp1* Δ*dcp2*; v) Δ*dcp1 dcp2*^{E148Q} ; vi) *dcp2*^{E148Q} . Similar phenotypes were observed for all Dcp2 mutant strains including the strain with a point mutation at Nudix domain (*dcp2*^{E148Q}). All strains were grown on solid MM with required supplements for 3 days at 37ºC.

To assess whether the *dcp2*^{E148Q} mutation will alter the aberrant polysome profile of Δ*dcp1* the Δ*dcp1 dcp2*^{E148Q} double mutant was subjected to the polysome analysis (Figure 6.1 (f)). Interestingly, the 60S peak was similar to the double mutant Δ*dcp1* Δ*dcp2* (Figure 6.1 (e)), suppressing the Δ*dcp1* specific profile. This suggests that the catalytic activity of Dcp2 is critical for the enhanced ribosome cleavage observed in the Δ*dcp1* strain although relatively minor degradation product of 28S rRNA appears in the 60S fraction (Appendix 4), as was also observed for Δ*dcp1* Δ*dcp2* (Appendix 2).

Figure 6.10. The point mutation disrupting the Nudix domain of *dcp2*. Amino acid alignment of Dcp2 with the point mutation introduced which alter the amino acid from glutamic acid (E) to glutamine (Q) (red box). Amino acid was aligned with Muscle (Edgar, 2004) and identical amino acid are shaded in purple using Jalview software (Waterhouse et al., 2009).

6.8. 3D analysis of 28S rRNA cleavage sites

To determine the location of cleavage sites within the 28S RNA, we undertook *in silico* 3D visualisation of 60S large ribosomal structure with the help from Dr. Sean Connell (CIC bioGUNE, Bilbao). In this analysis, the sequence from the degradation products (Figure 6.8) were aligned with the *S. cerevisiae* 60S subunit. Interestingly, the 3' cleavage sites for both the 5'-end and internal fragments were in close proximity within the ribosomal exit tunnel (Figure 6.11). The close positioning of these two cleavage sites may be significant and consistent with a common cleavage mechanism. All three mapped cleavage site are relatively accessible, consistent with cleavage of the structurally intact 28S rRNA.

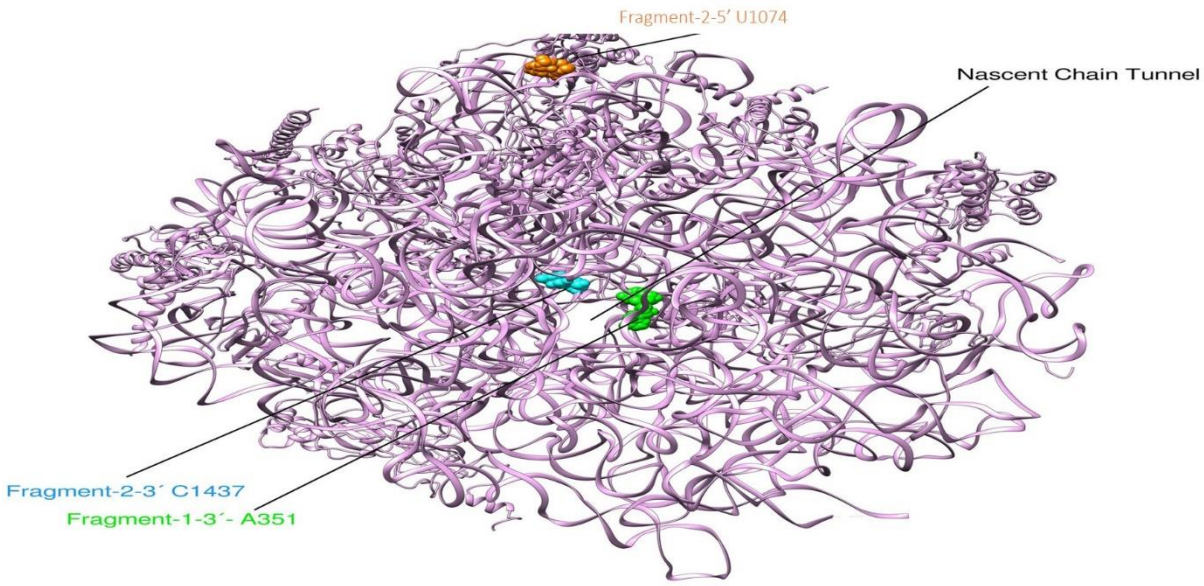

Figure 6.11. 3D analysis of 28S rRNA cleavage sites in *A. nidulans*. For both 28S rRNA fragments identified from the Δ*dcp1* strain the 3' cleavage sites from the 5' (green) and internal (blue) fragments are in lose proximity and within the ribosomal exit tunnel. The close positioning of two fragment 3' ends might increase the possibility of cleavage in 28S rRNA. The 5' cleavage site of the internal fragment (yellow) is at the surface of the large subunit.

6.9. Summary

The main objective of this part of the study was to analyse the polysome profile of strains disrupted for the decapping factors Dcp1 and Dcp2 in *A. nidulans*. An aberrant polysome profile was observed for Δ*dcp1* strains, where the 60S peak, associated with the large ribosomal subunit, was consistently greater than the 80S, monosome peak (Figure 6.1 (c)). The 40S subunit fraction was also relatively high. This observation distinguished Δ*dcp1* from WT and the phenotype of the Δ*dcp2* strain was intermediate between the two. The basis for the dramatic accumulation of free ribosomal subunits in the Δ*dcp1* strains was investigated further. There are several hypothesis that could explain the apparent accumulation of ribosomal subunits such as a defect in ribosome biogenesis including overexpression or the production of defective subunits, the reduced ability of mRNAs to be translated leading to ribosome disassembly or inhibition of initiation complex assembly (Mašek et al., 2011).

However, gel electrophoresis revealed that the Δ*dcp1* 60S fractions include a relatively high proportion of two RNA bands that were distinct from 28S and 18S rRNA with respect to migration on non-denaturing agarose gels. Northern analysis indicated that the two bands observed are both derived from 28S rRNA. Using probes from specific regions of the 28S rRNA, it was apparent that these bands include components derived from different regions of the 28S rRNA suggesting that it is not the product of progressive exonuclease degradation as has been observed for defective pre-rRNA in the nucleus (Dez et al., 2006) and TOR-induced ribosome degradation in the cytoplasm (Pestov and Shcherbik, 2012).

The sequence of cloning of RNA fragments from the principal aberrant band derived from the Δ*dcp1* mutant were consistent with this, as two fragments were identified which were non-contiguous and surprisingly each was only around 350 nucleotides in length. This was in contrast to the expected size which was in excess of 1500 nucleotides, based on gel migration. Of the 15 clones sequenced 14 derived from the 5' end of 28S rRNA (Figure 6.8 (a)). One was derived from the central region of the 28S rRNA (Figure 6.8 (b)). This suggests that in spite of using formaldehyde gels the degradation product observed is in fact composed of multiple small fragments that have not been fully denatured. This is consistent with polyacrylamide gel electrophoretic analysis of the rRNA fractions (Appendix 5) where a complex banding pattern was observed which did not reflect that observed by agarose gel electrophoresis (Figure 6.3 and Figure 6.6 (a)). This suggests that this band represents a complex structure derived from the 60S ribosomal subunit which has been cleaved at various positions but has maintained RNA-RNA interactions and structure in spite of the denaturing electrophoresis conditions used. It is possible that the lower band is equally complex as both 5' and 3' specific probes appeared to hybridise to sequences in a similar area of the gel (Figure 6.7 (b)).

The three cleavage sites identified were all accessible in the mature 28S ribosomal subunit based on mapping them on to the published structure for *S. cerevisiae*. The two of the 3' ends identified were in very close proximity within the ribosomal exit tunnel (Figure 6.11) perhaps indicating that the same activity is responsible for both events. The strong cloning bias towards 5' end fragments suggests that internal fragments present may be poor cloning substrates. One possibility is that the phosphorylation state is not optimal. This may reflect the cleavage reaction that produced them and may be overcome with pre-treatment of the extracted RNA with phosphatase and polynucleotide kinase to ensure that the fragments are mono-phosphorylated. We would predict that, based on the migration of the larger form, there are other RNA fragments within the complex and this should be investigated further.

The basis for the accumulation of ribosomal subunits, including the cleavage products, is of interest as is the more dramatic phenotype of Δ*dcp1* strains, compared to the far less striking Δ*dcp2* mutant phenotype. The accumulation of the subunits coinciding with the relatively high level of cleaved degradation products suggests that these may represent non-functional rRNA components, rather than functional subunits accumulating due to the repression of translational initiation. Supporting this is unpublished data, based on Western analysis, which demonstrates that the ribosomal proteins in the Δ*dcp1* strain have a very high level of ubiquitination (Parisi, personal communication). Interestingly non-functional rRNA decay (NRD), which specifically eliminates defective subunits, is triggered by ubiquitination of ribosomal proteins (Fujii et al., 2009).

Why defects in the primary decapping complex should lead to the accumulation of defective rRNA is intriguing. It is now known that mRNA decapping occurs while the transcripts are associated with the ribosomes (Hu et al., 2010) and there appears to be feedback between ribosomes and mRNA, in that cycloheximide with stalls the ribosomes stabilises transcripts, preventing 5' but not 3' degradation (Beelman and Parker, 1994; Morozov et al., 2000). The Dcp1/Dcp2 complex is also known to interact directly with the ribosomes (Nissan et al., 2010). One possibility is that the recycling of ribosomes at the point where decapping would normally be induced, for example in deadenylated transcripts, ribosome dissociation is in some way linked to decapping. Consequently by blocking decapping it may be that this recycling process is disrupted and the stalled ribosomes are then subject to degradation by an NRD like process.

Why Δ*dcp1* strains have a more striking Δ*dcp2* mutant phenotype with respect to the ribosomal profile and the level of degradation products is intriguing, considering that Dcp1 is an enhancer of Dcp2 and that at the level of mRNA degradation Dcp2 plays a more direct and greater role (Chapter 3). As both Δ*dcp2* and the non-catalytic mutant $dcp2^{E148Q}$ were both epistatic to *dcp1,*

the implication is that free Dcp2 is in some way exacerbating the Δ*dcp1* mutant phenotype. These data also indicate that the Nudix domain plays an important role consistent with the nuclease activity of Dcp2 acting directly to cleave the rRNA in the absence of Dcp1. However, it is important to note that the degradation products observed by Northern analysis in both the Δ*dcp1* and Δ*dcp2* strains appear very similar, even though the levels vary dramatically. This implies that Dcp2 is not responsible for this or it is one of a number of activities cleaving the rRNA in what appears to be a similar way.

CHAPTER 7: DISCUSSION

7.1. Overview.

This thesis details a number of studies aimed at determining the roles of known and novel decapping factors which potentially play key roles in the general transcripts degradation and NMD in *A. nidulans*. This study has involved a range of approaches including qRT-PCR, quantitative Northern blotting for RNA degradation rates, polysome analysis and confocal microscopy for the intracellular localisation of factors involved in transcripts degradation.

7.2. Decapping and NMD.

The main objective of this part of the study was to determine whether the disruption of decapping factors, Dcp2 and Dcp1 have an effect on NMD. In *A. nidulans*, NMD persists in both Δ*dcp1* and Δ*dcp2* mutants, however, the severity of the NMD is diminished as compared to the WT background. In WT, the expression level of PTC-containing transcripts (*uaZ14* and *hxA5*) reduced by 80% whereas in both Dcp1, Dcp2 and Lsm1, only 50% to 60%, respectively. These data are consistent with these proteins functioning in the same decapping mechanism but only playing a minor role in NMD. We also showed that Δ*lsm1* mutants partially suppress NMD. Lsm1 is known to form a large cytoplasmic complex with six other Lsm proteins, known as Lsm1-7 (Fillman and Lykke-Andersen, 2005), and this has been shown to recruit the Dcp1-Dcp2 decapping complex to deadenylated mRNAs (Tharun et al., 2000). These data would be consistent with the *A. nidulans* Lsm1-7 complex having a similar role in promoting decapping in response to NMD. To our knowledge, this is the first time that the role of the Lsm complex in NMD has been described.

The partial suppression of the NMD response in both Δ*dcp1* and Δ*dcp2* strains indicates the possibility of other decapping mechanisms are involved., In animal systems an endonuclease,

SMG6, is also implicated (Eberle et al., 2009). Another possibility is that there are other decapping factors in *A. nidulans* such as other Nudix family proteins (Song et al., 2013).

We have shown that Pat1 and Dhh1 are not required for NMD in *A. nidulans*, which is consistent with the results observed in *S. cerevisiae* (Swisher and Parker, 2011). Pat1 binds to the Lsm1-7 complex and interacts with Dhh1 and Xrn1, as part of the deadenylation-dependent decay pathway in eukaryotes. Based on the interaction with Lsm1-7 we would have postulated that disruption of Pat1 and Lsm1 resulting similar NMD phenotype. However, results obtained in this study shows differently and these data may suggest that Pat1's activity is perhaps limited to deadenylation-dependent decapping, whereas Lsm1-7 appears to have a wider function. It was discovered recently that Pat1 was bound to Lsm2 and Lsm3 in the complex and not with the Lsm1 (Wu et al., 2014) and therefore it is possible that Pat1's function is retained in Lsm1 mutants.

Surprisingly, we observed that deletion of *xrn1* did not have an effect on NMD in *A. nidulans*, unlike the situation in *S. cerevisiae* (Nagarajan et al., 2013; Sheth and Parker, 2006). We postulate that other exonucleases are profiting from redundancy. The most likely candidate is Rat1/Xrn2. In mammalian systems, Rat1 has been shown to be associated with NMD factors such as Upf1, Upf2, Upf3X, Dcp2, Xrn1, and exosome components PM/Scl100, Rrp4, and Rrp41 (Lejeune et al., 2003). Therefore, it is possible that Xrn1 is not solely responsible for NMD in *A. nidulans*. Rat1 has been successfully deleted from the *A. nidulans* genome, however, deleted strains show very poor growth and could not be cultured (Caddick, unpublished data).

Polysome profiling of the Δ*dcp2* and Δ*dcp1* mutants indicates that higher percentage of the *uaZ14* transcripts bind to the polysome fractions (~37%) as compared to the WT (~21%) (Figure 3.9). Similar results were observed in *S. cerevisiae* (Hu et al., 2010) where it was argued

that this support of the hypothesis that NMD induced decapping occurs while the transcripts are bound to the ribosome. Additionally, in a WT background, we found that transcripts bound to the non-translating, lighter fraction (RNPs) show an increase (~10%) in *uaZ14* as compared to the *uaZ*$^{+}$, which would be consistent with translational repression as a component of NMD in *A. nidulans*. However, our results had no similar effect as compared to the enrichment of NMD substrates in the polysome and monosome fraction observed for Δ*cutA* and Δ*cutB* mutants, which disrupt in 3' pyrimidine-tagging of transcripts induced by NMD (Morozov et al., 2012). This would suggest that this aspect of the Δ*cutA* and Δ*cutB* phenotype is not specifically associated with failure to activate *dcp2* mediated decapping.

An interesting observation was that the rate of *uaZ*$^{+}$ mRNA degradation was not affected by deletion of *dcp1* unlike deletion of *dcp2* (Figure 3.10). This suggests that for this transcript Dcp2 is acting independently of Dcp1. It will be important to test other transcripts to see if this is a general phenomena. Additionally, the fluorescence microscopy of Dcp1:GFP and Dcp2:RFP shows that both proteins localise into the expected P-body-like structures, however, a significant proportion of Dcp2 and Dcp1 did not co-localise and were therefore not in a complex at any one time. It will be important to test if this is an artefact of the C-terminal tagging of both proteins. However, the possibility that the Dcp2 activity is not dependent solely on Dcp1, suggesting a divergence between *A. nidulans* and *S. cerevisiae.*

Confocal microscopy analysis of the two ribonucleotidyltransferases, CutA and CutB, which are involved in 3'-tagging and important in promoting decapping (Morozov et al., 2012; Morozov et al., 2010) show that CutA were primarily localised in the cytoplasm with a low level in nucleus whereas CutB primarily, but not exclusively, located in the nuclei. Surprisingly, for both CutA and CutB, there was no punctate distribution suggesting that neither is preferentially localised to P-bodies. The apparent requirement for CutA in P-body formation (Morozov et al., 2010) suggests that this relates to a process that occurs upstream

from P-body formation. Interestingly, preliminary observation shows that the proportion of CutA in nuclei increased when CutB was disrupted. It shows that in the absence of CutB, CutA may enter nuclei to replace CutB. It was originally postulated that based on homology, CutB is likely to be associated with the nuclear TRAMP complex (Morozov et al., 2012), which is involved in various processes including maturation of structural RNAs and degradation of aberrant transcripts. This is fully consistent with the predominant localisation to the nuclei observed. One intriguing possibility is that in the absence of CutB, CutA can integrate into the TRAMP complex and this interaction anchors it in the nucleus. However, further experiments need to confirm the change in intracellular location and test this hypothesis. Additionally, Western blotting of CutA also shows that it associates with the ribosome (preliminary data not shown). If confirmed this result would support the evidence that the proposed role of CutA is in promoting decapping, which is known to occur while transcripts are associated with ribosomes.

7.3. Additional decapping activities in *A. nidulans*.

Recent studies show that multiple Nudix proteins possess decapping activity in mammalian systems (Song et al., 2013). Our observation of partial suppression of NMD in Dcp1 and Dcp2 mutants supported our postulation that *A. nidulans* have another decapping factor. This leads us to perform the phylogenetic analysis of Nudix proteins. From our analysis, three of the Nudix proteins encoded by *A. nidulans* (NdxA, NdxB and NdxD) were selected for further characterisation.

Of the three genes analysed, *ndxD* appeared to be the best candidate. Δ*ndxD* strains showed partial suppression of NMD for *uaZ14* (Figure 4.5) which is similar to the Δ*dcp1* and Δ*dcp2* mutants (see Figure 3.7). This is consistent with NdxD playing a significant role in NMD induced transcripts degradation in *A. nidulans*. However, the Δ*ndxD* Δ*dcp2* double mutant

restored WT levels of NMD. Interpreting this is not straightforward as the ratio observed is a product of more than one degradation rate; both degradation of wild type transcripts, probably mediated by deadenylation-dependent decapping, and separately NMD dependent degradation of *uaZ14* mRNA. Therefore, dramatic stabilisations of the wild-type transcript would result in an apparent increase in NMD. There is also the additional issue, not addressed here, that degradation rates and the associated machinery can influence transcription rates (Braun and Young, 2014; Sun et al., 2013). Consequently, the disruption of two factors potentially involved in RNA degradation may have a complex interplay that may have impacted on these data.

Preliminary results of general transcript stability also showed that disruption of NdxA and NdxB did not alter transcript stability. However, disruption of NdxD appeared to stabilise the *uaZ*$^{+}$ transcript, although not as dramatically as Δ*dcp2*. These data are consistent with NdxD playing a role in transcript degradation. Transcript degradation rate for the Δ*ndxA* Δ*dcp2* and Δ*ndxB* Δ*dcp2* double mutants have shorter half-lives as compared to the Dcp2 single mutant, while the Δ*ndxD* Δ*dcp2* strain showed a marginally longer half-life (Figure 4.9). These data are not sufficient to demonstrate additivity but are consistent with NdxD having decapping activity. Our phylogenetic analysis shows that NdxD is closely related to MutT, a protein which has been shown to possess decapping activity (Parrish et al., 2007). Previous studies have shown that Nudix/MutT motif possess decapping activity in various organisms such as vaccinia virus D10 protein (Parrish et al., 2007) and *S. cerevisiae* (Dunckley and Parker, 1999). These observations are all consistent with NdxD playing a role in *A. nidulans* decapping.

7.4. Development of decapping assay.

Decapping is one of the major steps in controlling the fate of transcripts in the cell. It would be useful if we could determine the proportion of decapped transcripts in different strains and

under different growth conditions. Currently, there are no reliable and sensitive methods that specifically detect and allow quantification of the mRNA in the decapped form. In order to achieve this goal, we developed an assay using the splinted-primer which has random nucleotides (N_8) at it's 5'-end so that it can potentially hybridise with any RNA sequence and facilitate the ligation of the RNA primer.

Our initial optimisation steps using the single mutant strain failed to amplify the decapped RNA for any of the strains used, except for the Δ*xrn1*. One possibility is that the decapped transcript is rapidly degraded by Xrn1, an exoribonuclease which is known to hydrolyzes RNA in the 5' to 3' direction (Blewett et al., 2011; Mullen and Marzluff, 2008). This is consistent with Xrn1 being the major exonuclease responsible for degradation of mRNA in *A. nidulans*, the decapped transcripts being stabilised in the Δ*xrn1* strain allowing them to be detected. However, this contradicts the hypothesis that Rat1 being implicated in NMD (Chapter 3). This may suggest that *A. nidulans* can differentiate between NMD and normal poly(A) dependent degradation. The assay showed that the proportion of decapped mRNA in strains disrupted for either *dcp2* or *ndxD* had a similarly significant effect. These data may suggest Dcp2 and NdxD are the primary decapping activities in *A. nidulans*. We attempted to make the triple mutant Δ*ndxD* Δ*dcp2* Δ*xrn1*, however, we were unable to achieve this. One possibility is that this strain is inviable as all other combinations were amongst the progeny tested.

One of the major concern of the assay developed is the different size of the final products from the qRT-PCR, which is smaller than expected size. One possibility is that the adaptor preferentially ligates to the smaller decapped/degraded transcript. Further optimisation steps are required to develop a robust assay. However, the assay developed in this chapter provides a good basis for further development.

7.5. Polysome analysis.

An interesting result from the polysome profile of Δ*dcp1* was achieved, where the large subunit (60S) represented the major peak. The accumulation of ribosomal subunits in the Δ*dcp1* mutant was also present but less striking in Δ*dcp2,* again indicating a distinction in the function between these two components of the decapping complex. The large 60S fraction from Δ*dcp1* strains included a high proportion of fragments derived from 28S rRNA, which we postulate to be 28S degradation products. Northern analysis and sequencing which suggests that the fragments identified are composed of small fragments which associate into a more complex structure directly derived from 60S ribosomal subunit. The three cleavage sites identified show two in a very close proximity within the ribosomal exit tunnel, suggesting the same activity may be responsible for both events. The third cleavage site is also accessible on the mature 60S subunit. The accumulation of the 60S subunits coinciding with the relatively high level of cleaved degradation products suggests that these may represent non-functional rRNA components, rather than functional subunits accumulating due to the repression of translational initiation. Supporting this is unpublished data, based on Western analysis, which demonstrates that the ribosomal proteins in the Δ*dcp1* strain have a very high level of ubiquitination (Parisi, personal communication). Interestingly non-functional rRNA decay (NRD), which specifically eliminates defective subunits, is triggered by ubiquitination of ribosomal proteins (Fujii et al., 2009). If deletion of *dcp1,* and to a lesser extent *dcp2,* leads to ribosome turnover, the basis of this is intriguing. We know that Dcp1 and Dcp2 associate with ribosomes and function to decap transcripts during translation. It is, therefore, possible that in the absence of the decapping complex the coordination of RNA degradation and translational termination are both inhibited/defective and this may in some way signal to a salvage mechanism to degrade apparently defective ribosomes.

Why Δ*dcp1* strains have both a more striking aberrant ribosomal profile and a proportionately higher level of degradation products as compared to Δ*dcp2* strains is intriguing, considering that Dcp1 is an enhancer of Dcp2 and that at the level of mRNA degradation Dcp2 plays a more direct and greater role (Chapter 3). As both Δ*dcp2* and the non-catalytic mutant $dcp2^{E148Q}$ were both epistatic to Δ*dcp1,* the implication is that free Dcp2 is in some way exacerbating the Δ*dcp1* mutant phenotype. These data also indicate that the Nudix domain plays an important role consistent with the nuclease activity of Dcp2 acting directly to cleave the rRNA in the absence of Dcp1. However, it is important to note that the degradation products observed by Northern analysis in both the Δ*dcp1* and Δ*dcp2* strains appear very similar, even though the levels vary dramatically. This implies that Dcp2 is not responsible for this or it is one of a number of activities cleaving the rRNA in what appears to be a similar way.

7.6. Future plans.

This study has produced numbers of interesting findings as to how decapping takes place in *A. nidulans*. Our results show that disruption of dcp1 has little effect in stabilising the uaZ^{+} transcript which contradicts the observation for the Δ*dcp2* mutant strain. Furthermore, fluorescence microscopy analysis also shows that only a small proportion of Dcp1 and Dcp2 co-localise and potentially form a complex in *A. nidulans* at any one time, which contradicts the results observed in yeast. Moreover, deletion of *dcp1* and *dcp2* produce related but distinct polysome profiles and proportions of 28S degradation products. Confirmation of these data is needed, with more extensive analysis of RNA degradation phenotypes, testing of different tagged versions of the proteins for fluorescence microscopy and alternative approaches such as immunoprecipitation to identify other interacting partners.

Studies have shown that Rat1 also possess the 5'-3' exonucleases activity in yeast, it is really interesting if we can produce a Rat1 mutant in *A. nidulans*. Although our group has successfully

produced a Δ*rat1* strain due to its very poor growth it difficult to assay. One possibility in generating a conditional mutant; i.e introducing the regulated promoter so that it will turn the protein off prior to NMD. However, it would also be desirable to destabilise the protein so that loss of Rat1 activity could be better controlled.

Finally, global transcript degradation should ideally be carried out using the various strains lacking various genes involved in mRNA degradation. This comparative method can help us understand the changes in mRNA degradation and synthesis rates in *A. nidulans*. However, this project will generate large sequencing data, thus expertise in bioinformatics is needed to perform the extensive analysis. Additionally, the cost of running this type of project needs to be taken into account.

It is interesting to know the positions of the cleavage sites of the 28S rRNA caused by the disruption of decapping factors Dcp1 and Dcp2. Although we have tried several methods, but we haven't managed to sequence all the fragments identified by Northern analysis. We predict that there are other RNA fragments within the complex and sequencing all would allow us to determine the cleavage positions comparing WT with different mutants.

APPENDIX 1a - Buffers and solutions for general molecular biology

0.5M EDTA (pH8.0), per 1 litre:

168.1 g EDTA

1X Tris-EDTA (TE) buffer, per 1 litre:

3.72 g EDTA, 12.11 g Tris-HCl (pH7.5), Autoclave

50X Tris Acetate EDTA buffer, per 1 litre:

242 g Trisbase, 57.1 ml glacial acetic acid, 100 ml 0.5 M EDTA (pH8.0)

20X sodium citrate (SSC) buffer, per 1 litre:

175.3 g NaCl, 88.2 g sodium citrate (pH7.0), autoclave

10X MOPS (for RNA electrophoresis), per 1 litre:

41.9 g MOPS, 4.1 g NaAc, 3.7 g EDTA, Autoclave

Proflavine:

1 mg of solid proflavine (Sigma) dissolved in 1 ml of sterile water

10X Gel-Loading buffer (RNA electrophoresis)

50 ml glycerol, 25 ml 1.0 M EDTA (pH8.0), 100 mg bromophenol blue

APPENDIX 1b – Fungal solutions and media

Aspergillus Salts Solution (1 litre):

KCl 26 g

MgSo4.7H2O 26 g

KH2PO4 76 g

Trace elements solution 50 ml

Solution stored at 4˚C

Vitamin solution (1 litre):

ϱ-amino benzoic acid (PABA) 0.4 g

Calcium pantothenate (Panto) 0.6 g

Pyridoxine (Pyro) 0.25 g

Riboflavin (Ribo) 0.1 g

Trace elements solution (1 litre)

Sodium tetraborate 0.04 g

Cupric sulphate 0.4 g

Ferric orthophosphate 0.8 g

Manganese sulphate 0.8 g

Sodium molybdate 0.8 g

Zinc sulphate 8.0 g

Complete medium (CM) (1 litre):

Glucose 10 g

Aspergillus salt solutions 20 ml

Vitamin solution 10 ml

Yeast extract 1 g

Peptone 2 g

Casamino acids 1 g

Adenine 75 mg

Adjust pH to pH6.5 using NaOH

Minimum medium (MM) (1 litre):

Glucose 10 g

Aspergillus salt solutions 20 ml

Adjust pH to pH6.5 using NaOH

For solid media, granulated agar was added at either 1% or 3% (w/v)

All media were autoclaved for 20 minutes at 15 psi and stored at 4˚C

Appendix 2

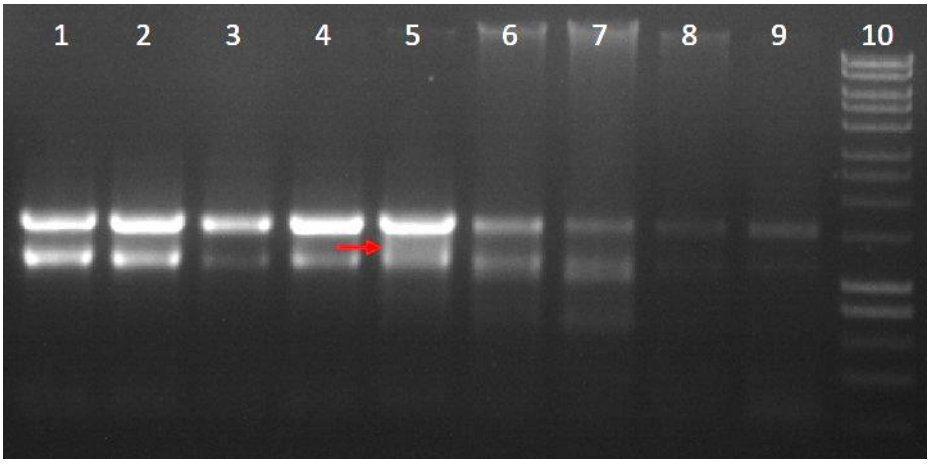

Gel picture of purified RNA from the Δ*dcp1* Δ*dcp2* polysome fractionation. Based on the picture, we can see a clear 18S and 28S rRNA bands in the polysome peaks and monosome peak (Lane 1,2,3,4), 60S (Lane 5). DNA Ladder (Hyperladder1)(Lane 10). Red arrow indicate the degradation product.

Appendix 3

```
Query  1    GGCTAGATGACTTGTGCGTCCGCTTCATTATAAACCTGCCCCGTGAGGAACTGGAATCGG  60
Sbjct  1    GGCTAGATGACTTGTGCGTCCGCTTCATTATAAACCTGCCCCGTGAGGAACTGGAATCGG  60

Query  61   TTGAGCGAATATGTTTCCAAGTCGAAGAAGCACAATGGTTTTACGAAGATTTCATCCGGC  120
Sbjct  61   TTGAGCGAATATGTTTCCAAGTCGAAGAAGCACAATGGTTTTACGAAGATTTCATCCGGC  120

Query  121  CGTTAGACCCAGCCCTCCCTTCGCTTTCACTGAAGGCTTTCGCCTTGCGGATTTTCCAGC  180
Sbjct  121  CGTTAGACCCAGCCCTCCCTTCGCTTTCACTGAAGGCTTTCGCCTTGCGGATTTTCCAGC  180

Query  181  ATTGTCCGCTTATGGCCAACTGGTCTCGATATCATCATATGACTGCCTTTTCTGAGTTCC  240
Sbjct  181  ATTGTCCGCTTATGGCCAACTGGTCTCGATATCATCATATGACTGCCTTTTCTGAGTTCC  240

Query  241  TTGCCTATAAAACTCGCGTTCCTGTTCGTGGAGCAATCATGTTGAACCAAGAAATGGATC  300
Sbjct  241  TTGCCTATAAAACTCGCGTTCCTGTTCGTGGAGCAATCATGTTGAACCAAGAAATGGATC  300

Query  301  AGGTTGTTTTAGTCAAGGGCTGGAAGAAGGGCGCTAACTGGAGTTTCCCTCGGGGGAAAA  360
Sbjct  301  AGGTTGTTTTAGTCAAGGGCTGGAAGAAGGGCGCTAACTGGAGTTTCCCTCGGGGGAAAA  360

Query  361  TCAACAAGGACGAAAAAGATCTTGACTGCGCGATCCGGGAGGTATATGAGCAAACTGGAT  420
Sbjct  361  TCAACAAGGACGAAAAAGATCTTGACTGCGCGATCCGGGAGGTATATGAGGAAACTGGAT  420

Query  421  ACGACGTACGAGAGGCGGGCTTGGTCCCGAACGATGA  457
Sbjct  421  ACGACGTACGAGAGGCGGGCTTGGTCCCGAACGATGA  457
```

The alignment of a point mutation at the Nudix domain of *dcp2* with the original *dcp2*. The confirmation of point mutation at the 442 was validated by sequencing (Red arrow).

Appendix 4

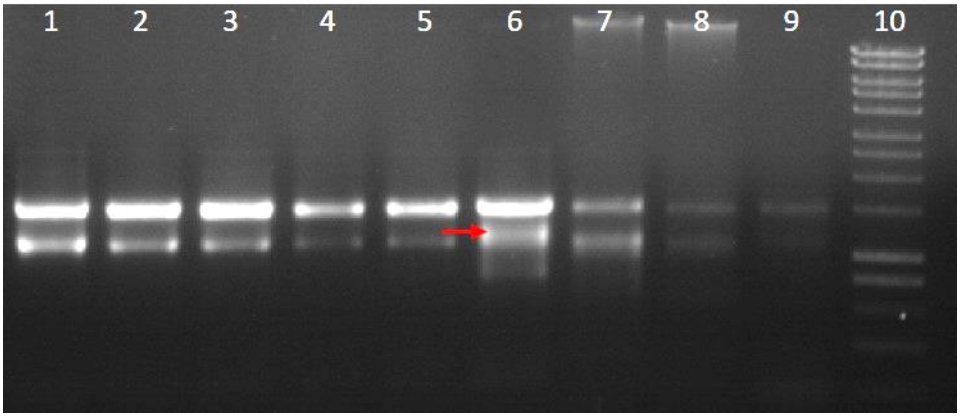

Gel picture of purified RNA from the Δ*dcp1 dcp2^{E148Q}* polysome fractionation. Based on the picture, we can see a clear 18S and 28S rRNA bands in the polysome peaks and monosome peak (Lane 1,2,3,4). 60S (Lane 5). DNA Ladder (Hyperladder1)(Lane 10). Red arrow indicate the degradation product.

Appendix 5

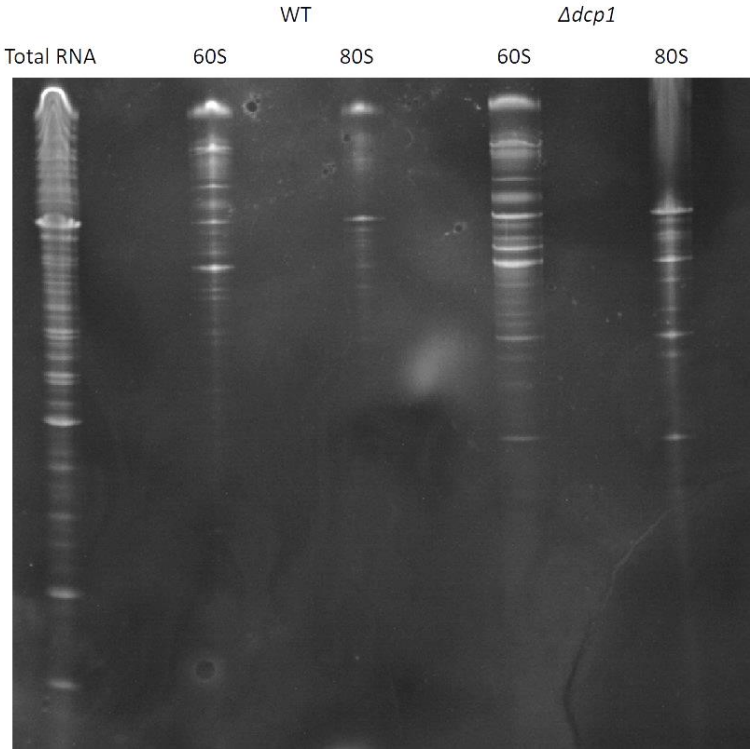

Separation of the purified RNA from the monosome (80S) and large subunit (60S) fractions from WT and Δ*dcp1*. 500 µg samples were loaded for each well and separated at 200 volts for 2.5 hours in 6% TBE-Urea gel (Thermo). Total RNA samples were used as a control sample.

References

1) Abdelhamid, R.F., Plessy, C., Yamauchi, Y., Taoka, M., de Hoon, M., Gingeras, T.R., Isobe, T., and Carninci, P. (2014). Multiplicity of 5′ Cap Structures Present on Short RNAs. PLoS ONE 9, e102895.
2) Amrani, N., Ganesan, R., Kervestin, S., Mangus, D.A., Ghosh, S., and Jacobson, A. (2004). A faux 3[prime]-UTR promotes aberrant termination and triggers nonsense-mediated mRNA decay. Nature 432, 112-118.
3) Amrani, N., Sachs, M.S., and Jacobson, A. (2006). Early nonsense: mRNA decay solves a translational problem. Nature reviews. Molecular cell biology 7, 415-425.
4) Archer, S.K., Shirokikh, N.E., Hallwirth, C.V., Beilharz, T.H., and Preiss, T. (2015). Probing the closed-loop model of mRNA translation in living cells. RNA Biology 12, 248-254.
5) Bail, S., Swerdel, M., Liu, H., Jiao, X., Goff, L.A., Hart, R.P., and Kiledjian, M. (2010). Differential regulation of microRNA stability. RNA (New York, N.Y.) 16, 1032-1039.
6) Baker, K.E., and Parker, R. (2004). Nonsense-mediated mRNA decay: terminating erroneous gene expression. Current Opinion in Cell Biology 16, 293-299.
7) Balagopal, V., Fluch, L., and Nissan, T. (2012). Ways and means of eukaryotic mRNA decay. Biochimica et Biophysica Acta (BBA) - Gene Regulatory Mechanisms 1819, 593-603.
8) Basturea, G.N., Zundel, M.A., and Deutscher, M.P. (2011). Degradation of ribosomal RNA during starvation: comparison to quality control during steady-state growth and a role for RNase PH. RNA (New York, N.Y.) 17, 338-345.
9) Beelman, C.A., and Parker, R. (1994). Differential effects of translational inhibition in cis and in trans on the decay of the unstable yeast MFA2 mRNA. J Biol Chem 269, 9687-9692.
10) Bessman, M., Frick, D., and O' Handley, S. (1996). The MutT proteins or "Nudix" hydrolases, a family of versatile, widely distributed, "housecleaning" enzymes. J Biol Chem 271, 25059-25062.
11) Blewett, N., Coller, J., and Goldstrohm, A. (2011). A quantitative assay for measuring mRNA decapping by splinted ligation reverse transcription polymerase chain reaction: qSL-RT-PCR. RNA (New York, N.Y.) 17, 535-543.
12) Borja, M.S., Piotukh, K., Freund, C., and Gross, J.D. (2011). Dcp1 links coactivators of mRNA decapping to Dcp2 by proline recognition. RNA (New York, N.Y.) 17, 278-290.
13) Borja, M.S., Piotukh, K., Freund, C., and Gross, J.D. (2011). Dcp1 links coactivators of mRNA decapping to Dcp2 by proline recognition. RNA (New York, N.Y.) 17, 278-290.
14) Borsuk, P.A., Nagiec, M.M., Stepien, P.P., and Bartnik, E. (1982). Organization of the ribosomal RNA gene cluster in Aspergillus nidulans. Gene 17, 147-152.
15) Braun, J.E., Truffault, V., Boland, A., Huntzinger, E., Chang, C.-T., Haas, G., Weichenrieder, O., Coles, M., and Izaurralde, E. (2012). A direct interaction between DCP1 and XRN1 couples mRNA decapping to 5′ exonucleolytic degradation. Nat Struct Mol Biol 19, 1324-1331.
16) Braun, K.A., and Young, E.T. (2014). Coupling mRNA Synthesis and Decay. Molecular and Cellular Biology 34, 4078-4087.

17) Brogna, S., and Wen, J. (2009). Nonsense-mediated mRNA decay (NMD) mechanisms. Nat Struct Mol Biol 16, 107-113.
18) Butler, J.S., and Mitchell, P. (2010). Rrp6, Rrp47 and Cofactors of the Nuclear Exosome. In RNA Exosome, T.H. Jensen, ed. (New York, NY: Springer US), pp. 91-104.
19) Caddick, M.X., Jones, M.G., van Tonder, J.M., Le Cordier, H., Narendja, F., Strauss, J., and Morozov, I.Y. (2006). Opposing signals differentially regulate transcript stability in Aspergillus nidulans. Mol Microbiol 62, 509-519.
20) Chamieh, H., Ballut, L., Bonneau, F., and Le Hir, H. (2008). NMD factors UPF2 and UPF3 bridge UPF1 to the exon junction complex and stimulate its RNA helicase activity. Nat Struct Mol Biol 15, 85-93.
21) Chang, C.-T., Bercovich, N., Loh, B., Jonas, S., and Izaurralde, E. (2014). The activation of the decapping enzyme DCP2 by DCP1 occurs on the EDC4 scaffold and involves a conserved loop in DCP1. Nucleic acids research.
22) Chang, H., Lim, J., Ha, M., and Kim, V.N. (2014). TAIL-seq: genome-wide determination of poly(A) tail length and 3' end modifications. Molecular cell 53, 1044-1052.
23) Chang, J.H., Xiang, S., Xiang, K., Manley, J.L., and Tong, L. (2011). Structural and biochemical studies of the 5′→3′ exoribonuclease Xrn1. Nat Struct Mol Biol 18, 270-276.
24) Chang, P.-K., Scharfenstein, L.L., Mack, B., and Ehrlich, K.C. (2012). Deletion of the Aspergillus flavus Orthologue of A. nidulans fluG Reduces Conidiation and Promotes Production of Sclerotia but Does Not Abolish Aflatoxin Biosynthesis. Applied and Environmental Microbiology 78, 7557-7563.
25) Chang, Y.F., Imam, J.S., and Wilkinson, M.F. (2007). The nonsense-mediated decay RNA surveillance pathway. Annual review of biochemistry 76, 51-74.
26) Chowdhury, A., Kalurupalle, S., and Tharun, S. (2014). Pat1 contributes to the RNA binding activity of the Lsm1-7–Pat1 complex. RNA (New York, N.Y.) 20, 1465-1475.
27) Coller, J. (2008). Chapter 14 Methods to Determine mRNA Half-Life in Saccharomyces cerevisiae. In Methods in Enzymology (Academic Press), pp. 267-284.
28) Coller, J. (2016). mRNA decapping in 3D. Nat Struct Mol Biol 23, 954-956.
29) Coller, J., and Parker, R. (2004). Eukaryotic mRNA decapping. Annual review of biochemistry 73, 861-890.
30) Coller, J.M., Tucker, M., Sheth, U., Valencia-Sanchez, M.A., and Parker, R. (2001). The DEAD box helicase, Dhh1p, functions in mRNA decapping and interacts with both the decapping and deadenylase complexes. RNA (New York, N.Y.) 7, 1717-1727.
31) Conti, E., and Izaurralde, E. (2005). Nonsense-mediated mRNA decay: molecular insights and mechanistic variations across species. Current Opinion in Cell Biology 17, 316-325.
32) Deana, A., Celesnik, H., and Belasco, J.G. (2008). The bacterial enzyme RppH triggers messenger RNA degradation by 5[prime] pyrophosphate removal. Nature 451, 355-358.
33) Decker, C.J., Teixeira, D., and Parker, R. (2007). Edc3p and a glutamine/asparagine-rich domain of Lsm4p function in processing body assembly in Saccharomyces cerevisiae. Journal of Cell Biology 179, 437-449.
34) Deshmukh, M.V., Jones, B.N., Quang-Dang, D.U., Flinders, J., Floor, S.N., Kim, C., Jemielity, J., Kalek, M., Darzynkiewicz, E., and Gross, J.D. (2008). mRNA decapping is promoted by an RNA-binding channel in Dcp2. Molecular cell 29, 324-336.

35) Dez, C., Houseley, J., and Tollervey, D. (2006). Surveillance of nuclear-restricted pre-ribosomes within a subnucleolar region of Saccharomyces cerevisiae. The EMBO Journal 25, 1534-1546.
36) Drążkowska, K., Tomecki, R., Stoduś, K., Kowalska, K., Czarnocki-Cieciura, M., and Dziembowski, A. (2013). The RNA exosome complex central channel controls both exonuclease and endonuclease Dis3 activities in vivo and in vitro. Nucleic acids research 41, 3845-3858.
37) Dunckley, T., and Parker, R. (1999). The DCP2 protein is required for mRNA decapping in Saccharomyces cerevisiae and contains a functional MutT motif. The EMBO Journal 18, 5411-5422.
38) Durand, S., Cougot, N., Mahuteau-Betzer, F., Nguyen, C.-H., Grierson, D.S., Bertrand, E., Tazi, J., and Lejeune, F. (2007). Inhibition of nonsense-mediated mRNA decay (NMD) by a new chemical molecule reveals the dynamic of NMD factors in P-bodies. The Journal of Cell Biology 178, 1145.
39) Durand, S., and Lykke-Andersen, J. (2013). Nonsense-mediated mRNA decay occurs during eIF4F-dependent translation in human cells. Nat Struct Mol Biol 20, 702-709.
40) Eberle, A.B., Lykke-Andersen, S., Muhlemann, O., and Jensen, T.H. (2009). SMG6 promotes endonucleolytic cleavage of nonsense mRNA in human cells. Nat Struct Mol Biol 16, 49-55.
41) Edgar, R.C. (2004). MUSCLE: multiple sequence alignment with high accuracy and high throughput. Nucleic acids research 32, 1792-1797.
42) Esposito, A.M., Mateyak, M., He, D., Lewis, M., Sasikumar, A.N., Hutton, J., Copeland, P.R., and Kinzy, T.G. (2010). Eukaryotic Polyribosome Profile Analysis. Journal of Visualized Experiments : JoVE, 1948.
43) Fenger-Gron, M., Fillman, C., Norrild, B., and Lykke-Andersen, J. (2005). Multiple processing body factors and the ARE binding protein TTP activate mRNA decapping. Molecular cell 20, 905-915.
44) Fillman, C., and Lykke-Andersen, J. (2005). RNA decapping inside and outside of processing bodies. Current Opinion in Cell Biology 17, 326-331.
45) Fischer, N., and Weis, K. (2002). The DEAD box protein Dhh1 stimulates the decapping enzyme Dcp1. The EMBO Journal 21, 2788-2797.
46) Franks, T.M., and Lykke-Andersen, J. (2008). The Control of mRNA Decapping and P-Body Formation. Molecular cell 32, 605-615.
47) Franks, T.M., Singh, G., and Lykke-Andersen, J. (2010). Upf1 ATPase-dependent mRNP disassembly is required for completion of nonsense- mediated mRNA decay. Cell 143, 938-950.
48) Fromm, S.A., Truffault, V., Kamenz, J., Braun, J.E., Hoffmann, N.A., Izaurralde, E., and Sprangers, R. (2012). The structural basis of Edc3- and Scd6-mediated activation of the Dcp1:Dcp2 mRNA decapping complex. The EMBO Journal 31, 279-290.
49) Fujii, K., Kitabatake, M., Sakata, T., Miyata, A., and Ohno, M. (2009). A role for ubiquitin in the clearance of nonfunctional rRNAs. Genes & development 23, 963-974.
50) Funakoshi, Y., Doi, Y., Hosoda, N., Uchida, N., Osawa, M., Shimada, I., Tsujimoto, M., Suzuki, T., Katada, T., and Hoshino, S.-i. (2007). Mechanism of mRNA deadenylation: evidence for a molecular interplay between translation termination factor eRF3 and mRNA deadenylases. Genes & development 21, 3135-3148.

51) Gabelli, S.B., Bianchet, M.A., Bessman, M.J., and Amzel, L.M. (2001). The structure of ADP-ribose pyrophosphatase reveals the structural basis for the versatility of the Nudix family. Nature structural biology 8, 467-472.
52) Gatfield, D., and Izaurralde, E. (2004). Nonsense-mediated messenger RNA decay is initiated by endonucleolytic cleavage in Drosophila. Nature 429, 575-578.
53) Ghosh, T., Peterson, B., Tomasevic, N., and Peculis, B.A. (2004). Xenopus U8 snoRNA Binding Protein Is a Conserved Nuclear Decapping Enzyme. Molecular cell 13, 817-828.
54) Glatigny, A., and Scazzocchio, C. (1995). Cloning and molecular characterization of hxA, the gene coding for the xanthine dehydrogenase (purine hydroxylase I) of Aspergillus nidulans. J Biol Chem 270, 3534-3550.
55) Gowda, M., Li, H., and Wang, G.-L. (2007). Robust analysis of 5[prime]-transcript ends: a high-throughput protocol for characterization of sequence diversity of transcription start sites. Nat. Protocols 2, 1622-1632.
56) Haas, G., Braun, J.E., Igreja, C., Tritschler, F., Nishihara, T., and Izaurralde, E. (2010). HPat provides a link between deadenylation and decapping in metazoa. The Journal of Cell Biology 189, 289.
57) Hall, B.G. (2013). Building Phylogenetic Trees from Molecular Data with MEGA. Molecular Biology and Evolution 30, 1229-1235.
58) Harigaya, Y., Jones, B.N., Muhlrad, D., Gross, J.D., and Parker, R. (2010). Identification and Analysis of the Interaction between Edc3 and Dcp2 in Saccharomyces cerevisiae. Molecular and Cellular Biology 30, 1446-1456.
59) He, F., Ganesan, R., and Jacobson, A. (2013). Intra- and Intermolecular Regulatory Interactions in Upf1, the RNA Helicase Central to Nonsense-Mediated mRNA Decay in Yeast. Molecular and Cellular Biology 33, 4672-4684.
60) He, F., and Jacobson, A. (2015). Control of mRNA decapping by positive and negative regulatory elements in the Dcp2 C-terminal domain. RNA (New York, N.Y.) 21, 1633-1647.
61) He, F., Li, X., Spatrick, P., Casillo, R., Dong, S., and Jacobson, A. (2003). Genome-Wide Analysis of mRNAs Regulated by the Nonsense-Mediated and 5′ to 3′ mRNA Decay Pathways in Yeast. Molecular cell 12, 1439-1452.
62) He, W., and Parker, R. (2001). The yeast cytoplasmic LsmI/Pat1p complex protects mRNA 3' termini from partial degradation. Genetics 158, 1445-1455.
63) Henry, T., Iwen, P.C., and Hinrichs, S.H. (2000). Identification of Aspergillus Species Using Internal Transcribed Spacer Regions 1 and 2. Journal of Clinical Microbiology 38, 1510-1515.
64) Hoefig, K.P., Rath, N., Heinz, G.A., Wolf, C., Dameris, J., Schepers, A., Kremmer, E., Ansel, K.M., and Heissmeyer, V. (2013). Eri1 degrades the stem-loop of oligouridylated histone mRNAs to induce replication-dependent decay. Nat Struct Mol Biol 20, 73-81.
65) Houseley, J., and Tollervey, D. (2009). The Many Pathways of RNA Degradation. Cell 136, 763-776.
66) Hu, W., Petzold, C., Coller, J., and Baker, K.E. (2010). Nonsense-mediated mRNA decapping occurs on polyribosomes in Saccharomyces cerevisiae. Nat Struct Mol Biol 17, 244-247.
67) Isken, O., and Maquat, L.E. (2008). The multiple lives of NMD factors: balancing roles in gene and genome regulation. Nat Rev Genet 9, 699-712.

68) Jacobson, A., and Peltz, S.W. (1999). Tools for Turnover: Methods for Analysis of mRNA Stability in Eukaryotic Cells. Methods 17, 1-2.
69) Johnson, A.W. (1997). Rat1p and Xrn1p are functionally interchangeable exoribonucleases that are restricted to and required in the nucleus and cytoplasm, respectively. Molecular and Cellular Biology 17, 6122-6130.
70) Karousis, E.D., Nasif, S., and Mühlemann, O. (2016). Nonsense-mediated mRNA decay: novel mechanistic insights and biological impact. Wiley Interdisciplinary Reviews: RNA 7, 661-682.
71) Kashima, I., Yamashita, A., Izumi, N., Kataoka, N., Morishita, R., Hoshino, S., Ohno, M., Dreyfuss, G., and Ohno, S. (2006). Binding of a novel SMG-1–Upf1–eRF1–eRF3 complex (SURF) to the exon junction complex triggers Upf1 phosphorylation and nonsense-mediated mRNA decay. Genes & development 20, 355-367.
72) Kervestin, S., and Jacobson, A. (2012). NMD: a multifaceted response to premature translational termination. Nature reviews. Molecular cell biology 13, 700-712.
73) King, H.A., and Gerber, A.P. (2014). Translatome profiling: methods for genome-scale analysis of mRNA translation. Briefings in Functional Genomics.
74) Kiss, D.L., Oman, K.M., Dougherty, J.A., Mukherjee, C., Bundschuh, R., and Schoenberg, D.R. (2016). Cap homeostasis is independent of poly(A) tail length. Nucleic acids research 44, 304-314.
75) Kowalinski, E., Kögel, A., Ebert, J., Reichelt, P., Stegmann, E., Habermann, B., and Conti, E. (2016). Structure of a Cytoplasmic 11-Subunit RNA Exosome Complex. Molecular cell 63, 125-134.
76) Krokowski, D., Gaccioli, F., Majumder, M., Mullins, M.R., Yuan, C.L., Papadopoulou, B., Merrick, W.C., Komar, A.A., Taylor, D., and Hatzoglou, M. (2011). Characterization of hibernating ribosomes in mammalian cells. Cell Cycle 10, 2691-2702.
77) Krol, K., Morozov, I.Y., Jones, M.G., Wyszomirski, T., Weglenski, P., Dzikowska, A., and Caddick, M.X. (2013). RrmA regulates the stability of specific transcripts in response to both nitrogen source and oxidative stress. Molecular Microbiology 89, 975-988.
78) Leeds, P., Peltz, S.W., Jacobson, A., and Culbertson, M.R. (1991). The product of the yeast UPF1 gene is required for rapid turnover of mRNAs containing a premature translational termination codon. Genes & development 5, 2303-2314.
79) Lejeune, F., Li, X., and Maquat, L.E. (2003). Nonsense-Mediated mRNA Decay in Mammalian Cells Involves Decapping, Deadenylating, and Exonucleolytic Activities. Molecular cell 12, 675-687.
80) Lejeune, F., Li, X., and Maquat, L.E. (2003). Nonsense-Mediated mRNA Decay in Mammalian Cells Involves Decapping, Deadenylating, and Exonucleolytic Activities. Molecular cell 12, 675-687.
81) Li, Y., Song, M., and Kiledjian, M. (2011). Differential utilization of decapping enzymes in mammalian mRNA decay pathways. RNA (New York, N.Y.) 17, 419-428.
82) Liu, H.-L., De Souza, C.P.C., Osmani, A.H., and Osmani, S.A. (2009). The Three Fungal Transmembrane Nuclear Pore Complex Proteins of Aspergillus nidulans Are Dispensable in the Presence of an Intact An-Nup84-120 Complex. Molecular Biology of the Cell 20, 616-630.
83) Liu, S.W., Jiao, X., Welch, S., and Kiledjian, M. (2008). Chapter 1 Analysis of mRNA Decapping. In Methods in Enzymology (Academic Press), pp. 3-21.

84) Livak, K.J., and Schmittgen, T.D. (2001). Analysis of relative gene expression data using real-time quantitative PCR and the 2(-Delta Delta C(T)) Method. Methods 25, 402-408.
85) Luciano, D.J., Hui, M.P., Deana, A., Foley, P.L., Belasco, K.J., and Belasco, J.G. (2012). Differential Control of the Rate of 5′-End-Dependent mRNA Degradation in Escherichia coli. Journal of Bacteriology 194, 6233-6239.
86) Lykke-Andersen, J., Shu, M.-D., and Steitz, J.A. (2000). Human Upf Proteins Target an mRNA for Nonsense-Mediated Decay When Bound Downstream of a Termination Codon. Cell 103, 1121-1131.
87) Lykke-Andersen, J., Shu, M.-D., and Steitz, J.A. (2001). Communication of the Position of Exon-Exon Junctions to the mRNA Surveillance Machinery by the Protein RNPS1. Science 293, 1836.
88) Lykke-Andersen, S., Brodersen, D.E., and Jensen, T.H. (2009). Origins and activities of the eukaryotic exosome. Journal of Cell Science 122, 1487.
89) Lykke-Andersen, S., and Jensen, T.H. (2015). Nonsense-mediated mRNA decay: an intricate machinery that shapes transcriptomes. Nature reviews. Molecular cell biology 16, 665-677.
90) Maderazo, A.B., He, F., Mangus, D.A., and Jacobson, A. (2000). Upf1p Control of Nonsense mRNA Translation Is Regulated by Nmd2p and Upf3p. Molecular and Cellular Biology 20, 4591-4603.
91) Mašek, T., Valášek, L., and Pospíšek, M. (2011). Polysome Analysis and RNA Purification from Sucrose Gradients. In RNA: Methods and Protocols, H. Nielsen, ed. (Totowa, NJ: Humana Press), pp. 293-309.
92) McCluskey, K., Wiest, A., and Plamann, M. (2010). The Fungal Genetics Stock Center: a repository for 50 years of fungal genetics research. Journal of biosciences 35, 119-126.
93) McLennan, A.G. (2006). The Nudix hydrolase superfamily. Cellular and molecular life sciences : CMLS 63, 123-143.
94) Milac, A.L., Bojarska, E., and Wypijewska del Nogal, A. (2014). Decapping Scavenger (DcpS) enzyme: Advances in its structure, activity and roles in the cap-dependent mRNA metabolism. Biochimica et Biophysica Acta (BBA) - Gene Regulatory Mechanisms 1839, 452-462.
95) Mildvan, A.S., Xia, Z., Azurmendi, H.F., Saraswat, V., Legler, P.M., Massiah, M.A., Gabelli, S.B., Bianchet, M.A., Kang, L.W., and Amzel, L.M. (2005). Structures and mechanisms of Nudix hydrolases. Archives of Biochemistry and Biophysics 433, 129-143.
96) Millevoi, S., and Vagner, S. (2010). Molecular mechanisms of eukaryotic pre-mRNA 3′ end processing regulation. Nucleic acids research 38, 2757-2774.
97) Miluzio, A., Beugnet, A., Volta, V., and Biffo, S. (2009). Eukaryotic initiation factor 6 mediates a continuum between 60S ribosome biogenesis and translation. EMBO Reports 10, 459-465.
98) Mitchell, P., and Tollervey, D. (2003). An NMD Pathway in Yeast Involving Accelerated Deadenylation and Exosome-Mediated 3′→5′ Degradation. Molecular cell 11, 1405-1413.
99) Morozov, I.Y., Galbis-Martinez, M., Jones, M.G., and Caddick, M.X. (2001). Characterization of nitrogen metabolite signalling in Aspergillus via the regulated degradation of areA mRNA. Molecular Microbiology 42, 269-277.

100) Morozov, I.Y., Jones, M.G., Gould, P.D., Crome, V., Wilson, J.B., Hall, A.J., Rigden, D.J., and Caddick, M.X. (2012). mRNA 3' tagging is induced by nonsense-mediated decay and promotes ribosome dissociation. Mol Cell Biol 32, 2585-2595.
101) Morozov, I.Y., Jones, M.G., Razak, A.A., Rigden, D.J., and Caddick, M.X. (2010). CUCU Modification of mRNA Promotes Decapping and Transcript Degradation in Aspergillus nidulans. Molecular and Cellular Biology 30, 460-469.
102) Morozov, I.Y., Jones, M.G., Spiller, D.G., Rigden, D.J., Dattenböck, C., Novotny, R., Strauss, J., and Caddick, M.X. (2010). Distinct roles for Caf1, Ccr4, Edc3 and CutA in the co-ordination of transcript deadenylation, decapping and P-body formation in Aspergillus nidulans. Molecular Microbiology 76, 503-516.
103) Morozov, I.Y., Martinez, M.G., Jones, M.G., and Caddick, M.X. (2000). A defined sequence within the 3′ UTR of the areA transcript is sufficient to mediate nitrogen metabolite signalling via accelerated deadenylation. Molecular Microbiology 37, 1248-1257.
104) Morozov, I.Y., Negrete-Urtasun, S., Tilburn, J., Jansen, C.A., Caddick, M.X., and Arst, H.N. (2006). Nonsense-Mediated mRNA Decay Mutation in Aspergillus nidulans. Eukaryotic Cell 5, 1838-1846.
105) Mühlemann, O., and Lykke-Andersen, J. (2010). How and where are nonsense mRNAs degraded in mammalian cells? RNA biology 7, 28-32.
106) Muhlrad, D., and Parker, R. (1999). Aberrant mRNAs with extended 3' UTRs are substrates for rapid degradation by mRNA surveillance. RNA (New York, N.Y.) 5, 1299-1307.
107) Mukherjee, C., Patil, Deepak P., Kennedy, Brian A., Bakthavachalu, B., Bundschuh, R., and Schoenberg, Daniel R. (2012). Identification of Cytoplasmic Capping Targets Reveals a Role for Cap Homeostasis in Translation and mRNA Stability. Cell Reports 2, 674-684.
108) Mullen, T.E., and Marzluff, W.F. (2008). Degradation of histone mRNA requires oligouridylation followed by decapping and simultaneous degradation of the mRNA both 5' to 3' and 3' to 5'. Genes & development 22, 50-65.
109) Mullen, T.E., and Marzluff, W.F. (2008). Degradation of histone mRNA requires oligouridylation followed by decapping and simultaneous degradation of the mRNA both 5′ to 3′ and 3′ to 5′. Genes & development 22, 50-65.
110) Nagarajan, V.K., Jones, C.I., Newbury, S.F., and Green, P.J. (2013). XRN 5'→3' exoribonucleases: Structure, mechanisms and functions. Biochimica et biophysica acta 1829, 590-603.
111) Nagarajan, V.K., Jones, C.I., Newbury, S.F., and Green, P.J. (2013). XRN 5'→3' exoribonucleases: Structure, mechanisms and functions. Biochimica et biophysica acta 1829, 590-603.
112) Nayak, T., Szewczyk, E., Oakley, C.E., Osmani, A., Ukil, L., Murray, S.L., Hynes, M.J., Osmani, S.A., and Oakley, B.R. (2006). A Versatile and Efficient Gene-Targeting System for Aspergillus nidulans. Genetics 172, 1557-1566.
113) Newbury, S., and Woollard, A. (2004). The 5′–3′ exoribonuclease xrn-1 is essential for ventral epithelial enclosure during C. elegans embryogenesis. RNA (New York, N.Y.) 10, 59-65.
114) Nilsen, T.W. (2013). Splinted Ligation Method to Detect Small RNAs. Cold Spring Harbor Protocols 2013, pdb.prot072611.

115) Nilsen, T.W. (2013). Splinted Ligation Method to Detect Small RNAs. Cold Spring Harbor Protocols 2013, pdb.prot072611.
116) Nissan, T., Rajyaguru, P., She, M., Song, H., and Parker, R. (2010). Decapping activators in Saccharomyces cerevisiae act by multiple mechanisms. Molecular cell 39, 773-783.
117) Nurenberg, E., and Tampe, R. (2013). Tying up loose ends: ribosome recycling in eukaryotes and archaea. Trends in biochemical sciences 38, 64-74.
118) Page, M.F., Carr, B., Anders, K.R., Grimson, A., and Anderson, P. (1999). SMG-2 Is a Phosphorylated Protein Required for mRNA Surveillance in Caenorhabditis elegans and Related to Upf1p of Yeast. Molecular and Cellular Biology 19, 5943-5951.
119) Park, E., and Maquat, L.E. (2013). Staufen-mediated mRNA decay. Wiley interdisciplinary reviews. RNA 4, 423-435.
120) Parker, R. (2012). RNA Degradation in Saccharomyces cerevisae. Genetics 191, 671-702.
121) Parker, R., and Sheth, U. (2007). P Bodies and the Control of mRNA Translation and Degradation. Molecular cell 25, 635-646.
122) Parker, R., and Song, H. (2004). The enzymes and control of eukaryotic mRNA turnover. Nat Struct Mol Biol 11, 121-127.
123) Parrish, S., Resch, W., and Moss, B. (2007). Vaccinia virus D10 protein has mRNA decapping activity, providing a mechanism for control of host and viral gene expression. Proceedings of the National Academy of Sciences of the United States of America 104, 2139-2144.
124) Peccarelli, M., and Kebaara, B.W. (2014). Regulation of Natural mRNAs by the Nonsense-Mediated mRNA Decay Pathway. Eukaryotic Cell 13, 1126-1135.
125) Pestov, D.G., and Shcherbik, N. (2012). Rapid Cytoplasmic Turnover of Yeast Ribosomes in Response to Rapamycin Inhibition of TOR. Molecular and Cellular Biology 32, 2135-2144.
126) Pestova, T.V., and Hellen, C.U.T. (2003). Translation elongation after assembly of ribosomes on the Cricket paralysis virus internal ribosomal entry site without initiation factors or initiator tRNA. Genes & development 17, 181-186.
127) Platt, A., Langdon, T., Arst, H.N., Kirk, D., Tollervey, D., Sanchez, J.M., and Caddick, M.X. (1996). Nitrogen metabolite signalling involves the C-terminus and the GATA domain of the Aspergillus transcription factor AREA and the 3' untranslated region of its mRNA. The EMBO Journal 15, 2791-2801.
128) Rissland, O.S., and Norbury, C.J. (2009). Decapping is preceded by 3[prime] uridylation in a novel pathway of bulk mRNA turnover. Nat Struct Mol Biol 16, 616-623.
129) Schaefer, B.C. (1995). Revolutions in Rapid Amplification of cDNA Ends: New Strategies for Polymerase Chain Reaction Cloning of Full-Length cDNA Ends. Analytical Biochemistry 227, 255-273.
130) Schindelin, J., Arganda-Carreras, I., Frise, E., Kaynig, V., Longair, M., Pietzsch, T., Preibisch, S., Rueden, C., Saalfeld, S., Schmid, B., et al. (2012). Fiji - an Open Source platform for biological image analysis. Nature methods 9, 10.1038/nmeth.2019.
131) Schmittgen, T.D., and Livak, K.J. (2008). Analyzing real-time PCR data by the comparative C(T) method. Nature protocols 3, 1101-1108.
132) Schneider, C., Leung, E., Brown, J., and Tollervey, D. (2009). The N-terminal PIN domain of the exosome subunit Rrp44 harbors endonuclease activity and tethers Rrp44 to the yeast core exosome. Nucleic acids research 37, 1127-1140.

133) Schneider, C., and Tollervey, D. (2014). Looking into the barrel of the RNA exosome. Nat Struct Mol Biol 21, 17-18.
134) Schwartz, D., Decker, C.J., and Parker, R.O.Y. (2003). The enhancer of decapping proteins, Edc1p and Edc2p, bind RNA and stimulate the activity of the decapping enzyme. RNA (New York, N.Y.) 9, 239-251.
135) Sharif, H. (2014). Structural and biochemical characterization of eukaryotic mRNA decapping activators. (Ludwig-Maximilians-Universität München).
136) Sharif, H., and Conti, E. (2013). Architecture of the Lsm1-7-Pat1 Complex: A Conserved Assembly in Eukaryotic mRNA Turnover. Cell Reports 5, 283-291.
137) Shatkin, A.J., and Manley, J.L. (2000). The ends of the affair: Capping and polyadenylation. Nature structural biology 7, 838-842.
138) She, M., Decker, C.J., Svergun, D.I., Round, A., Chen, N., Muhlrad, D., Parker, R., and Song, H. (2008). Structural basis of Dcp2 recognition and activation by Dcp1. Molecular cell 29, 337-349.
139) Sheth, U., and Parker, R. (2006). Targeting of Aberrant mRNAs to Cytoplasmic Processing Bodies. Cell 125, 1095-1109.
140) Shimizu, M., Masuo, S., Fujita, T., Doi, Y., Kamimura, Y., and Takaya, N. (2012). Hydrolase controls cellular NAD, sirtuin, and secondary metabolites. Mol Cell Biol 32, 3743-3755.
141) Shimizu, M., and Takaya, N. (2013). Nudix Hydrolase Controls Nucleotides and Glycolytic Mechanisms in Hypoxic Aspergillus nidulans. Bioscience, Biotechnology, and Biochemistry 77, 1888-1893.
142) Sivan, G., Kedersha, N., and Elroy-Stein, O. (2007). Ribosomal Slowdown Mediates Translational Arrest during Cellular Division. Molecular and Cellular Biology 27, 6639-6646.
143) Solinger, J.A., Pascolini, D., and Heyer, W.-D. (1999). Active-Site Mutations in the Xrn1p Exoribonuclease of Saccharomyces cerevisiae Reveal a Specific Role in Meiosis. Molecular and Cellular Biology 19, 5930-5942.
144) Sonenberg, N., and Dever, T.E. (2003). Eukaryotic translation initiation factors and regulators. Current opinion in structural biology 13, 56-63.
145) Sonenberg, N., and Hinnebusch, A.G. (2009). Regulation of Translation Initiation in Eukaryotes: Mechanisms and Biological Targets. Cell 136, 731-745.
146) Song, J., Song, J., Mo, B., and Chen, X. (2015). Uridylation and adenylation of RNAs. Science China. Life sciences 58, 1057-1066.
147) Song, M.G., Bail, S., and Kiledjian, M. (2013). Multiple Nudix family proteins possess mRNA decapping activity. RNA (New York, N.Y.) 19, 390-399.
148) Song, M.-G., Li, Y., and Kiledjian, M. (2010). Multiple mRNA Decapping Enzymes in Mammalian Cells. Molecular cell 40, 423-432.
149) Steiger, M., Carr-Schmid, A., Schwartz, D.C., Kiledjian, M., and Parker, R.O.Y. (2003). Analysis of recombinant yeast decapping enzyme. RNA (New York, N.Y.) 9, 231-238.
150) Streit, S., Michalski, C.W., Erkan, M., Kleeff, J., and Friess, H. (2008). Northern blot analysis for detection and quantification of RNA in pancreatic cancer cells and tissues. Nat. Protocols 4, 37-43.
151) Sun, M., Schwalb, B., Pirkl, N., Maier, Kerstin C., Schenk, A., Failmezger, H., Tresch, A., and Cramer, P. (2013). Global Analysis of Eukaryotic mRNA Degradation Reveals Xrn1-Dependent Buffering of Transcript Levels. Molecular cell 52, 52-62.

152) Sweet, T., Kovalak, C., and Coller, J. (2012). The DEAD-Box Protein Dhh1 Promotes Decapping by Slowing Ribosome Movement. PLOS Biology 10, e1001342.
153) Swisher, K.D., and Parker, R. (2011). Interactions between Upf1 and the Decapping Factors Edc3 and Pat1 in Saccharomyces cerevisiae. PLoS ONE 6, e26547.
154) Szewczyk, E., Nayak, T., Oakley, C.E., Edgerton, H., Xiong, Y., Taheri-Talesh, N., Osmani, S.A., and Oakley, B.R. (2007). Fusion PCR and gene targeting in Aspergillus nidulans. Nat. Protocols 1, 3111-3120.
155) Tabb-Massey, A., Caffrey, J.M., Logsden, P., Taylor, S., Trent, J.O., and Ellis, S.R. (2003). Ribosomal proteins Rps0 and Rps21 of Saccharomyces cerevisiae have overlapping functions in the maturation of the 3′ end of 18S rRNA. Nucleic acids research 31, 6798-6805.
156) Tamura, K., Peterson, D., Peterson, N., Stecher, G., Nei, M., and Kumar, S. (2011). MEGA5: molecular evolutionary genetics analysis using maximum likelihood, evolutionary distance, and maximum parsimony methods. Mol Biol Evol 28, 2731-2739.
157) Taylor, M.J., and Peculis, B.A. (2008). Evolutionary conservation supports ancient origin for Nudt16, a nuclear-localized, RNA-binding, RNA-decapping enzyme. Nucleic acids research 36, 6021-6034.
158) Tharun, S., He, W., Mayes, A.E., Lennertz, P., Beggs, J.D., and Parker, R. (2000). Yeast Sm-like proteins function in mRNA decapping and decay. Nature 404, 515-518.
159) Thompson, D.M., and Parker, R. (2007). Cytoplasmic Decay of Intergenic Transcripts in Saccharomyces cerevisiae. Molecular and Cellular Biology 27, 92-101.
160) Thompson, J.D., Higgins, D.G., and Gibson, T.J. (1994). CLUSTAL W: improving the sensitivity of progressive multiple sequence alignment through sequence weighting, position-specific gap penalties and weight matrix choice. Nucleic acids research 22, 4673-4680.
161) Tilburn, J., Scazzocchio, C., Taylor, G.G., Zabicky-Zissman, J.H., Lockington, R.A., and Davies, R.W. (1983). Transformation by integration in Aspergillus nidulans. Gene 26, 205-221.
162) Todd, R.B., Davis, M.A., and Hynes, M.J. (2007). Genetic manipulation of Aspergillus nidulans: meiotic progeny for genetic analysis and strain construction. Nat. Protocols 2, 811-821.
163) Tucker, M., Valencia-Sanchez, M.A., Staples, R.R., Chen, J., Denis, C.L., and Parker, R. (2001). The Transcription Factor Associated Ccr4 and Caf1 Proteins Are Components of the Major Cytoplasmic mRNA Deadenylase in Saccharomyces cerevisiae. Cell 104, 377-386.
164) Valkov, E., Muthukumar, S., Chang, C.-T., Jonas, S., Weichenrieder, O., and Izaurralde, E. (2016). Structure of the Dcp2-Dcp1 mRNA-decapping complex in the activated conformation. Nat Struct Mol Biol 23, 574-579.
165) Wang, W., Czaplinski, K., Rao, Y., and Peltz, S.W. (2001). The role of Upf proteins in modulating the translation read-through of nonsense-containing transcripts. The EMBO Journal 20, 880-890.
166) Wasmuth, E.V., Januszyk, K., and Lima, C.D. (2014). Structure of an Rrp6-RNA exosome complex bound to polyA RNA. Nature 511, 435-439.
167) Waterhouse, A.M., Procter, J.B., Martin, D.M.A., Clamp, M., and Barton, G.J. (2009). Jalview Version 2—a multiple sequence alignment editor and analysis workbench. Bioinformatics 25, 1189-1191.

168) Wiederhold, K., and Passmore, L.A. (2010). Cytoplasmic deadenylation: Regulation of mRNA fate. Biochemical Society transactions 38, 1531-1536.
169) Wieser, J., Lee, B.N., Fondon, J.W., and Adams, T.H. (1994). Genetic requirements for initiating asexual development in Aspergillus nidulans. Current Genetics 27, 62-69.
170) Wu, D., Muhlrad, D., Bowler, M.W., Jiang, S., Liu, Z., Parker, R., and Song, H. (2014). Lsm2 and Lsm3 bridge the interaction of the Lsm1-7 complex with Pat1 for decapping activation. Cell Res 24, 233-246.
171) Xiang, S., Cooper-Morgan, A., Jiao, X., Kiledjian, M., Manley, J.L., and Tong, L. (2009). Structure and function of the 5[prime][rarr]3[prime] exoribonuclease Rat1 and its activating partner Rai1. Nature 458, 784-788.
172) Xu, J., Yang, J.-Y., Niu, Q.-W., and Chua, N.-H. (2006). Arabidopsis DCP2, DCP1, and VARICOSE Form a Decapping Complex Required for Postembryonic Development. The Plant Cell 18, 3386-3398.
173) Yamashita, A., Chang, T.-C., Yamashita, Y., Zhu, W., Zhong, Z., Chen, C.-Y.A., and Shyu, A.-B. (2005). Concerted action of poly(A) nucleases and decapping enzyme in mammalian mRNA turnover. Nat Struct Mol Biol 12, 1054-1063.
174) Yamashita, A., Izumi, N., Kashima, I., Ohnishi, T., Saari, B., Katsuhata, Y., Muramatsu, R., Morita, T., Iwamatsu, A., Hachiya, T., et al. (2009). SMG-8 and SMG-9, two novel subunits of the SMG-1 complex, regulate remodeling of the mRNA surveillance complex during nonsense-mediated mRNA decay. Genes & development 23, 1091-1105.
175) Zheng, D., Ezzeddine, N., Chen, C.-Y.A., Zhu, W., He, X., and Shyu, A.-B. (2008). Deadenylation is prerequisite for P-body formation and mRNA decay in mammalian cells. The Journal of Cell Biology 182, 89-101.